Superparamagnetic Iron Oxide Nanoparticles (SPION) for the Treatment of Device Related Infections

By Erik N. Taylor

Doctoral Thesis

The Center for Biomedical Engineering

May 2012

Brown University

This dissertation by Erik N. Taylor is accepted in its present form by the School of Engineering as satisfying the dissertation requirement for the degree of Doctor of Philosophy.

Date_____ _____
Thomas J. Webster, Advisor

Recommended to the Graduate Council

Date_____ _____
Thomas J. Webster, Reader

Date_____ _____
Keiko Tarquinio, Reader

Date_____ _____
Anubhav Tripathi, Reader

Date_____ _____
Robert Hurt, Reader

Date_____ _____
Rinti Banerjee, Reader

Approved by the Graduate Council

Date_____ _____
Peter Weber, Dean of the Graduate School

Erik N. Taylor

Brown University, Box D ♦ Providence, RI 02912 ♦ Erik_Taylor@brown.edu

EDUCATION

BROWN UNIVERSITY — Providence, RI
Center for Biomedical Engineering
***Doctorate of Philosophy**, Biomedical Engineering* — Class of 2012

- Thesis Title: "Superparamagnetic Iron Oxide Nanoparticles (SPION) for Treatment of Orthopedic Device Related Infections."
- Research Advisor: Thomas Webster (Ph.D.), Assoc. Prof. of Engineering (2008 – Present).
- VA Mentor: Roy K. Aaron (M.D.), Prof. of Orthopaedics (VA Fellowship; 2010 – 2012)

UNIVERSITY OF TEXAS — Austin, TX
***Bachelor of Science**, Biomedical Engineering* — May 2008

- Senior Design Project: "An arthroscopic tool for the delivery of a thermo-sensitive hydrogel into damaged knee cartilage."
- Professional outreach experience gained during MRS 2007 conference in Boston, MA

HONORS AND AWARDS

Center for Integration of Medicine and Innovative Technology – Shared $10,000 prize (2012)
Biomedical Engineering Society - Graduate Student Extended Abstract Award (2011)
Fulbright Full Research Grant-Nehru Award to India at IIT Bombay (Awarded 2011; Planned for 2012)
Publication in Nanotechnology was access over 250 times after the first quarter year (2008&2011)
Stevens Conference on Bacteria-Material Interactions - Student Travel Award (2011)
United States Department of Veterans Affairs – Pre-doctoral Research Fellowship (Awarded 2010)
Society for Biomaterials - Student Travel Award Recognition (STAR; 2010)
NSF Graduate K-12 Teaching Fellowship at Brown University (maximum duration; 2008&2009)
Office of the Vice President Undergraduate Research Fellowship at University of Texas (2006&2007)
National Science Foundation Research Experience for Undergraduates at Brown University (2007)
National Science Foundation Research Experience for Undergraduates at University of Missouri (2006)

PEER REVIEWED PUBLICATIONS

1. Erik Taylor, Keiko Tarquinio, and Thomas J Webster, "Outperforming Antibiotics through the Design of Multifunctional and Magnetic Nanoparticles." (In submission)
2. Erik Taylor, Batur Ercan, Ece Alpaslan, and Thomas J Webster, "Diameter of titanium nanotubes influences anti-bacterial efficacy." Nanotechnology, Volume 22, Number 29, 2011, Pages 295102-295113.
3. Erik Taylor and Thomas J. Webster, "Reducing infections through nanotechnology and nanoparticles." The International Journal of Nanomedicine, Volume 6, 2011, Page 1463-1473.

4. Erik Taylor and Thomas J. Webster, "Multifunctional magnetic nanoparticles for orthopedic and biofilm infections." The International Journal of Nanotechnology, Volume 8, Number 1-2, 2011, Pages 21–35.
5. Erik Taylor, Sabrina D. Puckett, Theresa Raimondo, and Thomas J. Webster, "The relationship between the nanostructure of titanium surfaces and bacterial attachment." Biomaterials, Volume 31, Issue 4, 2010, Pages 706-713.
6. Nhiem Tran, Rajesh A. Pareta, Erik Taylor, and Thomas J. Webster, "Iron oxide nanoparticles: novel drug delivery materials for treating bone disease." Advanced Materials Research, Volumes 89-91, 2010, Pages 411- 418.
7. Erik Taylor, and Thomas J. Webster, "Multifunctional superparamagnetic iron-oxide nanoparticles (SPION) for orthopedic and biofilm infections." Bioengineering Conference, IEEE 35th Annual Northeast, 2010, New York, NY, Pages 1 – 2.
8. Erik Taylor, and Thomas J. Webster, "Multifunctional superparamagnetic iron-oxide nanoparticles (SPION) for orthopedic and biofilm infections." Bioengineering Conference, IEEE 35th Annual Northeast, 2010, New York, NY, Pages 1 – 2.
9. Erik Taylor, Anubhav Kaviratna, Rinti Banerjee, and Thomas J. Webster, "Vesicular Lipid Nanoparticles (Liposomes) for the Treatment of Medical Device Infections." Proceedings of the Materials Research Society, Volume 1316, 2010, Number QQ12-23.
10. Erik Taylor, George E. Aninwene II, and Thomas J. Webster, "Using Antibiotic Conjugated Magnetic Nanoparticles and a Magnetic Field for the Treatment of Bone Prosthetic Infections." Proceedings of the Materials Research Society, Volume 1316, 2010, Number QQ09-08.
11. George E. Aninwene II, Erik Taylor, Amy Mei, Gregory D. Jay, and Thomas J. Webster, "Decreased Attachment of Bacteria to Lubricin Coated Intraocular Lenses." Proceedings of the Materials Research Society, Volume 1316, 2010, Number QQ12-31.
12. A. P. Horton, K. Kumar, H. Liu, L. Cheng, N. Lane, E. Taylor, H. R. Garner, J. W. Uhr, and X. J. Zhang, "Quantitative immunophenotyping of circulating tumor cells in blood using microfluidic screening chip integrated with hyperspectral microscope." The 15th International Conference on Solid-State Sensors, Actuators, and Microsystems (Transducers'09), 2009, Denver, CO, Pages 77-80.
13. Justin Seil, Erik Taylor, and Thomas J. Webster, "Reduced activity of Staphylococcus epidermidis in the presence of sonicated piezoelectric zinc oxide nanoparticles." Bioengineering Conference, IEEE 35th Annual Northeast, 2009, Boston, MA, Pages 1 – 2.
14. Erik Taylor, and Thomas J. Webster, "Multifunctional magnetic nanoparticles for prosthesis biofilm disruption." Bioengineering Conference, IEEE 35th Annual Northeast, 2009, Boston, MA, pp. 1 – 2.
15. Erik Taylor and Thomas J. Webster, "The use of superparamagnetic nanoparticles for prosthetic biofilm prevention." The International Journal of Nanomedicine, Volume 4, 2009, Pages 145–152.
16. Erik Taylor and Thomas Webster, "Decreased bacterial infection using nanostructured magnetic particles", Materials Research Society Conference Proceedings, Boston, MA, 2009.
17. Phong Anh Tran, Erik Taylor, Love Sarin, Robert Hurt, and Thomas J. Webster, "Novel anti-cancer, anti-bacterial coatings for biomaterials applications: selenium

nanoclusters." Proceedings of the Materials Research Society, Volume 1209, 2009, Number YY08-04.
18. Erik Taylor, Rajesh A Pareta, and Thomas J. Webster, "Increased osteoblast density in the presence of novel calcium phosphate coated magnetic nanoparticles." Nanotechnology, Volume 19, Number 26, 2008, Page 265101-265108
19. Mihail Popescu, Dong Xu, Erik Taylor, "GoFuzzKegg: Mapping Genes to KEGG Pathways Using an Ontological Fuzzy Rule System." Proceedings of the 2007 IEEE Symposium on Computational Intelligence in Bioinformatics and Computational Biology (CIBCB 2007), Hawaii, USA, 2007, Pages 298-303.

PRESENTATIONS

1. Erik Taylor and Thomas J. Webster, Oral Presentation: "Multifunctional Superparamagnetic iron oxide nanoparticles designed to outperform antibiotics against *Staphylococcus aureus* biofilms." Biomedical Engineering Society, Hartford, CT, 2011.
2. Erik Taylor and Thomas J. Webster, Oral Presentation: "Superparamagnetic iron oxide nanoparticles could be better than antibiotics at reducing *Staphylococcus aureus* biofilms." Stevens Conference on Bacteria, Hoboken, NJ, 2011.
3. Erik Taylor and Thomas J. Webster, Oral Presentation: "Nanotechnology for the reduction of device related infections." Society for Plastic Engineers, Boston, MA, 2011.
4. Erik Taylor and Thomas J. Webster, Oral Presentation: "Superparamagnetic iron oxide nanoparticles for the treatment of device related infections." Nanotechnology Showcase, Troy, NY, 2011.
5. Erik Taylor and Thomas J. Webster, Oral Presentation: "Superparamagnetic iron oxide nanoparticles that decrease infection under external control." North East Bioengineering Conference, Troy, NY, 2011.
6. Erik Taylor and Thomas J. Webster, Oral Presentation: "Magnetic nanoparticles and a magnetic field designed for the treatment of prosthetic infections." Society for Biomaterials, Orland, FL, 2011.
7. Erik Taylor and Thomas J. Webster, Poster Presentation: "Decreasing biofilm formation through the use of superparamagnetic iron oxide nanoparticles (SPION)." Materials Research Society, Boston, MA, 2011.
8. Erik Taylor and Thomas J. Webster, Oral Presentation: "Superparamagnetic iron oxide nanoparticles designed for the treatment of device related infections." Biomedical Engineering Society, Austin, TX, 2010.
9. Erik Taylor and Thomas J. Webster, Oral Presentation: "Decreasing biofilm formation through the use of superparamagnetic iron oxide nanoparticles." Society for Biomaterials, Seattle, WA, 2010.
10. Erik Taylor and Thomas J. Webster, Oral Presentation: "The relationship between nanostructure of titanium surfaces and bacterial attachment." Orthopedic Research Society, New Orleans, LA, 2010.
11. Erik Taylor, Justin Seil, Karen Haberstroh, and Tim Herbert, Oral Presentation: "The graduate student experience in NSF-GK-12." Biomedical Engineering Society, Pittsburgh, PA, 2009.

12. Erik Taylor and Thomas J. Webster, Poster Presentation: "Antibacterial properties of superparamagnetic nanoparticles." Biomedical Engineering Society, Pittsburgh, PA, 2009.
13. Phong Tran, Erik Taylor, Love Sarin, Robert Hurt, and Thomas J. Webster, Co-presentation: "Creating anti-bacterial, anti-cancer orthopedic implants: The role of selenium nanocluster coatings," Biomedical Engineering Society, Pittsburgh, PA, 2009.
14. Erik Taylor and Thomas J. Webster, Oral Presentation: "Magnetic Nanoparticles for Decreasing Biofilm Formation," Nano/Bio Materials and Applications, IC4N, Rhodes, Greece, 2009.
15. Erik Taylor and Thomas J. Webster, Oral Presentation "Superparamagnetic Iron Oxide Nanoparticles for Biofilm Disruption and Bone Regeneration." Society for Biomaterials, San Antonio, TX, 2009.
16. P. Tran, L. Sarin, E. Taylor, R. Hurt, and T.J. Webster, Co-presentation: "Selenium nanocluster coatings for anti-cancer, anti-bacterial biomaterial applications," TERMIS'2009, Seoul, South Korea, 2009.
17. Phong Anh Tran, Erik Taylor, Love Sarin, Robert Hurt, and Thomas J. Webster, Co-pesentation: "Selenium nanocluster coatings for anti-cancer, anti-bacterial orthopedic applications." American Institute of Chemical Engineers, Nashville, TN, 2009.
18. Erik Taylor, Domingo Ferrer, and Jose-Miguel Yacaman, Poster Presentation: "Gold and palladium nanoparticles with unique stellated polyhedral shape and optical properties." Material Research Society – Fall Meeting, Boston, MA, 2008.
19. Erik Taylor and Thomas J. Webster, Oral Presentation: "Superparamagnetic iron oxide nanoparticles with novel calcium phosphate coating for bone regeneration in osteoporosis." Biomedical Engineering Society, Los Angeles, CA, 2008.

BOOK CHAPTER

1. Erik N. Taylor, Dave A. Stout, George Aninwene II, and Thomas J. Webster, "Tissue engineering *in vivo* with nanotechnology." Nanomedicine: Principles and Perspectives, Volume 1, Springer, 2011 (Final Draft Submitted).

Acknowledgements

I would like to thank the following:

- VA Pre-doctoral Research Fellowship with support from Dr. Roy K. Aaron
- NSF GK-12 with Karen Haberstroh, Tim Herbert, and Dan Bisaccio for support
- Keiko Tarquinio, M.D. for guidance during weekly bacteria group lab meetings
- All members of the Nanomedicine Laboratory for help with bacterial studies
- And, Professor Thomas J. Webster

www.WebsterNano.com

Table of Contents

1. Introduction

1.1 Introduction to medical device infections

1.1.1 A novel approach to infection control through nanotechnology

This chapter outlines the relevance of medical device infections beginning with some statistical analysis of infections, and moving towards understanding why medical device infections are an increasing problem clinically today. Specifically, the underlying premise of this thesis is that antibiotics are not effective at eradicating medical device infections due to antimicrobial resistance caused by the evolution of genetically tolerant bacteria, or due to biofilm formation.[1-3] While numerous investigators have been creating different implant chemistries or designing new drugs, nanotechnology, or the science that deals with technologies on the scale of one billionth of a meter (10^{-9} m = 1 nm), is only recently being investigated as a means for infection control on medical devices.[4-7]

Nanomaterials are materials with structural units, grains, particles, fibers or other constituent components smaller than 100 nm in at least one dimension[8] and will be introduced as the basic building blocks of nanotechnology for infection control. Next, this chapter will review the studies that have been conducted so far, with a focus on the application of nanomaterials either as nanofeatured biomaterials, or as systemic nanoparticles, emphasizing the progress made, and the prospects necessary to be made. Finally, this chapter will then finish with an introduction to the core novel

nanotechnology explored here for infection control: superparamagnetic iron oxide nanoparticles (or SPION).

1.1.2 Medical device infections

Medical device infections can be frequent and costly depending on the device location and their duration of use.[3] Yet, the benefits from medical devices far outweigh this detriment, and therefore continue to be used clinically. For example, peripheral or central intravenous catheters (CVCs) resulting in bloodstream infections (BSI) occur in about 4–5 out of every 1000 CVC devices inserted,[9,10] with an attributed cost per infection estimated at US$34,508–$56,000,[11,12] and the annual cost of caring for patients with CVC-associated BSIs ranges from $296 million to $2.3 billion.[13] However, CVCs are necessary for the delivery of fluids and medication for monitoring patient health (such as through the drawing of blood or monitoring of blood pressure). Thus, their use, despite infection, is necessary. Additional examples are percutaneous orthopedic implant devices (implanted orthopedic devices which are fixed across the skin), which are susceptible to bacterial invasion at the biomaterial skin exit site,[14] and includes intramedullary nails, external-fixation pins (which are more likely to become infected than intramedullary nails), plates, and screw.[15] As bacteria colonize either the implant surface or adjacent damaged tissue sites, biomaterial exit sites become the gateway to infection,[16-18] with overall rates averaging 5%, or up to 57% (pin tract infection rate),[15,18] possibly leading to bacteria spreading internally and causing osteomyelitis (an infection of bone).[18,19] According to previous studies, the occurrence of osteomyelitis after insertion of an

external bone fixator can be up to 4%.[16-18] In addition to osteomyelitis, infection leads to bone implant loosening and fracture malunion or nonunion, leading to early failure of the device.[17] Yet, implantation of percutaneous orthopedic devices is necessary such as external fixators for setting bones which cannot be fixed through a cast, and is an extremely cost effective method for fixing bone,[18] or as an intraosseous transcutaneous amputee prosthesis (ITAP), the most promising technique to return mobility to war amputees, or others who have lost limbs, and therefore will continue to be used.[5,20,21]

In addition to the high infection rates stated above for transcutaneous extracorporeal devices or other medical devices that are constantly exposed to the non-sterile environment outside the body, implanted devices are also susceptible to infections, resulting in implant failure.[22] For example, orthopedic prosthetic joint replacements are permanently implanted to alleviate pain, promote mobility, and improve the quality of life, but such implantations suffer from the risk of infection, leading to the burden of revision surgery.[22] Recent studies estimate the infection burden on all revision surgeries is 25% for total knee arthroplasties (TKA) and 15% for total hip arthroplasties (THA), in the USA.[22-24] Such periprosthetic implant infections, which are also known as septic failures, cost about US$70,000 per episode, and are the most common reason for removal of all TKAs (79%) and THAs (74%).[22-24] Such orthopedic prosthetic device infections are some of the most striking medical device infections due to their widespread use, but other implanted medical devices (see **Table 1.1**), such as cardiac devices including mechanical heart valves, pacemaker-defibrillator, and vascular grafts can similarly suffer from infection, or others, and could benefit from new therapies beyond antibiotics.[3]

Table 1.1 A summary of the impact medical device infections have as a rate of infection related procedures and the cost associated with these procedures using surgical or other medical treatment methods.

Device type	Impact of infection	Cost for care
Catheters - Peripheral or central intravenous catheters (CVCs)	Resulting bloodstream infections (BSI) occur in about 4–5 out of every 1000 CVC devices inserted[9,10]	$34,508–$56,000,[11,12] and the annual cost of caring for patients ranges from $296 million to $2.3 billion[13]
External Orthopedic – Percutaneous implant devices	overall rates averaging 5%, or up to 57% (pin tract infection rate)[15,18]	$5,000 for pin tract infections or up to $25,000 for intramedullary nail infections[15]
Orthopedic - Total knee arthroplasties (TKA) and total hip arthroplasties (THA)	Infection burden on all revision surgeries is 25% for TKA and 15% for THA in the USA[22-24]	periprosthetic implant infections cost about US$70,000 per episode[22-24]
Cardiovascular – mechanical heart valve, pacemaker-defibrillator, or vascular graft	Average rates of infections for initially implanted cardiovascular devices or grafts are about 4%, which is lower than for revision implants[15]	Medical and surgical combined costs of $50,000 for mechanical heart valves, $40,000 for pacemaker-defibrillators, and $35,000 for vascular grafts[15]

1.1.3 Problems with current methods to limit infections

The three primary strategies to limit infections in the orthopedic settings are to first prevent the infection, treat the infection through surgery, and/or to use drugs to limit the spread of the infection. A summary of these strategies through prevention, surgery, or drugs are listed below in **Table 1.2** below.

Table 1.2 A summary of the strategies used to limit infections used today in hospitals.

Strategy	Method	Problems with method
Prevention	Sterilization of surfaces	The patient's skin, or surgeon's hands are a reservoir for contamination[6,7]
Prevention	Coatings and drug release	Limited lifetime,[8] decreases device performance,[9] or toxic[10,11]
Surgery	Device removal and joint washout	Extra cost to patient, decreases quality of life, impaired mobility, and device fails[12]
Surgery	Retention of devices	Only useful for early or late haematogenous (blood) infections[13]
Drugs	I.V. or oral antibiotics	Immuno-incompetent zone, biofilm, or poor availability at the site of infection[14]

The first step for prevention of infections is sterilization of the implant surface. Limitations of this method are that the hospital environment is a constant source of

bacteria that cannot be completely decontaminated. This is because there is no technology available which is able to remove all sources of contamination from areas such as hospital beds, health workers hands, the patient's skin, and other surfaces. To show how astounding the impact of these factors can be, one study found that of surgical instruments used in arthroplasty, 63% were contaminated after surgery, and although the clinical significance of this is unknown at this point, this could indicate a route for infections to develop.[25] Moreover, it is unrealistic to completely decontaminate human surfaces, and it has been hypothesized that complete elimination of one organism from the entire body, such as *Staphylococcus epidermidis*, would create the potential colonization and spread of more virulent organisms, such as MRSA.[26,27]

Coatings and methods for drug release from implants are another method to prevent infections, and is an approach that is being attempted for medical devices. Yet, limitations of this method are the limited lifetime,[28] decreased device performance,[29] or toxicity.[30,31] In particular, decreased mechanical stability, delamination of coatings (such as stent delamination or others which has limited the use of these devices recently as discovered during *in vivo* testing,) and decreased cell adhesion and tissue integration of devices.[32] Additionally, coatings have a limited lifetime, and therefore are only a temporary solution to limit infections, especially for devices that are exposed to bacterial continuously such as with catheters or endotracheal tubes, where the coating may only delay the onset of infection.[33]

Once bacterial infection prevention has failed, device removal combined with antibiotic therapy is the standard in the clinic for the treatment of infection. After biofilm formation occurs, the most straight forward way to treat infection is to remove the

infected surface which contains the sticky biofilm matrix. The standard surgical procedure in the clinic for prosthetic removal in a multi-step procedure[34] which requires joint washout and device removal with antibiotic treatment followed by prolonged oral antibiotics (which promotes the emergence of antibiotic resistant strains). During this process, the defect site is not mechanically stable until reinsertion of a new device. These procedures are expensive to the patient in terms of extra cost and decreased quality of life and clearly, new materials or procedures are needed to reduce infections.

Retention of devices after debridement (removal of infected tissue) and antibacterial therapy is more recently considered as a favorable procedure for the patient and surgeon in terms of ease of surgery, time, and cost-effectiveness.[35] Yet, the procedure has only been found effective for early post-operative infections or late acute haematogenous (blood associated) staphylococcal infections[35] and is in part dependent on microbiological findings such as antibiotic resistances, as such would limit success.[36] These limitations have caused variable success rates for different studies between 2.8%– 100%.[36] Due to such limitations, novel therapeutics able to treat late-stage infections, or antibiotic resistant infections associated with medical devices, would be useful. Problems with antibiotic treatments, especially through oral or intravenous routes, have been associated with the formation of an immune-incompetent zone (fibrous capsule formation,) poor availability of drugs at the site of infection, and the formation of biofilm.[37]

1.1.4 Problems with gentamicin loaded bone cements

Because standard antibiotics treatments are ineffective, local drug delivery might be preferable.[37] In particular, bone cements loaded with gentamicin have been used (i.e. for

hip replacements or revision surgeries).[37] For these treatments, the bone cement can be used during placement of the prosthetic device, yet may lead to device failure (**Figure 1.1** shows a hip prosthesis with loosening which could be due to infection).

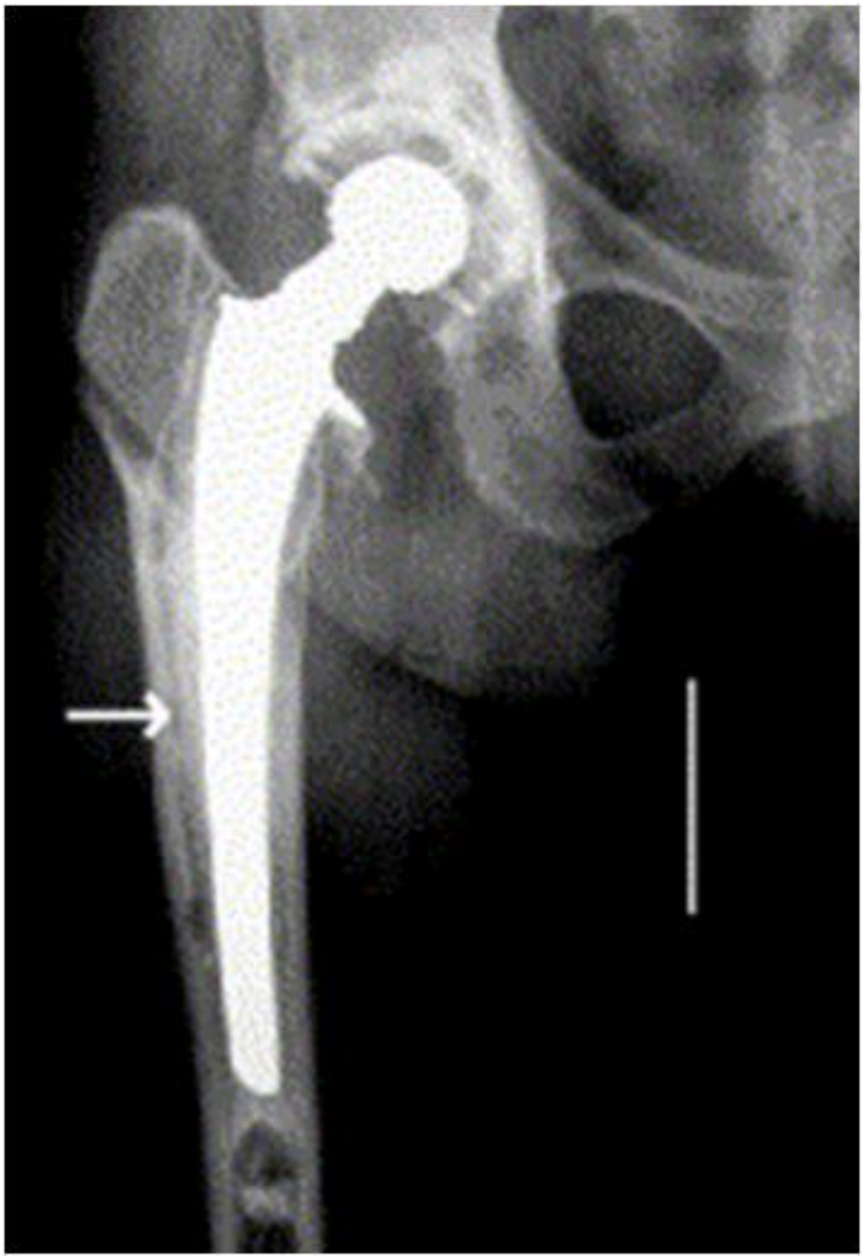

Figure 1.1 Hip prosthesis showing loosening around bone cement could be due to infection (White scale bar represents 5 cm; image from reference).[37]

Of available antibiotics, gentamicin was selected because it has outstanding heat stability, long shelf-life, is autoclavable, and has broad spectrum activity including both gram-positive (such as Staphylococcus genus) and gram negatives. Yet, there are problems with this technique, in particular the coating decreases mechanical stability of the cement, is not food and drug administration (FDA) approved, and may not warrant additional costs for these reasons.[37] Gentamicin used in bone cements can also lead to emergence of antibiotic resistant strains, in particular because it is a broad spectrum antibiotic, and thus targets a wide variety of bacteria that can then develop resistance.[37] Finally, when used instead as a treatment during revision surgery, the failure rate is still 5-23%, and thus better treatments are still needed which can further reduce these high reinfection rates.[37]

1.1.5 Why antibiotics don't work: antibiotic resistance

When it comes to device related infections, multiple drug resistant *Staphylococcus aureus* (MRSA) infections have caused great concern, with implant infections (including grafts and implantable medical devices) being the third most common cause of potential MRSA infections leading to hospitalization between 1999 and 2005.[38] More recent in-depth analysis found that 56% of all device-associated infections with *Staphylococcus aureus* were reported as MRSA between 2006 and 2007.[39] The International Nosocomial Infection Control Consortium (INNIC) also reported that of all *Staphylococcus aureus* isolated, 84.1% contained MRSA internationally (with the most recent data from 2008).[40] Of equal concern, MRSA infections are costing the health care system up to an estimated US$9.7 billion excess costs, and the percentage of infections with MRSA are expected to continue to increase.[38,40]

Briefly on the history of antibiotic resistance, penicillin resistance was observed as early as 1940's, as mediated by the emergency of β-lactamase enzymes produced by resistant bacteria (**Figure 1.2.A** is an outline of this brief history).[41] These are enzymes which are be produced by the bacteria, and break down penicillin. New drugs were produced which overcame this resistance, and yet in the 1980's, the emergency of methicillin resistance and emergence of multiple drug resistant *Staphylococcus aureus* (or MRSA) was observed.[41] This bacteria produced novel penicillin binding proteins (PBPs), named as such due to discovery via binding with radio-labeled penicillin, and is an enzyme that normally cross-links the peptidoglycan bacterial cell wall layer, a major structural component of the bacterial cell.[41] MRSA at the time began to produce PBPs which did not bind to β-lactam antibiotics (such as penicillin, oxacillin, and methicillin) and thus the bacteria could survive increasing concentrations of the antibiotic drugs in this class.[41] More recently, as early as 1992, vancomycin resistance was observed. This resistance was mediated by the gene, VanA, the gene product of which is a bacterial ligase, an enzyme able to incorporate methionine or phenylalanine into peptide subunits of peptidoglycan, and thus does not allow binding of vancomycin.[41] Finally, as the name of MRSA suggests, this type of bacteria is also resistant to other antibiotics such as aminoglycosides, including gentamicin, which normally binds to bacterial 30S subunits and inhibit protein synthesis. Gentamicin resistance in MRSA is mediated through the production of enzymes that modify the antibiotic via either amino groups, through acetylation, or hydroxyl groups, through adenylation or phosphorylation, thus allowing the bacteria to continue protein synthesis (**Figure 1.2.B**).[42]

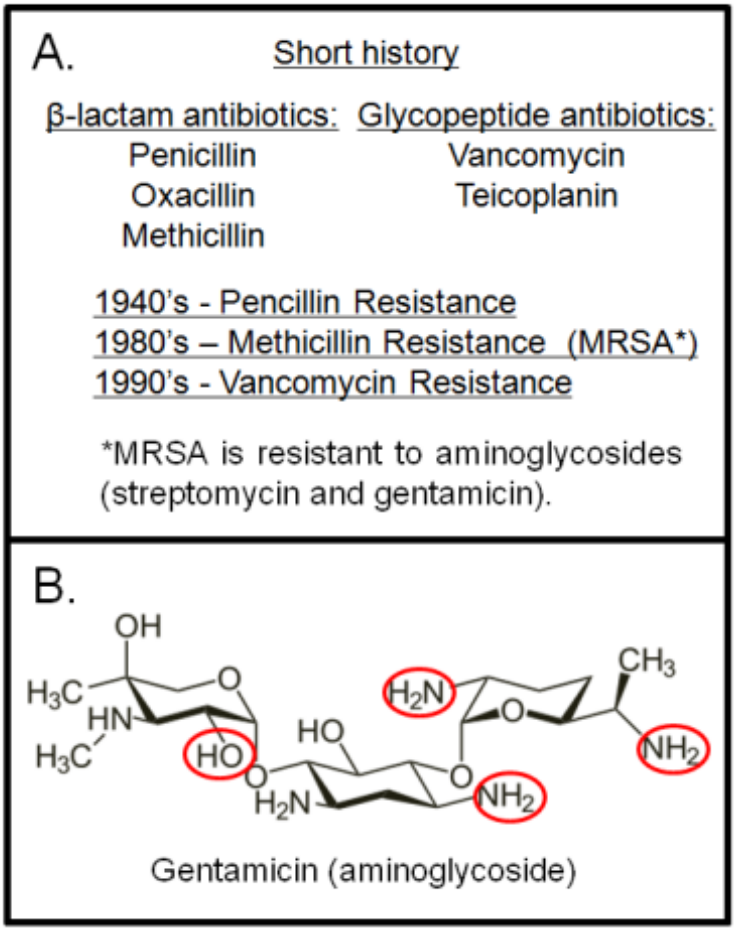

Figure 1.2 A description of the brief history of antibiotic resistance, and antibiotics used clinically. **A.** In particular, β-lactam antibiotics, including penicillin, methicillin, and oxacillin, and more recently glycopeptides antibiotics vancomycin and teicoplanin are used, especially for treating *Staphylococcus aureus* or other Gram-positive infections. Resistance to these antibiotics has been observed as early as 1940 for penicillin, 1980 for methicillin resistance, and the emergence of multidrug resistant *Staphylococcus aureus* (MRSA), and vancomycin resistance as early as 1992.[41] MRSA is also resistance to aminoglycosides. **B.** MRSA resistance to aminoglycosides is mediated by the production of enzymes that modify the antibiotic, and don't allow it's binding to 30S ribosomal subunits, an important component in bacterial protein synthesis. In particular, amino groups and hydroxyl groups are modified, thus inactivating gentamicin (image adapted from reference; groups open to modification are circled red).[42]

The mechanisms of these resistances are now well understood in these examples of penicillin, methicillin, and vancomycin, through the emergence of bacterial genes able to synthesize proteins including penicillinases, novel penicillin binding proteins, or novel ligases that enables biochemical modification of cell-wall components for resistance to the respective antibiotics.[41] **Figure 1.3** provides a detailed description these mechanisms of antibiotic resistance in bacteria for these three antibiotics, or other antibiotics in similar classes of β-lactams (penicillin, methicillin, and oxacillin) and glycopeptides (vancomycin). Furthermore, bacterial tolerance to vancomycin is a great concern, because it was long considered to be the antibiotic of last resort.[41]

Concerns are growing for the tolerance of antibiotics by all microorganisms. In addition to bacteria, fungi are also becoming tolerant to current antibiotic treatments. *Candida albicans* is the most frequent of these human pathogens, with various strains isolated from the clinical setting exhibiting resistance to antifungals, such as triazole,[43] or developing antibiotic-resistant biofilms,[44] posing a significant threat to the infected individual through increased resistance to antifungal treatments. Other pathogenic *Candida* species also have multidrug tolerances, such as *Candida krusei*.[45]

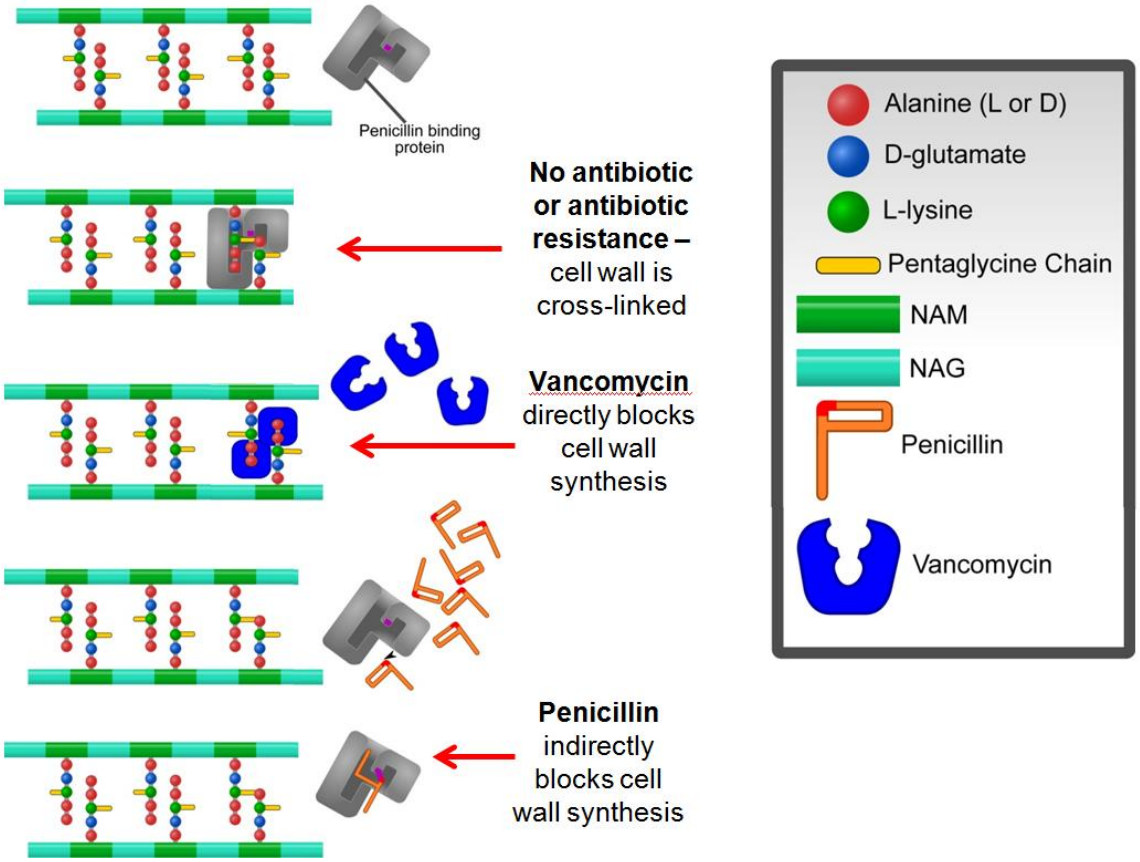

Figure 1.3 Antibiotic resistant bacteria continue to function in the presence of antibiotics such as penicillin, methicillin, and vancomycin by cross-linking of the polysaccharide cell wall, similar to bacteria without the presence of antibiotics. For vancomycin resistance, this is achieved by biochemical modification of the alanine binding cell wall component shown above, decreasing the antibiotics effectiveness.[46] In penicillin resistance, β-lactamases are produced, an enzyme that enables penicillin degradation by bacteria, effectively lowering the concentration of the active antibiotic.[47] Alternatively, modified versions of the penicillin binding protein (PBP) are produced with lowered binding affinity for the antibiotic,[47] as observed in methicillin resistant bacteria (which acts by an identical mechanism to penicillin).[41] Non-resistant strains are susceptible; antibiotics such as penicillin, methicillin, and vancomycin block cell wall synthesis through prevention of this cross-linking either via direct binding to penicillin binding protein or binding to the alanine repeats on the surface of the cell wall, respectively (image adapted from citation).[48]

1.1.6 Biofilm antibiotic tolerance and other stress factors

In addition to the evolution of antibiotic resistant bacteria, such as MRSA, VRE, or others, the tendency of bacteria to form biofilms during an infection on medical devices seriously complicates eradication. Formed as a sticky matrix through the incorporation of biopolymers including polysaccharides, proteins, and DNA, the biofilm is a physical and chemical protective barrier.[49,50] Significantly, antibiotic therapy is ineffective against biofilm bacteria, indicating another mode of bacterial resistance.[3,51,52] Furthermore, because biofilm bacteria are far more resistant to antibiotics, larger quantities of the drugs must be used, further contributing to the emergence of antibiotic resistant bacteria, as destruction of natural bacteria can help to spread bacterial resistance.[53]

Biofilm formation is hypothesized to be a highly conserved evolutionary means for bacteria to resist various antimicrobial agents, as mediated by the colonization of biotic surfaces (biologically derived, such as tissues and bone) and abiotic surfaces (engineered, such as medical devices).[1] Along these lines, antibiotics are rendered ineffective when biofilms form due to their relative impermeability into the biofilm matrix, slow growth, and the presence of persister cells (**Figure 1.4**).[1] Of these mechansisms, the biofilm matrix protects the bacteria from antibiotics, for example due to the charge of the biofilm, which can trap the antibiotic molecules.[1] Slow growth allows the bacteria to survive until the antibiotic concentration decreases, since most antibiotics target bacterial metabolism (such as cell-wall or protein synthesis).[1] Finally, persister cells could be antibiotic resistant, or phenotypticall resistant due to slow growth, or small size.[1]

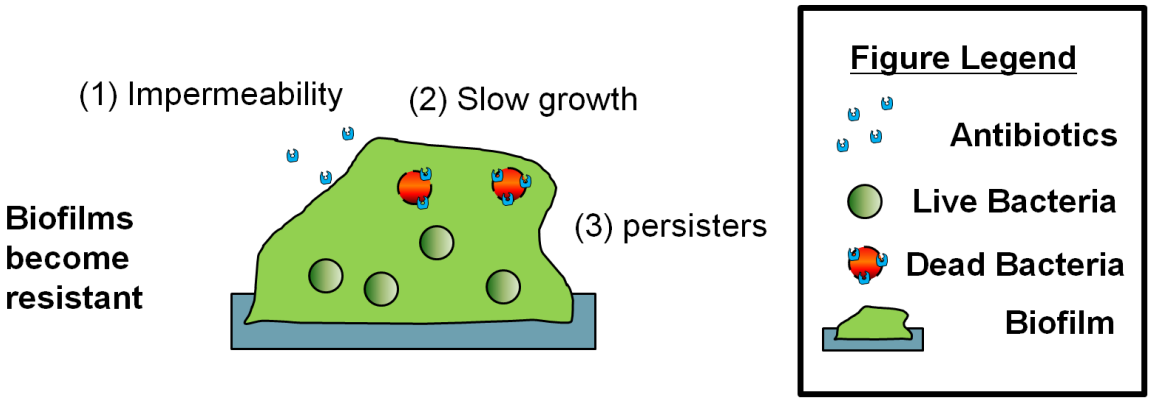

Figure 1.4 Bacteria can resist antibiotics due to evolutionarily conserved mechanisms of antibiotic resistance.[1] In particular, (1) antibiotics can have low permeability into the biofilm matrix, (2) the bacteria grow very slowly, or (3) the presence of persister cells allow bacteria in the biofilm to survive antibiotics.

Another hypothesis about why antibiotics don't work against biofilm is because the required pharmokinetics cannot be achieved *in vivo*. In work by Kerry L. LaPlante and Suzanne Woodmansee, this hypothesis was studied, that if biofilms increased resistances to antibiotics, then required antibiotic be concentrations could be pharmokinetically unachievable.[54] Using an experimental model of endocarditis, these researchers showed that the pharmokinetics of vancomycin in presence of the biofilm were impossible to achieve; more specifically, minimum biofilm eradication concentration (MBEC) was observed to be 64 to 128 μg/ml of vancomycin, yet the maximum achievable concentration in the pharmacokinetic model was 42.32 +/- 11.9 μg/ml vancomycin.[54] This study showed that, it is possible that antibiotics don't work *in vivo* against biofilm bacteria because the concentration required to eradicate a biofilm is higher than what is achievable.[54] Some limitations of this study are that 1) the limit of detection was 2.4 CFU/ml, which means that bacteria could still viable after treatments, and 2) no proof

was provided that the antibiotic was completely washed out after treatment during MBEC analysis (according to the referenced method, the biofilm was only rinsed only rinsed 1 time with PBS).[55] Finally, in the case of catheters that are used intermittently, "vancomycin lock therapy" can be used, where antibiotics solutions are left in the catheter volume when it is not in use, and thus the catheter is exposed for longer times, rather than systemically. Despite these limitations, or other therapies to overcome the issues with system delivery of antibiotics, the MBEC method[55] does seem to be useful for clinical predictions about comparing which antibiotic is the best candidate for use *in vivo*, and also if theoretical pharmocokinetics parameters enable clinical concentrations to be achievable during systemic use of antibiotics.[54]

A coincident theory is being developed, along with this growing hypothesis that antibiotics are ineffective against biofilms; antibiotics could even increase biofilm formation, as has been observed for biofilm formation by pathogenic microorganisms including *Staphylococcus epidermidis* and *Staphylococcus aureus* at sub-lethal concentrations of antibiotics.[56-58] For example, when various strains of biofilm forming *Staphylococcus epidermidis* were cultured at 10^4–10^5 CFU/ml (colony forming units per ml) in tryptic soy broth supplemented with antibiotics including vancomycin, tigecycline, linezolid, and novobiocin, a maximum of 9.1 fold increase in biofilm formation was found with tigecycline (at 0.02 µg/ml), or a up to a 2.1 fold increase with vancomycin (at 1.7 µg/ml), both at concentrations that would not kill the planktonic bacteria (sub-minimum inhibitory concentration; MIC).[56] In this study, Kaplan et al. found that this increase was related to the release and incorporation of extracellular DNA into biofilm.[56] Another mechanism was determined by Rachid et al., found that tetracycline and

quinupristin-dalfopristin antibiotics can lead to enhanced polysaccharide synthesis or biofilm formation at similar concentrations.[58] These authors concluded that antibiotic induced biofilm formation is both strain and antibiotic dependent.[56-58] Perhaps such increases in biofilm formation are part of an evolutionary adaptation to defend against natural antibiotics produced by bacteria and fungus.[59]

In a study by Hess et al., it was observed that the presence of an existing biofilm protects against antibiotics, and can lead to increased biofilm formation upon exposure to antibiotics.[60] In this study using a 10^5 *Staphylococcus aureus* inoculum per well in a 6-well plate, biofilms were produced on silk sutures, where it was found that subsequent addition of gentamicin increased the amount of biomass at both sub-inhibitory and lethal (1-4 µg/ml minimum bactericidal concentration; MBC) concentrations of gentamycin.[60] This novel finding indicated that concentrations of gentamicin of up to 20 µg/ml increased biofilm formation, and at the highest concentration tested of 100 µg/ml, the biofilm resident *Staphylococcus aureus* were still significantly viable.[60] Yet, after mechanical dispersal via ultra-sonication at ~50 joules with 100% amplitude for 5 s and 20kHz, bacterial growth was inhibited at 1-2 µg/ml. These results indicated that the biofilm was not only required for resistance to antibiotics, but could furthermore act as a reservoir for subsequent biofilm formation, enabling resident biofilm bacteria to enhance biofilm production in response to up to 20X the MIC of gentamicin in this study.[60]

Furthermore, biofilm formation is more generally understood as a stress response mechanism (**Figure 1.5**). In addition to antibiotic stresses as described above and elsewhere,[56-60] other factors are important and lead to biofilm formation such as nutritional limitations,[61-63] including no iron availability,[63] along with environmental

stress factors,[58,61,62,64-66] such as low oxygen (i.e. anaerobic conditions),[65] osmotic stress (up to 5.6% NaCl),[62,64,66] ethanol (up to 4%)[62,66] and heat response (up to 42°C).[58] These factors can mediate biofilm formation directly through gene expression leading to the release of polysaccharide intracellular adhesin[61,65] or proteins which mediate multicellular aggregation.[62] Alternatively, genes involved in surface attachment to medical devices could be activated, and thus contribute to subsequent biofilm formation.[67-69] Iron-limited medium can cause gene transcription in *Staphyloccus epidermidis*, resulting in the release of siderophores that mediate the covalent bonding of the bacterium to metal surfaces.[67,68] Biofilm pathogenesis of *Staphylococcus aureus* has been implicated by the expression of an extracellular adherence protein (Eap) and extracellular matrix binding protein (Emp) which are induced by iron restriction.[69] Interestingly, such regulation doesn't appear to be unidirectional, as biofilms grown from *Pseudomonas aeruginosa* strains obtained in the sputum of cystic fibrosis patients have been disrupted and cleared by switching to iron-rich medium in flow chamber and microtiter tests (minimum concentration of 5.2 µg/ml of free iron contributed from ferric ammonium citrate).[70]

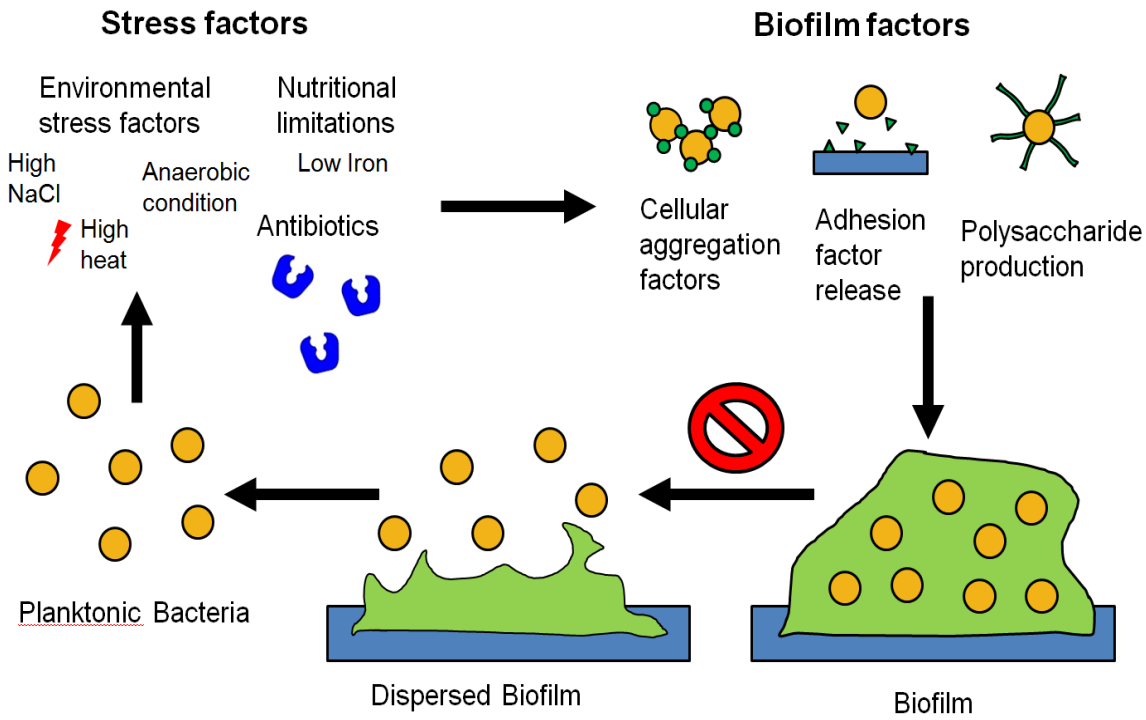

Figure 1.5 Biofilm formation is understood to be a stress response to various factors such as antibiotics,[56-60] nutritional limitations,[61-63] along with environmental stress factors.[58,61,62,64-66] Under these conditions, biofilm formation is mediated by biofilm factors including proteins which mediate multicellular aggregation,[62] released polysaccharide intracellular adhesin (PIA),[61,65] or activation of genes involved in surface attachment to medical devices.[67-69] Recent studies have also shown that these effects are reversible, leading to biofilm dispersal, as is evidenced by reintroduction of nutrients.[70,71]

1.1.7 Biofilms on medical devices

When a device must be removed to eradicate an infection, it is often because bacteria have produced a sticky biofilm matrix on the device surface,[72] and formed a strong adhesion (estimated at 2.3 times the shear forces to which the biofilm was exposed).[73] Biofilm resistance to antibiotic treatment enables the infection to reactive without

prolonged treatment or removal of the device.[1] After biofilm formation occurs, the simplest way to treat the infection is to remove the infected surface, which contains the sticky biofilm matrix.[72] Yet, with permanent fixtures, such as orthopedic prosthetic devices, device removal can be difficult or debilitating to the patient, especially if they are very young or old.[72] In addition, chronic infections that do not respond to antibiotic treatment and require removal of adjacent devitalized bone and soft tissue, and may also require plastic surgery.[72]

Along these lines of the difficulty of treating infections on medical devices is the hypothesis that biofilm, a physical matrix, provides protection for the embedded live bacteria.[1] An outline of biofilm pathogenicity demonstrating macroscopic biofilm dissemination, a representative micrograph of biofilm morphology on medical devices, and a schematic of biofilm formation is shown in **Figure 1.6**.

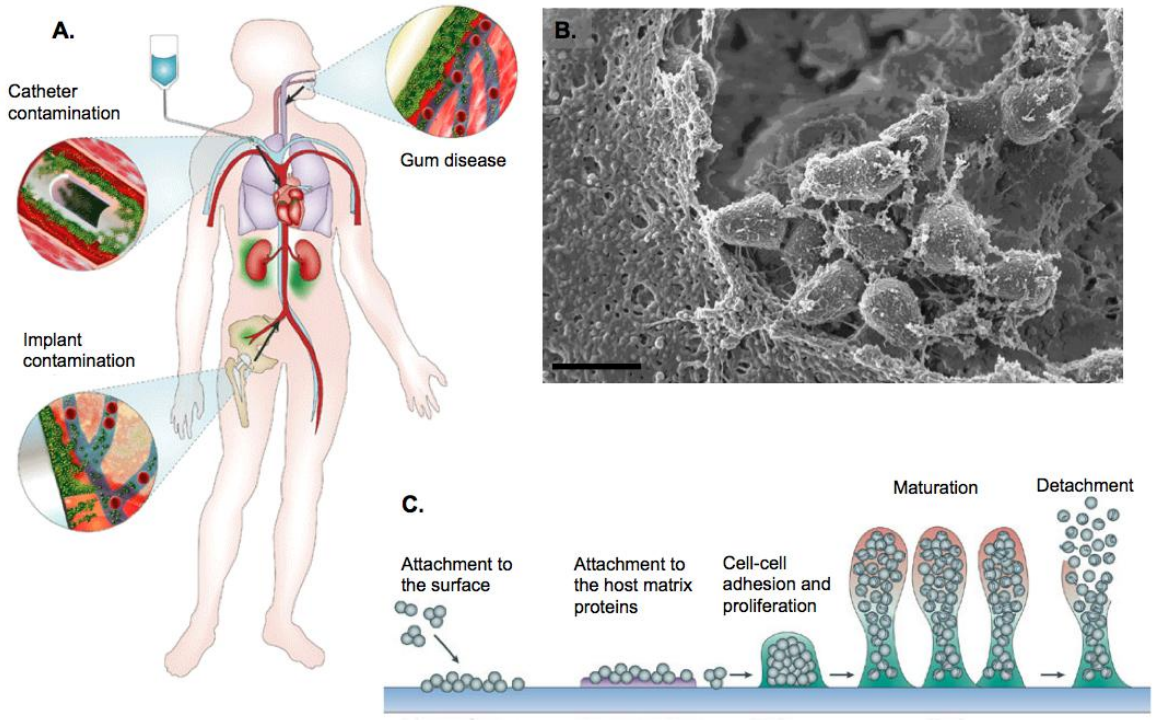

Figure 1.6 Bacterial pathogenicity in humans is mediated significantly by entry of medical devices into the body, acting as a source for biofilm matrix formation. (**A**) Possible routes of biofilm dissemination around the body originate from sites such as gum disease, catheter placement, or implant contamination.[1] (**B**) Scanning electron micrographs (SEM) of a biofilm matrix, offering protection of resident bacteria from eradication, imaged from a clinical endotracheal tube identified as S*treptococcus pneumonia*. Scale bar shown is 1 μm. (**C**) Schematic of biofilm-mediated device-related infection, starting with bacterial attachment to a device or adsorbed host proteins, leading to biopolymer mediated cell–cell adhesion, maturation, and eventual detachment leading to the spread of infection through the body.[53]

1.1.8 Tissue damage in the presence of infection

Biofilm infections can also lead to loss of bone mass, and thus bone-building agents would benefit regeneration of bone during or after an infection.[74] Bacteria degrade bone

by three mechanisms outlined by Nair and colleagues.[74] The first mechanism is the production of degradative products that destroy the non-cellular components of bone. Second, bacteria produce toxins (such as endotoxins)[75] which promote cellular processes stimulating degradation of bone (osteoclast activity).[74] Third, bacteria inhibit new bone formation through the disruption of osteoblast functions. There is mounting evidence to suggest that the last two are responsible for the majority of bone loss in various musculoskeletal infections.[75] This has been studied more thoroughly *in vitro*, where both the number and spreading area per osteoblast cell decreases with increasing density of adherent *Staphyloccus epidermidis.*[76] This may also be in part due the consumption of nutrients (such as iron and oxygen) by the active infection, which decreases the viability of osteoblasts,[77] while potentially simultaneously enhancing biofilm formation as described above and previously.[63,65]

Reversing low bone density is not, however, limited to infection. Other conditions (such as osteoporosis, bone cancer, arthritis and bone fractures) would also benefit from highly effective bone-building strategies. In all of these cases, the site specific anabolic behavior of a drug delivery system would be advantageous. Anabolic treatments are the most promising agents to build bone mass resulting in increased osteoblast activity and a reduction of 65–70% of vertebral and about 50% of nonvertebral fractures.[78] However, some anabolic treatments (like the use of bone morphogenetic proteins), while potent, are not selective inducers of bone mass and, thus, generate calcium deposits in areas not desirable (like the liver). At present some other drugs are available to treat low bone density such as bis- and di-phosphonates, estrogen modulators, etc. Anti-resorptive bone agents are primarily used to prevent further breakdown of bone. A common example is

the class of drugs, bis-phosphonates, which act by inhibiting the differentiation to and inducing apoptosis in osteoclasts (the bone resorbing cells).[79,80] Yet, the non-specific action of bis-phosphonates on other cell lines has been shown including decreasing the proliferation of osteoblasts (bone forming cells) and inducing apoptosis in macrophages.[81,82] Another limitation is the inability of these agents to increase bone growth, instead only working to prevent further loss.

1.1.9 Inflammation during implantation and in the presence of infection

Inflammation is considered a normal part of healing, and is closely linked to the activation of the immune system.[83] There are predictable stages to the inflammation and foreign body response that follows any injury or implantation. **Figure 1.7** shows this inflammatory cascade, while **Table 1.3** describes the primary cells involved in these inflammatory and wound healing processes. For the inflammatory cascade, the first step is nonspecific protein absorption and adhesion of cells, such as monocytes, leukocytes and platelets.[84] This is followed by the formation of giant cells and cytokine release.[84] Neutrophils arrive on the scene very early after any tissue damage, and in an attempt to kill any microbes they may flood the damaged area with free radicals that kill many otherwise-healthy host cells as well as the target infectious agents.[85] This becomes a major issue in chronic wound situations, and may lead to chronic inflammation and scarring.[85] In the case of implanted materials the implanted device may be encapsulated by fibrous tissue if excessive inflammatory processes take place, which can lead to failure of the implanted device, for example due to being cut-off from blood supply, in the case of a cardiovascular device, or the poor juxtaposition with bone, in the case of an

orthopedic device.[84] The materials that are considered to be biocompatible reduce the inflammation process by either avoiding the initiation of the foreign body response, by avoiding or reducing the initiation of one or more steps in the foreign body response, or by acceleration the process to reduce the inflammation period.

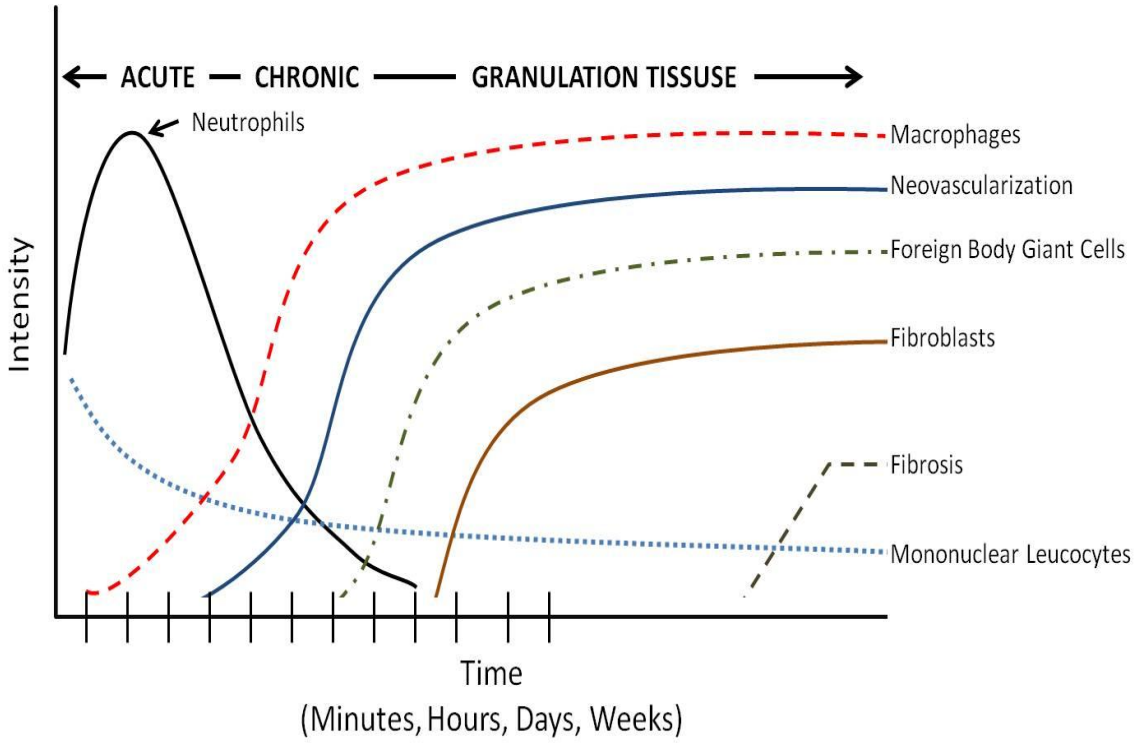

Figure 1.7 The above figure illustrates the temporal variation in the acute inflammatory response, chronic inflammatory response, granulation tissue development, and foreign body reaction to implanted biomaterials. The intensity and time variables are dependent upon the extent of the injury created in the process of the implantation, and the size shape topography, and chemical and physical properties of the implanted material (adapted from citation).[86]

Table 1.3 Major cells involved in the normal wound healing process (Adapted from [85])

Cell Type	Source	Timing and Behavior
Keratinocytes	Epidermal wound edges and cut appendage stumps	Migration commences after a brief lag phase
Fibroblasts/ myofibroblasts	Connective tissue wound edges and fibrocytes from circulation	Invasion to form wound granulation tissue commences early, but transformation into myofibroblasts is later
Endothelial cells	Nearby blood vessels	Vasculature near to wound site becomes activated rapidly to allow diapedesis, but sprouting is later
Platelets	Spill from damaged blood vessels	Immediately at the site of tissue damage
Mast cells	Small numbers resident in tissue; others by migration through the pores in blood vessels, diapedesis from adjacent vessels	Appear to have an early role in regulating the later inflammatory response by neutrophils
Neutrophils	Diapedesis from adjacent vessels	Earliest of the leukocytes to derive from the blood
Macrophages	Some tissue-resident cells but majority derive from blood-borne monocytes	Secondary influx from the blood after neutrophils have killed the immediate foreign-organism invaders

Implanted devices cause inflammation which may lead to device failure.[87] While there may be several reasons why an implant may fail, inflammation of the implant area is both a major cause, and major indicator of implant failure. According to one study, in their set of 282 cases of failed stainless steel orthopedic implants, 10.6% exhibited inflammation of the surrounding tissues.[87] Inflammation rates may change depending on the material implanted, location of implantation, and the function of the implanted device; however, inflammation is still a major issue to consider when developing a new implantable material or wound treatment. Implanted materials that cause excess inflammation lead to significant damage of the surrounding tissues and result in the loosening or total failure of the implanted material.

Moreover, in the case of an infected prosthesis, biofilm can cause such excesses of inflammation, leading to the failure of an implanted prosthesis.[87] Recent studies have shown that in many cases of aseptic loosening, which may impact up to 25% of all implanted prosthetic implants, and leads to subsequent implant failure, there were lipopolysaccharides (LPS) present (inflammatory inducing bacterial surface molecules).[88] Although aseptic failures can occur without the presence of bacteria, there is clear evidence that, in a number of cases, these processes may be initiated by LPS, or possibly other bacterial processes, such as undetectable infections on the surface of implants, or possibly metabolically inactive biofilm bacteria, which would incorrectly lead to the assumption that the implant is aseptic.[88] Staphylococci, the most prominent infectious organisms, and do not produce LPS, but they do produce other inflammatory products, which could remain associated with implants, and lead to loosening.[88] For example, endotoxin production by staphylococci, such as toxic shock syndrome toxin-1, induces

the production of cytokines IL-1β, IL-6, and TNFα which prevents osteoblastic growth and functions, and causes tissue damage.[75] These combined effects cause a greater inflammatory response to the implanted medical device.[75] Significantly, biofilms protect bacteria from immune responses and clearance by the body, because the biofilm matrix can lower diffusion of immune proteins or limit access of immune cells, thus the bacteria themselves could lead to further inflammatory cascades in the case of septic, and possibly even aseptic (if undetectable) implant failures.[88-90]

1.1.10 Protein mediated bacteria and cellular functions

Increased select protein adsorption on surfaces has been correlated to the improved functions of osteoblasts.[91-94] Previous studies have also shown that by varying the surface roughness of a biomaterial, bacteria adhesion decreases.[5,7,95] With selectively improved bone cell responses, as already demonstrated, and decreased bacteria adhesion, integration between bone and the implant surface would be promoted, thus, improving the success rate of orthopedic prosthetics, through better bone integration, and decreased inflammation, as has been observed *in vivo* through animal trials conducted to date.[96-98]

Compared to conventional surfaces, nanostructured materials have excellent biocompatibility properties due to enhanced protein interaction (including adsorption and conformation) resulting in improved cellular adhesion and tissue growth.[91-94,96-98] It has been demonstrated previously there is a linear relationship between nano-roughness, surface energy, and protein adsorption.[5] More specifically, a surface that has more nanorough features possesses increased surface energy which leads to greater protein adsorption.[91-94] Furthermore, research has also shown that increased protein adsorption,

such as fibronectin, results in decreased bacteria attachment.[99,100] Among these studies are others that determined it is possible to improve stem cell differentiation,[101,102] increase bone growth,[91-94,96-98,103,104] improve bladder stent urothelialization,[105] decrease inflammation,[98,106] and increase vascular stent endothelialization[107] by increasing the nanoroughness of an implant material.

Such studies are promising, and further research needs to go into understanding how these factors can be used to better improve implant materials, along with evaluation of long term *in vivo* performance. Yet, to treat biofilm infections under the condition that bacteria do adhere (even under the case of decreased bacteria on nanofeatured implant materials), agents must be developed to specifically target the biofilm. Some studies have suggested that nanofeatured surface may buy more time for antibiotics to go into effect after bacterial exposure.[107,108] Yet, it has also been observed that agents that kill bacteria, such as antibiotics, could lead to further bacterial adhesion as mediated by released protein factors.[29,109] For example, dead or dying *P. aeruginosa* can release intracellular lectins to promote the adhesion of living bacteria.[109] In a similar manner, *S. aureus* can release an intercellular protein upon death to enhance the adhesion to other microorganisms.[29] Clearly, the release of such compounds from adherent dead bacteria may promote subsequent live bacterial adhesion at the site of implantation. Therefore, compounds or other agents must still be developed which can decrease bacterial functions after adhesion to the implant surface, such as through the disruption of biofilm.

1.2 Current strategies to control device related infection

1.2.1 Ion implantation in antibacterial biomaterials

Techniques have been developed to improve the antibacterial properties of existing metals, ceramics, and polymers used in implant devices. Ion impregnation is one such technique, which uses a high energy ion beam to bombard the surface with antibacterial ions, resulting in an ion impregnation, and an observed improvement in antibacterial properties.[110-112] Both successes and issues with this technique will be explained below.

In a study by Wan et al., silver and copper ions were implanted into various medical grade metals, namely 317L stainless steel, titanium, and Ti-Al-Nb by a metal vapor vacuum arc (MEVVA) ion source, and antibacterial properties were determined under different ion beam implantation doses (a range between $0\text{-}2*10^{17}$ ions/cm^2 were tested). Wan and colleagues determined that both silver and copper were antibacterial against *Staphyloccocus aureus* after ion implantation, inhibiting 99.7-100% of colonies at the highest implantation dose, yet toxicity studies on mammalian cells were not conducted.[112]

Yoshinari and colleagues used a similar method of ion beam impregnation towards improved antibacterial activity in dental implant applications.[110,111] The later of these studies found that fluorine ion-implanted Ti surfaces contained fewer viable colony forming units (*Porphyromonas gingivalis* and *Actinobacillus actinomycetemcomitans*), suggesting antibacterial properties of fluorine, while other ions such as zinc, silver, calcium, platinum, tin, and nitrogen had no effect.[110] This study demonstrated that fluorine ions were not released, suggesting that the formation of metal fluoride bonds were sufficient for producing antibacterial effects; the lack of such bonds for other ions to

titanium may explain why antibacterial properties where not found in this study (the different bond structures were confirmed by X-ray diffraction and X-ray photoelectron spectroscopy in this study)[110] in addition to a lower ion dose of $5*10^{16}$ ions/cm^2 compared to the study by Wan.[112] Toxicity studies were also performed for the fluorine ion impregnated titanium, and no difference in L929 fibroblasts were found at 3 or 10 days of culture.[110]

Although the antibacterial properties of ion impregnated materials are promising, as found in studies by Wan, Yoshinari, and others,[110-112] these processes could result in more complications. Some studies suggest that ion impregnation could even increase the chances of infection.[5,113-116] For example, increasing the concentration of surface ions on glass or metal oxide surfaces has been shown by Li and collegues to increase the binding of bacteria to the surface for both gram positive (*Bacillus subtilis*) and gram negative (two *Pseudomonas aeruginosa* strains, three *Escherichia coli* strains, and two *Burkholderia cepacia* strains).[113] This observation was not affected by the surface charge or hydrophobicity/hydrophilicity of the bacteria surface.[113] Other studies have shown that surface impregnated fluorine increases bacterial adhesion of *Streptococcus mutans*, *Staphylococcus epidermidis*, *Staphylococcus aureus*, and *Pseudomonas aeruginosa* on ceramics, metals, and polymers;[5,114-116] some of this discrepancy could be that antibacterial properties result in bacterial death, and after fluorine kills bacteria, released factors such as lectins or other proteins to promote the adhesion of living bacteria.[29,109] Additionally, ion impregnation may also result in some toxicity to certain cells of the body, for example free silver ions can results serious cytotoxic activity against various host cells including keratinocytes and fibroblasts important in the wound healing

process,[30,31] while copper may be even more toxic, for example causing substantial DNA damage and oxidative lesions in lung cells.[117]

1.2.2 Microtechnology: release platforms, coatings, and microspheres

Control of medical materials and drugs on the scale of one millionth of a meter (10^{-6} m = 1 μm) offers the advance of microtechnology, and is the common standard used in medicine today for both drug delivery and medical device technology.[118] Although microtechnology offers benefits over less controlled technological processes (which do not control microstructure,) there are significant advances beyond microtechnology through smaller fabrication techniques, such as nanotechnology, that have been made to date, and could further benefit anti-infection medicine.

Briefly on the advances here, microparticles are the standard used in drug delivery, with the size range of 1 μm to 1000 μm (1 mm), offering improvements over free drugs by enhanced delivery across a number of natural and artificial membranes.[118] Specifically, microparticles below the size of 4-5 micrometers can pass through blood capillaries, and can enter the lymphatic portals of the gut, and uptake is increased in relation to smaller particle size (while larger size microparticles will be trapped); these are important properties for the systemic use of these particles in treatment of infections (through either injection or peroral ingestion).[118]

Microparticles can also be incorporated into medical devices, such as with multi-layered fabrication procedures, allowing controlled release rates.[119,120] In one study, a hyaluronan microparticles fabricated with a combined freeze-drying/air drying method were loaded with silver sulfadiazine, and then incorporated into collagen membranes by cross-linking

with ultraviolet light.[119] In this study by Lee and colleagues, release was controlled for up to six days, and *Pseudomonas aeruginosa* growth was inhibited for up to four days as determined using a Bauer-Kirby disk diffusion method.[119] Also important, the microparticles loaded with silver sulfadiazine exhibited decreased toxicity when compared to free silver sulfadiazine alone during fibroblast L929 exposures of 2 days, and also showed promise in a guinea pig animal model of wound repair when applied as a dressing for 14 days, although the epidermidis was not completely restored.[119]

Microparticles can also be loaded with antibiotics to control release, allowing better localization at the site of infection.[28,121] In a study by Schlapp and colleagues, microparticles were prepared using polylactic-co-glycolic acid (PLGA) 50:50 copolymer ratio in a water/oil/water microemulsion technique, yielding 370 +/- 130 μm particles, with a load of up to 15 +/- 3% gentamicin (an aminoglycoside antibiotic that inhibits protein synthesis), and 50% encapsulation efficiency.[28] These microparticles were loaded into an insoluble fibrous bovine tendon collagen, and prepared as a sponge for a tissue engineering construct using a lypholization freeze drying technique.[28] Using this combination, release could be sustained for up to 7 days, or an additional dose of 2 mg gentamicin per 2.8 mg collagen was also added in some cases, resulting in a burst release upon implantation.[28] One limitation of this study is that the authors did not characterize the impact of these release profiles on bacteria, instead only assuming that the antibiotic would be useful and effective. Smaller PLGA microparticles were prepared in a study by Yenice et al. and loaded with teicoplanin (glycopeptides antibiotic with similar activity to vancomycin).[121] The microparticles for this study were prepared using an emulsion/solvent evaporation process from PLGA at a copolymer ratio of 75:25, for a

particle size of 29 +/- 4.57, with a theoretical drug load of 10% weight drug per weight of polymer (w/w), and a low encapsulation efficiency of 1.73%.[121] Using these ratios, the authors of this study were able to achieve 5 weeks of release, although 40% of drug was released immediately, 65% of drug was released after the first week, and after two weeks 80% was released.[121] Finally, an animal study was conducted on locally raised White New Zealand Rabbits according to the Hacettepe University Local Animal Ethics Committee in Anarkara, Turkey. PLGA microparticles detectably released teicoplanin into the synovial fluid of the joints for 10 days, with antimicrobial activity sustained, as determined by agar gel tests with *Staphylococcus aureus*; yet, in all groups at two weeks, excessive infections prevented further readings, and, furthermore, 86% of the animals had wound infection complications. This study provides evidence that although the microparticles were well designed to release antibiotic for up to 5 weeks, complications from unexpected antibiotic tolerances, such as via biofilm formation, may have arose *in vivo*, allowing the infections to subsist. Instead, more recent advances suggest that nanotechnology may alleviate some of these problems faced by those authors working with microtechnology, and nanomaterials are now showing promise to decrease medical device related infections.

1.3 Nanotechnology for infection control

1.3.1 The potential of nanomaterials and nanoparticles

Nanomaterials have a variety of applications in biomedicine, such as incorporation into medical devices and drugs. Recent applications of these materials look to improved antimicrobial properties. Zinc oxide (ZnO) nanoparticles are shown in **Figure 1.8.A** as viewed through a scanning electron micrograph (scale bar: 20 μm).[122] High surface area, as shown in this image, is an important property of nanomaterials, because small particle size (12 +/- 2 nm) and high surface area (90 m^2/g) were determined to be important factors in increasing antibacterial activity of ZnO nanoparticles in this study, among others.[7,122-129] Carbon nanotubes (as shown in **Figure 1.8.B**)[130] are growing in importance for biomedical applications such as conductive biomaterials, in situ sensors, drug delivery vehicles, or tissue engineering scaffolds.[92,130-143] Recent studies are also showing that carbon nanotubes can increase the antimicrobial properties of such technologies, and therefore could be used for this purpose.[130,134-137,142] Titanium is a material widely used in medical device technologies, especially in orthopedic implants and vascular stents.[5,21,94-98,101,102,104-108,144-148] TiO_2 nanotubes (shown in **Figure 1.8.C**)[5] can be easily fabricated in arrays on the surface of titanium, and are being explored for implant applications, offering possible control of stem cell differentiation,[101,102] increased bone growth,[91-94,96-98,103,104] improved bladder stent urothelialization,[105] decreased inflammation,[98,106] increased vascular stent endothelialization,[107] and decreased bacterial attachment[95,108] by increasing the nanoroughness of an implant material, in addition to the potential for loading of antibiotics and other drugs to control release.[149,150] Finally, polyurethane or

other materials can be loaded with silver nanoparticles to improve the antimicrobial response, and slow the release rate of silver ions compared to other loading techniques.[151-154] One key factor for the effectiveness of silver biomaterials a good dispersion of the nanoparticles throughout the biomaterial (as is shown in **Figure 1.8.D** at 30 ppm silver.)[151]

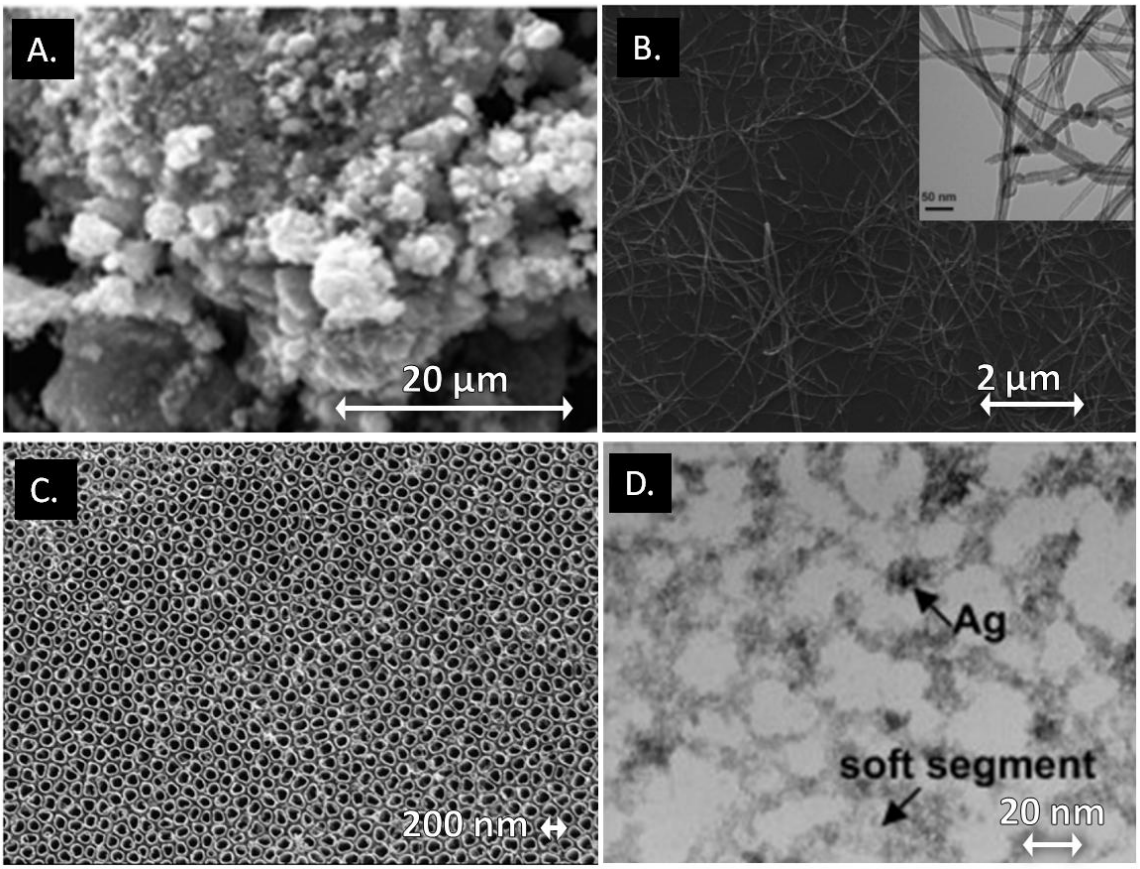

Figure 1.8 The use of nanomaterials is a growing new approach to the design of medical devices that have improved resistance to biofilm-mediated, drug-resistant, and device centered infections.[7,95,108,122-130,134-137,142,151-154] For these anti-infection applications, various nanomaterials are being developed, such as nanoparticles and nanotubes, for direct use as biomedical devices; such nanomaterials can be used alone, incorporated onto surfaces, into composites, or as components in sensors such as zinc oxide (ZnO) nanoparticles, carbon nanotubes, titanium dioxide nanotube arrays, and silver nanoparticle-polymer composites, respectively in A.-D. (A.,[122] B.,[130] C.,[5] and D.,[151] are from citations listed**)**. These examples, and others, will be further reviewed here briefly to understand their antibacterial activity and potential applications.

1.3.3 Antibacterial mechanism of action for nanoparticles

Metal nanoparticles are growing in applications, especially for antibacterial uses. In particular, metal ions are good candidates antibacterial chemicals which can also elicit anti-biofilm activity depending on the type of ion selected,[155] and benefit in terms of increased antibacterial activity through incorporation into nanoparticles.[4,129,156,157] Below, the differences between metal ions, and nanoparticles will be explained for several examples of silver nanoparticles, zinc oxide nanoparticles, and zero valence iron. Because some of the mechanism of carbon nanotube antibacterial activity is similar, and also enlightening, these materials will also be included in this discussion.[130,134-137,142]

1.3.3.1 Zinc oxide nanoparticles antimicrobial mechanism of action

Nanoparticles fabricated from zinc oxide (ZnO) are under investigation for their inherent antimicrobial properties, which are enhanced, or may only exist, when the materials are in the nanometer size and in relation to surface area. Greater ZnO antibacterial activity has been observed as particle size decreases into the nanometer level in relation to surface area.[122] Using nitrogen gas (N2) isotherms and the Brunauer–Emmett–Teller equation in the relative pressure range (*P*/*P*o) of 0.05–0.30, researchers have found a direct correlation between surface area, particle size (calculated from surface area), and antibacterial activity of ZnO, with activity ranging from ~5%–90% decreased bacteria viability among surface areas of 90.4–3.49 m^2/g (corresponding to calculated ZnO particle sizes from 12 to 307 nm).[122] Furthermore, the authors found that the 4–7 mM ZnO colloidal suspension with the highest surface area (90.4 m^2/g) inhibited 95% of MRSA, *Enterococcus faecalis*, a high-biofilm-producing strain *Staphylococcus*

epidermidis, and various other clinically relevant pathogen growths.[122] Despite such positive results, the ZnO suspension was least effective against *Salmonella typhimurium*, inhibiting only 50% of growth;[122] because this is still a relevant pathogen (there was, for example, a peanut butter-related outbreak in 2009[158]), further studies should focus on the mechanism of ZnO nanoparticle resistance in this pathogen.

These studies and others determined that ZnO nanoparticles antibacterial activity could be mediated by increasing reactive oxygen species (ROS) production,[124,126] due to metal ion release (which is related to surface area,) or through their interaction with ultraviolet (UV) light (which also depends on particle size).[124] Such events would also be accelerated through the increased surface area of nanometer compared with micron particles, especially when such nanoparticles penetrate the bacteria.

A very detailed analysis of ZnO nanoparticle ROS generation was carried out recently by Lipovsky et al.[125] In this study, it was found that, when using electron paramagnetic resonance coupled with the spin-trapping technique, the formation of hydroxyl radicals and singlet oxygen in water suspensions of ZnO nanoparticles resulted, but the possibility of superoxide anion production was ruled out.[125] Moreover, the level of oxy radicals increased considerably when the suspension was irradiated with visible light at the range 400–500 nm, demonstrating the ability of nondestructive visible light (as opposed to UV light) to stimulate ROS production in ZnO.[125] One limitation of this study was that the possibility of H_2O_2 production by ZnO was not discounted, as has been previously observed in suspensions of ZnO as a primary mediator of antibacterial activity.[126-128]

Other metal oxide nanoparticles also act in a similar way to ZnO. Similar to ZnO, for example, size-dependent antibacterial properties of magnesium oxide nanoparticles have

been observed against *Escherichia coli* and *S. aureus*, where it was shown that for 23, 18, 15, 11, and 8 nm particles, the smallest 8 nm particles decreased bacteria growth the most.[157]

There are limitations of ZnO based technologies for anti-infection applications. ZnO is known to be very stable, and thus it biodegrades very slowly. The impact of this is that the ZnO nanoparticles can accumulate inside the cell, and then release free radicals, cause oxidant injury, excite inflammation, and finally cause cell death as was shown *in vitro* with RAW 264.7 (mouse leukaemic monocyte macrophage cell line) and BEAS-2B (human bronchial epithelial cell line).[159] Moreover, these materials can accumulate in tissues of the body causing a toxic effect, for example showing pathological damage in the stomach, liver, heart, and spleen of healthy adult CD-ICR (institute for cancer research) mice administered with 120 nm ZnO, or in the liver, spleen, and pancrease with 20 nm ZnO in one study (this study also demonstrates how particle size varies tissue distribution and toxic impact).[160] From a more practical standpoint, ZnO is also more difficult to fabricate than other nanomaterials, and is frequently obtained from bulk materials through grinding.[129] The disadvantage of grinding procedures are that the polydispersity of the ZnO is large, and thus a lot of studies use low quality (polydisperse) ZnO dispersions, which are not ideal for biomedical applications.[129]

1.3.3.2 Titanium Dioxide nanoparticles and UV light

Self-cleaning surfaces based on nanomaterials are already making a significant impact as antimicrobial paints for buildings and hospitals.[161] One of the most popular self-cleaning coatings is based on UV light–activated photocatalytic TiO_2 thin-films.[162] Yet, it is only

recently, through the application of nanotechnology and enhanced optical properties, that the production of antimicrobial coatings activated in visible light (such as by fluorescent light bulbs) has become possible. In a study by Caballero et al, it was found that by including TiO_2 nanoparticles in a paint formulation, bacteria were inactivated in the presence of fluorescent lighting alone.[161]

The mechanism of TiO_2 antimicrobial activity is different from ZnO in that it is only active in the presence of light. The antimicrobial properties of which have been understood for over a decade, because the materials were first used in thin-film technologies as described above.[162] When in the presence of both oxygen and light, the primary ROS with antimicrobial activity generated by TiO_2 nanoparticles are hydroxyl radicals, superoxide, and hydrogen peroxide.[162] Initially, the reactions of a photogenerated hole-electron (h^+ and e^-) pair[163] are shown in equations **(1.1)** and **(1.2)** below respectively:

$$H_2O + h^+ \rightarrow OH^\bullet + H^+ \qquad \textbf{(1.1)}$$

$$O_2 + e^- \rightarrow O_2^- \qquad \textbf{(1.2)}$$

These free radicals can then further react to product hydrogen peroxide as shown below in equations **(1.3-1.4)** for the generated superoxide radical (O_2^-) or through combination of the hydroxyl radicals produced by hole generation **(1.5)**:

Generation of hydrogen peroxide from superoxide:

$O_2^{-} + H^+ \rightarrow HO_2^{\bullet}$ **(1.3)**

$HO_2^{\bullet} + e^{-} H^+ \rightarrow H_2O_2$ **(1.4)**

Generation of hydrogen peroxide from hydroxyl radicals:

$OH^{\bullet} + OH^{\bullet} \rightarrow H_2O_2$ **(1.5)**

The primary effects occurring through generation of these radicals are inactivation of bacteria through oxidation of the bacterial membrane, and eventual destruction of the bacterial cell.[162] The two main effectors are hydroxyl radical, and hydrogen peroxide. Moreover, hydroxyl radicals are short lived, and therefore most reactions either occur at the TiO2 surface, or are through hydrogen peroxide generation.[162]

Although popular in paints and coatings as mentioned above,[161] there are limitations to TiO_2 based technologies for anti-infection applications. Specifically, it is difficult to activate the nanoparticles with UV light, turning on the antibacterial activity, for example one study determined a required exposure time of 60-90 minutes direct UVA exposure for complete inactivation of *Staphylococcus aureus*, and even the authors of this study admitted that this time is still too long, and must be shortened before clinical use in implants.[164] Additionally, TiO_2 has a low biodegradability, and thus the nanoparticles may accumulate in the body and result in toxicity.[165]

1.3.3.3 Silver nanoparticles mechanism of action

The use of colloidal silver for minimizing infection has been investigated for over 50 years, but with recent advances in chemical, biological, and material characterization techniques, silver is being more widely adopted in the medical community.[156] By binding with DNA, with enzymes that control respiration and other critical cell functions, or with chemical functionality or receptors on the cell membrane, nanoparticles of silver is attractive due to activity against many otherwise intractable infectious organisms (such as MRSA and other antibiotic-resistant microorganisms).[166] Importantly, silver nanoparticles releases ions more slowly compared to free silver, thus controlling release, a major advantage for biomedical applications.[167]

Along these lines, the mechanism of action for nanosilver is most well understood in terms of released silver ions.[167] Because silver ions are highly reactive with various biological molecules and chemical entities, thus rendering the ion almost useless alone, the ability to control release from nanosilver has enabled the numerous applications now being explored in antimicrobial biomedicine.[167] Specifically, of these mechanisms, binding of silver ions to thiols groups in L-cysteine residues of proteins is the most widely known bactericidal mechanism, because this binding event inactivates enzymatic function.[168,169] More recently, the production of ROS by silver ions and nanoparticles in the presence of bacteria has been considered as an important mechanism in killing bacteria.[170,171] In a study by Park and colleagues, superoxide was generated in the presence of oxygen, either via blocking of free radical scavenging enzymes (such as superoxide dismutases) or impairing the respiratory chain.[170] Furthermore, the authors demonstrated that this mechanism accounted for about half of the antimicrobial activity

of silver ions, as determined by aerobic growth of bacteria in the presence of silver ions (which eliminated ROS production).[170] This mechanism of free radical generation is unique, because the biological entity is required for free radical generation.[170] Once again, it should be emphasized that this mechanism is in relation to silver ions, and is not unique to silver nanoparticles alone.[170,171]

Although release of ions is the main mode of antibacterial activity for silver nanoparticles, there are additional benefits of nanoparticles compared to free ions.[171] A study by Hwang et al. has shown that silver nanoparticles disrupt the ion efflux system, and therefore bacteria cannot effectively extrude silver ions, and as a result silver nanoparticles cause more damage than do silver ions.[171] Furthermore, this phenomenon is linked with the size of the particles, because larger micro-meter sized silver particles did not cause any detectable membrane damage.[171]

Silver nanoparticles are a very useful antimicrobial tool, and yet there are some disadvantages **(Figure 1.9)**. For drug delivery applications, the surface of silver nanoparticles must be coated, and such coatings can inhibit the release of silver ions from the surface;[167] therefore, a limitation is that these coatings must be developed and proven effective for treating infections. Also, even if silver was delivered to the site of infection, biofilm can resist silver ions in a time dependent manner according to the "restricted penetration" hypothesis.[155,172,173] According to this hypothesis, exopolymeric substances (EPS) that encapsulates the biofilm can restrict the diffusion of silver ions, providing protection for the biofilm cells.[172] The negatively charged EPS is effective in protecting cells by reducing the permeation of positively charged molecules.[172] In the case of metals, the penetration through the EPS can be reduced; and, the time to penetrate the

matrix is likely dependent on the reactivity of the metal.[172] Under the restricted penetration hypothesis, slow release of silver into the biofilm is a disadvantage for the silver nanoparticles, because the biofilm would lower it's susceptibility in a time dependent manner. Clinically, biofilm and bacterial resistance to silver has also been observed, and furthermore, such bacterial resistance to silver is growing because of the numerous applications of silver in medicine and industrial technologies.[174] In addition to these disadvantages of nanoparticles for drug delivery, silver ions can cause serious cytotoxic activity against various host cells, for example impairing the wound healing process, as ROS generation, and enzyme inactivation are non-specific mechanism.[30,31,170,171] Therefore, there is still need for novel nanoparticles that penetrate the biofilm, possibly through physical means; quickly release silver, ROS, or other metals into the biofilm; and moreover, release some other agent that inhibits biofilm function.

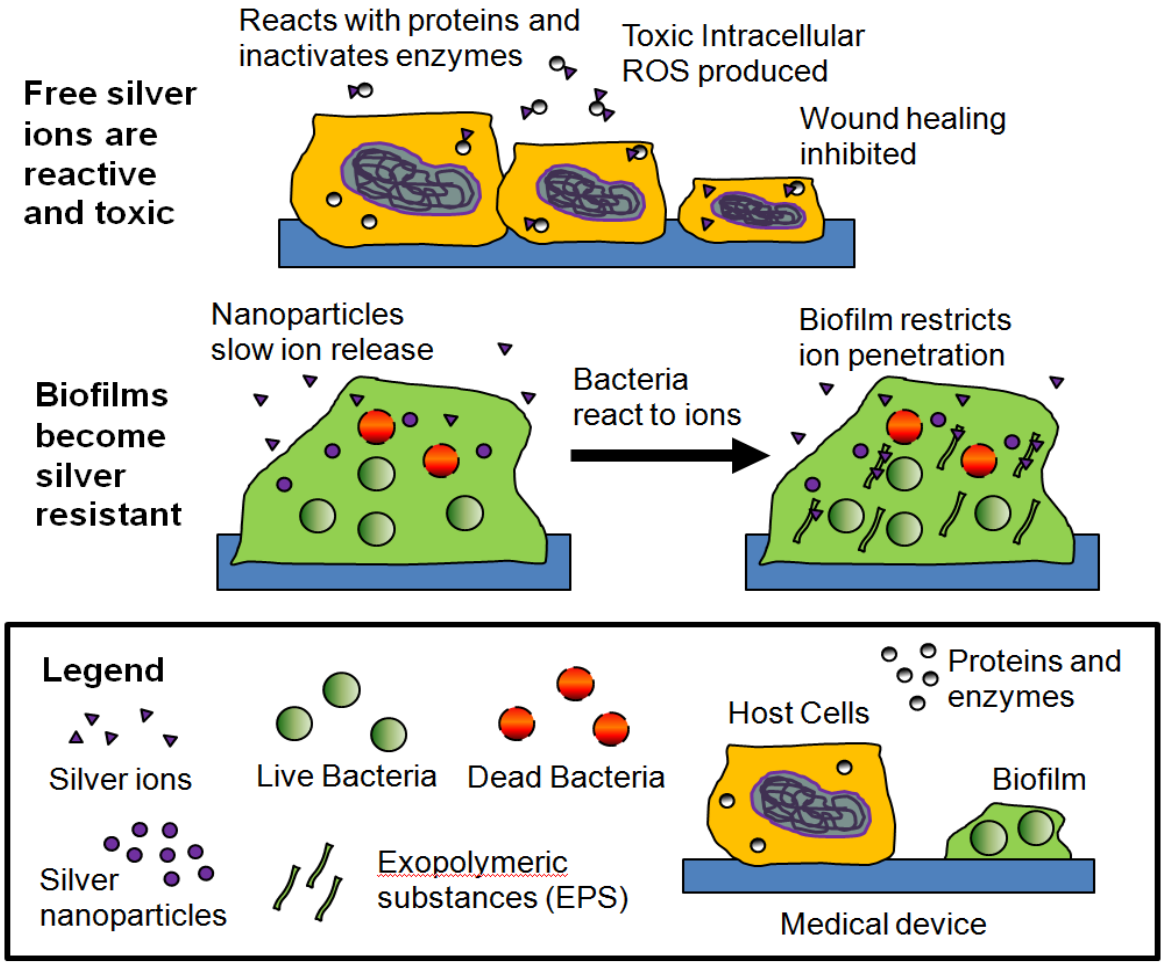

Figure 1.9 Silver is an effective biocide, and yet there are disadvantages to its use in drug delivery as a free ion or nanoparticle. Silver ions alone are reactive with proteins, inactivate enzymes, and produce intracellular ROS, thus producing cytotoxic effects that inhibit wound healing.[30,31,170,171] Silver nanoparticles slow the release of silver ions, and therefore are more likely to reach the site of infection. Yet, coatings are required to prevent aggregation, and further slow silver ion release,[167] and furthermore, under the restricted penetration hypothesis, slowed release gives the opportunity for bacteria to react by producing extrapolymeric substrances (EPS) in the biofilm, thus decreasing silver ion penetration, and improving bacterial resistance to silver.[155,172,173] Bacteria can also resist silver through other means, and thus complete eradication would be more desirable, or other methods must be developed to inhibit biofilm formation, such that antimicrobial are effective. [174]

1.3.3.4 Nanoscale zero-valent iron synergistic mechanism of action

The duel effect of both generating ROS and releasing metals can also act synergistically to create antimicrobial products. For example, iron ions generate oxygen free radicals by converting hydrogen peroxide (H_2O_2) to the more reactive hydroxyl radical via the Fenton reaction.[175] Hydroxyl radicals generated by these iron ions can depolymerize polysaccharides, cause DNA strands to break, inactivate enzymes, and initiate lipid peroxidation.[176] One nanomaterial capable of amplifying this effect is nanoscale zero-valent iron (or nZVI; this nanoparticles is made of Fe^0),[177-179] which, according to **equations 1.6-1.8**, is known to oxidize in the presence of oxygen **(1.6)**, generating hydrogen peroxide and free iron **(1.7)**, and finally ending with hydroxyl radical production via the Fenton reaction **(1.8)** as shown below, and previously in citation:[179]

$$Fe^0 + O_2 + 2H^+ \rightarrow Fe^{2+} + H_2O_2 \qquad \textbf{(1.6)}$$

$$Fe^0 + H_2O_2 \rightarrow Fe^{2+} + 2OH^- \qquad \textbf{(1.7)}$$

$$Fe^{2+} + H_2O_2 \rightarrow Fe^{3+} + OH^{\bullet} + OH^- \qquad \textbf{(1.8)}$$

After exposure to the hydroxyl radicals as produced by free iron release from nZVI, and via the fenton reaction, bacterial death occurs.[177,179] More specifically, the hydroxyl radical causes lysis through oxidation of the bacterial membrane.[179] Although effective, these nZVI based nanomaterials also are very sensitive to oxygen exposure, and quickly oxidize, releasing free radicals.[177-179] The primary limitation of the material is the ability to achieve site-specific delivery, while simultaneously slowing the oxidation reaction (through limits on oxygen exposure) for a long enough time period, allowing the

nanomaterial to be delivered to the site of infection. Otherwise, the nZVI would show non-specific toxicity to numerous other cells of the body, as has been shown previously for microglia and neurons.[178]

1.3.3.5 Selenium nanoparticles mechanism of action

Selenium nanoparticles are being developed for various biological and medical applications, including as a dietary supplement, because it is a micronutrient required in at least 25 human selenoproteins and enzymes.[180] Importantly, nano-selenium (also called red nano-selenium) has lower toxicity than free selenium compounds, and has good bioavailability, whereas bulk selenium (selenium black) is relatively inert.[180] More recent developments using selenium nanomaterial are as coatings for implants, or as free nanoparticles, in order to inhibit bacterial growth and cancer (selenium is also known to have anti-cancer properties).[181,182]

For antibacterial applications, it is hypothesized that selenium nanoparticles work by depletion of intracellular low molecular weight (LMW) thiols. In doctoral work by Phong Tran, it was shown that the after soaking polymers coated with nano-selenium in fresh bacterial media (tryptic soy broth), the media contained selenium (as determined by inductively coupled plasma atomic emission spectroscopy; or ICP-AES), and moreover this supernatant was sufficient to deplete intracellular LMW thiols in *Staphylococcus aureus*, as detected by monochlorobimane.[183] This same study was repeated with selenium nanoparticles in the media, and a even greater depletion was detected (95% with collected supernatant vs. 90% depletion with nanoparticles).[183] Furthermore, it was shown that the selenium nanoparticles do not produce superoxide, a common free radical,

although the production of other ROS species was not ruled out.[183] One limitation of this study was that selenium's effectiveness as an antimicrobial agent for implant coatings or drug delivery applications still requires improvement (for example 10% intracellular LMW thiol reduction in bacteria might not be enough, and studies have only shown up to a 1 log reduction in bacteria growth *in vitro*).[182,183]

The probe used for detection of LMW thiols in this dissertation work was monochlorobimane;[183] importantly, unlike other bimanes such as monobromobimane, monochlorobimane forms fluorescent adducts exclusively with glutathione, and not with other LMW thiols in human or animal tissues and cells.[184] Therefore, the suspected LMW thiol could be glutathione, because it is a ubiquitous LMW thiol;[183] but, importantly, glutathione is conspicuously absent from most Gram-positive bacteria, including *Staphylococcus aureus*.[185,186] Other candidates are therefore necessary, which could be detected by monochlorobimane as was observed previously.[183] In particular, bacillithiol is a LMW thiol present in many bacteria species in the Bacilli class of bacteria (the Bacilli class defines many bacteria including the Staphylococcus genus of bacteria, including *Staphylococcus aureus*, and the Bacillus genus, including the common bacteria *Bacillus subtilis*), and does form adducts with monochlorobimane.[186,187] Therefore, this must be the molecule which was detected in previous studies with selenium, because of the absence of glutathione and the specificity of monochlorobimane to either glutathione or bacillithiol. Moreover, bacillithiol is a LMW thiol, and may be adept at chelating metal ions, an important buffering property which could protect intracellular cytosolic chemistry from irreversible protein damage via oxidation of cysteines.[186,188] Therefore, in this mechanism, elemental selenium could either catalyze the oxidation of bacillithiol, or

alternatively release selenium ions, resulting in bacillithiol depletion that leads to irreversible protein damage and cell death.[183]

In addition to pure selenium nanoparticles, selenium is also a common component of quantum dots such as CdSe, a type of fluorescent nanoparticle.[189] Quantum dots generate ROS in the presence of light, including superoxide and subsequently hydroxyl radicals, and these ROS compounds exhibit antimicrobial properties.[189] In addition to ROS production in light, the quantum dots also corrode in light (the process of photobleaching for quantum dots), and thus release metals, such as both cadmium and selenium (in CdSe nanoparticles), both of which have antimicrobial properties (in addition that cadmium is very toxic and carcinogenic).[189]

1.3.3.6 Carbon nanotubes mechanism of action

Medical devices are being designed through the incorporation of carbon nanotubes into sensors[141,143] to serve as feedback loops to detect bacteria and release antibiotics only when needed (as has been previously shown with carbon nanotube–coated titanium, which was used, after sensing an infection, to break down a thin film of polypyrrole containing antibiotics[131]). Moreover, researchers also benefit from the antimicrobial properties of these nanomaterials when incorporated into biomedical devices. For example, the antimicrobial properties of carbon nanotubes have been documented, with a dependence on carbon nanotube diameter. In a series of studies, it was found that multiwalled carbon nanotubes (MWNTs) and single-walled carbon nanotubes (SWNTs), created as mat-like surfaces, inactivated free bacteria when mixed with cultures or adherent bacteria **(Figures 1.10.A and 1.10.C)**.[130,134-137,142] Furthermore, SWNTs

exhibited a greater inactivation percentage, as demonstrated by decreased viability and metabolic activity, under both conditions.[130,135] To explain this observation, gene expression of *E. coli* during exposure to the nanotubes was studied; it was found that stress-related gene products were especially high in the presence of SWNTs, leading to the conclusion that the diameter of nanotubes determined the amount of stress and damage caused to the bacteria (MWNTs have larger diameters than SWNTs; see **Figures 1.10.B and 1.10.D** for a comparison of *E. coli* morphology on the two surfaces).[135]

Large limitations of carbon nanomaterials are that although they do improve antimicrobial properties, they have apparent toxicity, causing fibrotic reactions, causing cell death, and causing inflammation such as has been observed in the lungs in a similar manner to asbestos (depending on the aggregation state, methods used in fabrication of the nanotubes, nanotube length, and purity, these properties vary).[190-192] Therefore, the therapeutic window, which would decrease bacteria, and yet increase tissue growth, has not been proven, and is also hindered because the antimicrobial properties aren't as high as other nanomaterials.[117]

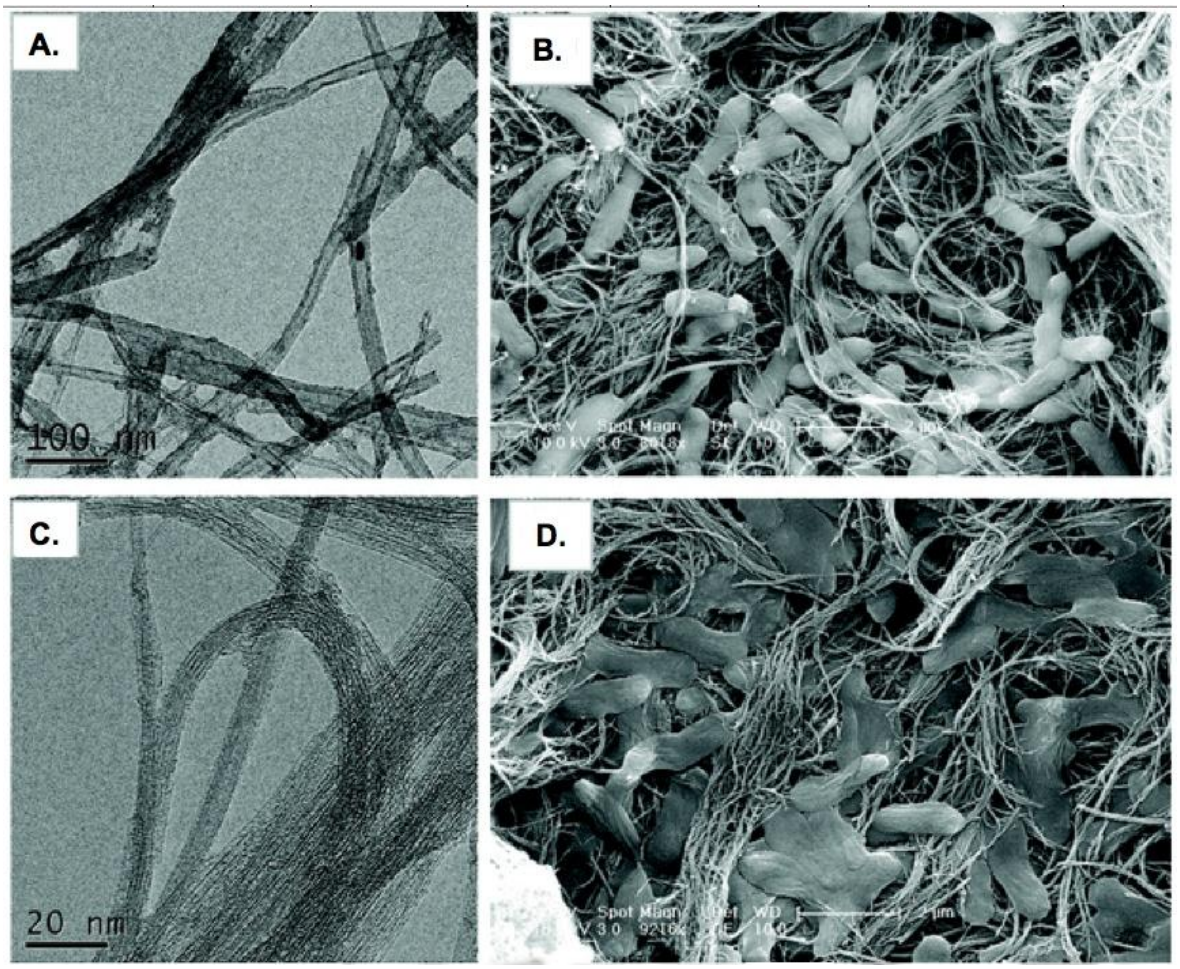

Figure 1.10 The diameter of the carbon nanotubes determined by transmission electron microscopy (**A** and **C**) predicts antimicrobial behavior as visible in scanning electron micrographs (**B** and **D**).53 A mat-like surface made of multiwalled carbon nanotubes (**A**) inactivates a small percentage of *Escherichia coli*, visible as abnormal and flattened bacteria on the surface (**B**). Single-walled carbon nanotubes (**C**), having a smaller diameter, inactivate a greater percentage of bacteria, causing significant structural disruption and bacterial death (**D**).

1.3.3.7 Comparison of mechanisms of action between nanomaterials

There are many nanomaterials, with a variation in mechanisms of action that can kill bacteria such as nanoparticles of zinc oxide, titanium dioxide, silver, zero valent iron, selenium, selenium based quantum dots, and carbon nanotubes. Some of these are more useful, because the same toxicity mechanisms don't kill host cells. Yet, many of the nanomaterials outlined thus far have limitations for use in antimicrobial technologies that will be used to treat medical device related infections or to coat the devices to inhibit infection. These mechanisms of action are outlined in **Table 1.4**, along with the disadvantages that the use of each nanomaterial brings**.**

Table 1.4 A list of nanomaterials is here including antimicrobial action and disadvantages.

Nanomaterial (abbreviation)	**Primary antimicrobial mechanisms of action**	**Disadvantages to use in biomedicine**
Zinc oxide (nano-ZnO)	Particle size;[122] Zinc ion release;[124] ROS generation[125-128]	ROS toxicity; [159] may accumulate in tissues of the body; [160] difficult to fabricate[129]
Titanium dioxide (nano-TiO_2)	ROS generation in the presence of UV light[162]	Antimicrobial activity requires UV light;[162] may accumulate in tissues of the body[165]
Silver (nano-Ag)	Silver ion release leads to enzyme inactivation[168,169] and intracellular ROS production;[170,171] nanoparticle disruption of membrane and ion efflux[171]	High reactivity of silver ion results in toxicity and limited usefulness in drug delivery;[30,31,167,170,171] bacterial and biofilm resistance to silver ions[155,172-174]
Zero-valent iron (nZVI)	Iron ion release leads to ROS production in the presence of oxygen[177-179]	Extremely reactive, the nanomaterial is consumed within one hour;[177-179] ROS are toxic[178]
Selenium (nano-Se)	Intracellular bacillithiol depletion[183]	Effectiveness not optimized for antimicrobial use[182,183]
Quantum Dots (e.g. CdSe)	ROS production;[189] cadmium and selenium ion release[189]	Toxic and carcinogenic[189]
Carbon Nanotubes (CNT)	Penetration and activation of stress related genes[130,135]	Toxic, carcinogenic, and may accumulate in the lungs[190-192]

1.3.4 Surface active and multifunctional systemic nanoparticles

Modular nanopharmaceutical systems are being designed to address multifunctional capabilities for the ideal bacterial treatment, with the ability to mix and match appropriate functions such as targeting of bacteria with antibodies, crossing the blood brain barrier, and improving antibiotics. One way to achieve such multi-functionality would be to tailor nanoparticles for specific applications through surface conjugation. Surface conjugation is the final chemical modification of nanoparticles, providing the opportunity to deliver drugs to the site of infection to selectively interact with (and penetrate) the biofilm and bacteria targeted. Nanoparticle conjugation can also improve drug efficacy by increasing the number of active drug loading sites (through conjugation of multiple selected agents onto one nanoparticle).

1.3.4.1 Antibody targeting of nanoparticles

One method of targeting biofilms is through the incorporation of antibodies to a nanocarrier. Antibody targeting is highly specific and requires identification of an epitope (such as a molecule or protein) in the bacterial biofilm for nanoparticle delivery. In particular, Suci et al found that *Staphylococcus aureus* biofilm targeting could be achieved through the use of a viral nanoparticle, cowpea chlorotic mottle virus (CCMV), coated with antibodies to protein A (which is a *Staphylococcus aureus* surface protein and virulence factor).[193] It was found that CCMV bound to the surface of *Staphyloccus aureus* in biofilms (~30 μm thick), penetrated 17.6 (standard deviation 3.3) μm during an 80-minute exposure.[193] The cage-like protein structure of CCMV could simultaneously be loaded with the magnetic resonance imaging (MRI) contrast agent gadolinium (Gd)

achieving a concentration of 1.8×10^5 Gd atoms per cell, as determined by inductively coupled plasma atomic emission spectroscopy.[193] This technology was shown to be very useful for biofilm imaging applications, but activity against the biofilm, towards prevention or reduction of infection, was not proven by this study.[193]

1.3.4.2 Nanoparticles could improve the activity of antibiotics

Overcoming antibiotic resistance of one strategy for the use of nanoparticles in anti-infection medicine, and has been achieved through the combination of nanoparticles with antibiotics.[194-197] It has been shown that antibiotic resistance can be overcome in vancomycin-resistant bacteria using gold nanoparticles coated with vancomycin (ie, gold functionalized with vancomycin [Au@Van]).[194,195] Vancomycin is an inhibitor of cell-wall synthesis, normally binding to D-alanine repeat units (D-ala-D-ala) on the bacterial cell surface, but in vancomycin-resistant bacteria, such as VRE, modifications of terminal cell-surface peptides (such as to D-lactate) lower antibiotic activity. In a study by Gu et al, Au@Van with activity against VRE was prepared through the interaction of synthetic gold nanoparticles with bis(vancomycin) cystamide, through gold and sulfur interactions lowering the minimum inhibitory concentration (MIC) of resistant bacteria to between 2 and 4 μg/mL,[194] closer to a value in non-resistance bacteria (~1-8 μg/ml).[198] It was hypothesized that antibacterial activity increased as a consequence of close contact among vancomycin molecules (~31 per nanoparticle), changing the binding properties in a phenomenon called "polyvalent inhibition."[196] In a more recent study by Fayaz et al, a novel preparation of Au@Van effectively inhibited the growth of vancomycin-resistant *S. aureus* at an MIC of 8 μg/mL.[195] In this study, gold nanoparticles were synthesized

biologically using the fungus *Trichoderma viride* and vancomycin was bound to the surface by ionic interactions, allowing the positively charged amine groups of vancomycin to interact with the negatively charged gold nanosurface. It was hypothesized that the nanoparticles bound nonspecifically to cell-surface peptides involved in cell-wall synthesis, but no further evidence of this was provided. Interestingly, both studies with Au@Van found activity against *Escherichia coli* growth, which is normally not inhibited due to the inability of vancomycin to penetrate the gram-negative bacteria outer membrane.[194,195] Fayaz et al proposed that Au@Van penetrated the gram-negative bacteria membrane, as evidenced by pitting that was visible in the cell membrane under transmission electron microscopy.[195]

Nanoparticles are also being used as an injectable or topical to improve tissue responses and wound healing to antibiotics. In one set of *in vivo* studies, polyacrylate nanoparticle emulsions were used for topical wound healing or systemic applications.[197] This study found that the antibiotic-conjugated polyacrylate nanoparticles had activity against MRSA *in vitro* and no cytotoxicity against human dermal cells. The water-based emulsion is capable of solubilizing lipophilic antibiotics for systemic administration, and has shown to protect antibiotics from hydrolytic cleavage by penicillinases, thus improving the activity of penicillin against resistant bacteria. This study demonstrated the favorable activity in murine models of the drug for systemic application by intraperitoneal injection or topical application in a wound abrasion model. *In vivo*, both routes were favorable, showing no signs of inflammation, such as redness or abnormal cytokine release, and when topically applied, the emulsion enhanced wound healing by an average 3 to 5 days.

Such nanoparticles might afford promising opportunities for treating both skin and systemic infections.[194-197] The primary improvement the authors were able to demonstrate for these technologies are the potential to overcome very specific mechanisms of antibiotic resistance, and the other benefits of drug delivery afforded from nanoparticle delivery vehicles such as increased cellular or bacteria penetration; and yet, it is likely that bacteria will eventually evolve mechanisms to overcome these nanoparticle formulations, since they are basically just improvements to existing antibiotics.[194-197]

1.3.4.3 Nanoparticles for crossing the blood brain barrier

Targeting drugs across the blood–brain barrier (BBB) to fight neural tissue infection is another issue with traditional infection drug design that is currently being addressed by nanotechnology. When targeting brain infection, such as meningitis, nanoparticles may be able to cross the BBB and kill a broad spectrum of microorganisms. For example, one study by Liu et al found that self-assembled cationic peptide nanoparticles synthesized through the incorporation of a cationic peptide (composed of six arginine residues), a TAT peptide sequence (recognized by the BBB for cell-membrane translocation), and a cholesterol core were useful for fighting neural tissue infection.[199] Broad antimicrobial activity was achieved, with higher efficacy in killing bacteria and fungi than many currently available antibiotics.[199] Moreover, using an *in vivo* mouse model, it was found that the nanoparticles that targeted brain infections by crossing the BBB were equally as effective as vancomycin alone.[199] This shows that, through the application of nanotechnology and self-assembly, new antimicrobial therapeutics can be designed to target brain infections. One limitation of this study is that the authors did not show any

improvements over vancomycin, or other existing antibiotics *in vivo*, and therefore this technology might have difficulty competing against these other drugs that have already been developed and work for this application (such as vancomycin).[199]

1.3.5 Nanotextured surfaces as antimicrobial biomaterials

Towards the goal of infection prevention, studies are being conducted to examine the implications of nanotechnology in response to microbial challenges. This growing direction in tissue engineering focuses on improved antimicrobial response in biomaterials. As many of these studies move from in vitro to in vivo, this will also be a focus of this section, and the animal model will be explained.

1.3.5.1 Wound repair with silver nanomaterials

An overwhelming number of studies focus on improving the wound healing response of materials incorporating silver. For example, waterborne polyurethane-silver nanocomposites have been used in this manner to fabricate biomaterials for preventing infection in catheters & subcutaneous wounds.[151] Using polyurethane (PU) with nanosilver (~5nm size), the material could be loaded up to 30 ppm with a good dispersion, as confirmed by transmission electron microscopy, whereas at higher concentrations the nanosilver aggregated. Important previous observations using nano-gold and nano-silver contributed to the design of this study through determination that the nanoparticle component improved material properties such as microphase separation on the surface of H_{12}MDI-based PU for enhanced the biostability and biocompatibility *in vitro* and *in vivo*, with nanosilver at 30 ppm being more effective.[152] In conjunction with

similar materials property improvements also found in this study, the nano-components enhanced fibroblast attachment and endothelial cell response, while allowing a reduction in monocyte and platelet activation, relative to PU alone or nanocomposites with other silver concentrations, and biocompatibility was confirmed in a subcutaneous rat model using adult Sprague-Dawley rats. The adhesion of *Bacillus subtilis*, *Escherichia coli*, or Ag-resistant *Escherichia coli* on PU-Ag nanocomposites was significantly lower at all concentrations of nanosilver tested, in addition to bacteriostatic ability, whereas PU did not. Commercial catheters were also coated with PU-nanosilver at 30 pmm, and these were inserted into rat jugular veins for evaluation. The results indicated milder inflammation after 3 months, with the wall thickness of the veins being smaller than that with the commercial catheters or the pure PU-coated catheters. Finally, it was concluded that the PU-nanosilver could reduce vein occlusion and improve blood compatibility through an overall better anti-fouling response.

1.3.5.2 Bone repair with silver nanomaterials

The design of orthopedic implant materials for reducing infection could also benefit from the application of nanotechnology. In one such study, a concern about bone tissue infection, termed osteomyelitis, has prompted researchers to incorporate antimicrobial aspects into bone tissue engineering systems. In one such study, the use of bone morphogenic protein 2 (BMP-2) coupled with nanosilver-PLGA composite grafts to induce bone repair in grossly infected segmental defects used materials for treating infection and healing bone defects.[154] The authors of this study used metallic nanosilver (20-40nm) combined with PLGA composite grafts. To make grafts, the authors mixed

PLGA with various weight percentages of nanosilver (with respect to PLGA), and poured the mixture over a bed of sieved sugar particles (200-300 μm) to generate a paste. This process was used to generate porosity in the structure after removal of the sugar particles via soaking in water. The paste was stacked in a Teflon mold to generate cylindrical grafts, dried for 12 hours, lyophilized for 4 hours, and washed with distilled water to leach out the sugar, and finally sterilized with 70% ethanol and further dried. BMP-2, an osteoinductive protein used to repair many bone fractures and bone defects, was also injected into some grafts to prepare BMP-2/NS/PLGA bone grafts. The authors used a vancomycin and methicillin resistant clinical strain of *Staphylococcus aureus*, Mu50, and cultured the microorganisms in the presence of grafts with up to 2 % nanosilver. The authors found that with an *in vitro* challenge of 10^7 CFU/graft, 0.1% nanosilver resulted in only a slight decrease of growth, a 0.5% nanosilver graft slowed the emergence of exponential phase by 13 hours, and weight percentages of 1% or higher completely inhibited growth. Using a higher inoculate of 10^8 CFU/graft, 0.1% and 0.5% nanosilver had no significant effect, 1 % and 1.5% slowed the emergence of exponential phase by 10 and 15 hours respectively, and 2% completely inhibited growth. Using this information, the authors decided to use an *in vivo* rat femoral segmental defect model, and with PLGA grafts of 0%, 1%, or 2% nanosilver implanted into SD rats along with an injection of 10^8 CFU (**Figure 1.11**). The silver composite grafts were able to heal a femoral defect implanted with the BMP-2 coupled with 2% nanosilver-PLGA, where the BMP-2 in PLGA grafts without silver failed to heal the defects. This study shows that healing can occur in the presence of silver, but only proves this for the incidence that the cost of infection is greater than the detriments of silver to the healing process.[154]

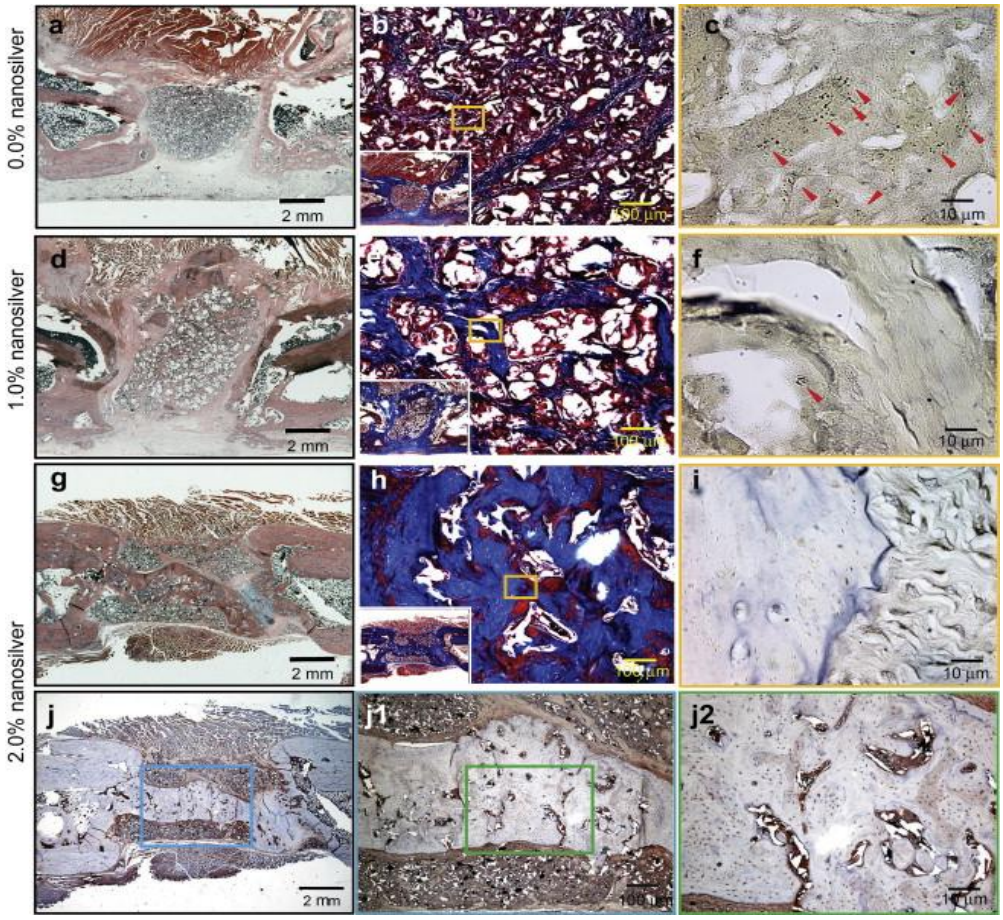

Figure 1.11 H&E staining (a, d, and g), Masson's trichrome staining (b, e, and h), Taylor modified Brown and Brenn gram stain (c, f, and i) and immunostaining of OCN (j, j1, and j2) of 10^8 CFU *S. aureus* Mu50 contaminated rat femoral segmental defects implanted with 0.0% (a–c), 1.0% (d–f), and 2.0% (g–j2) nanosilver-PLGA bone grafts coupled with 30 μg/ml BMP-2 at 12 weeks post implantation, respectively. Almost no bone regenerated in BMP-2/0.0%-NS/PLGA (control BMP-2 coupled control PLGA) implanted groups (a, and b) with obvious continued bacterial contamination (c, red arrows). Less bone regenerated in the defect area of BMP-2/1.0%-NS/PLGA implanted groups (d and e), while only limited bacterial colonies were observed (f, red arrow). BMP-2/2.0%-NS/PLGA grafts promoted significantly greater bone formation to form a mineralized bony bridge between the two defect ends (g, h, and j) by eliminating bacteria in the defect area (i), Higher magnification figures show active bone regeneration around the mineralized bridge and in the marrow-like cavities in the bridge (j1, and j2).[200]

1.3.5.3 Nanosheets in applications of tissue repair

Understanding of nanotechnology as a tool to improve antimicrobial response is growing as more nanomaterials are being developed and tested. Yet, few *in vivo* studies of nanomaterials have stepped outside of wound repair and bone repair towards improved bacteria inhibition on tissue engineering devices. One exception is gastrointestinal abdominal tissue repair with nanosheets, which has been investigated and will be described below.

Nanotechnology has been used in the production of antibiotic-loaded nanosheets for the treatment of gastrointestinal tissue defects.[201] In a series of studies, ultrathin polymer films (nanosheets) composed of polysaccharides were used as a wound dressing in gastrointestinal tissue defects (see **Figure 1.12** for details about preparation of and tissue repair with nanosheets). To prepare these materials, the authors used a layer-by-layer assembly method using biocompatible and biodegradable chitosan and sodium alginate, whereby single layers, each approximately 29 nm, were prepared via electrostatic interactions by spin-coating on SiO_2 substrates.[202] Because the nanosheets are too thin to lift and use surgically alone, a water soluble polyvinyl alcohol (PVA) with a thickness of about 70 μm was incorporated, which could be dissolved upon placement at the site of injury by the simple addition of saline.[202] These nanosheets showed favorable properties as a tissue engineering device sealing gastrointestinal or other tissues, acting as a physical barrier to bacteria, while attaining equal performance in sealing to sutures, with a less invasive procedure, and without postoperative adhesions.[201-203] Despite the sealing and healing effects, it was found that bacteria could penetrate through the wound dressing because of the ultra-thin structures.[201,203] To reduce bacterial penetration, tetracycline was

incorporated between a polyvinyl-acetate (PVAc) layer and polysaccharide nanosheets.[201] The tetracycline was released for 6 hours under physiological conditions. *In vivo* studies showed that overlapping therapy significantly increased mouse survival rate after cecal puncture, suppressing intraperitoneal bacterial count and leukocyte count, therefore showing the antibacterial and anti-inflammatory properties of the wound covering, and providing an efficient way for surgeons to repair tissues in various scenarios. This is an interesting application of nanotechnology, but further improvements still need to be made. Specifically, antibiotics are still incorporated into the device, which bacteria can develop resistance to; moreover, this technology only inhibits bacterial penetration (for example for sealing of gastrointestinal tract, which is a large reservoir of *Escherichia coli*, among others) and yet does not necessarily inhibit biofilm formation and even bacterial growth alone, on this or other surfaces.[201] In combination with new drugs able to inhibit bacterial growth and biofilm formation, nanosheets would become a more promising technology for various applications.

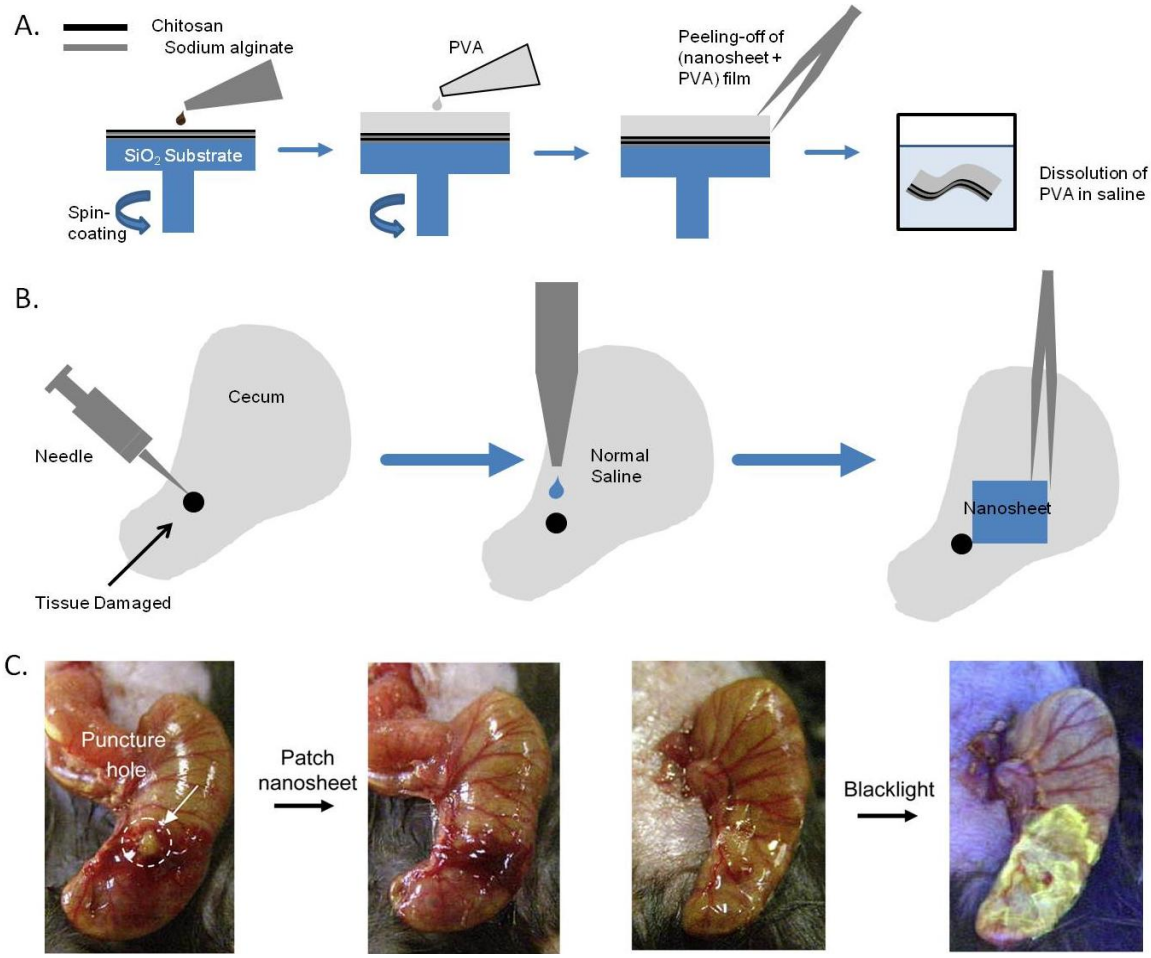

Figure 1.12 Overview of the methods required for tissue repair using biocompatible and biodegradable nanosheets. (A.) Nanosheets composed of chitosan and sodium alginate were prepared by layer-by-layer assembly on a SiO_2 substrate, a thicker 70 µm polyvinyl alcohol (PVA) layer allows handling with tweezers, and dissolution of the PVA layer takes place in normal saline. (B.) After tissue damage caused by a needle puncture into the cecum, the defect site is prepared with normal saline, and the nanosheet is simply applied to the site of damage resulting in PVA dissolution and sealing. (C.) Macroscopic images of tissue repair after treatment with antibiotic loaded nanosheets containing tetracycline (TC), where the TC nanosheets are viewed under a blacklight in the final image (the nanosheet is visible due to fluorescence of TC), thus preventing penetration of bacteria. Image in A. and B. are adapted and redrawn from previous work.[201,202]

1.5.4 Limitations of current antimicrobial nanomaterial developments

While many of these biomaterials are promising to reduce infections, either through the incorporation of nanosilver, as has been shown for polymers and bone graft materials, or through the incorporation of tetracycline or other antibiotics in nanosheets, these studies have not shown that it is possible to reduce biofilm infections in the event that they do occur.[151,152,154,201,202,204] Moreover, the antimicrobial activity of silver or antibiotics in biomaterials will eventually run out, because the mechanism of these nanomaterials is the release of either silver ions, or antibiotic, each of which are exhaustible. Also, the toxicity of silver is a concern, especially in consideration of the long term impact on tissue regeneration as is required for implant applications.[30,31] Finally, many devices have already been implanted which do not incorporate antibacterial drugs, and therefore there is a need for new drugs which can treat biofilm infections, since antibiotics don't work. With these limitations apparent, there is a need for novel materials developed which can effectively be delivered to the site of infection, limiting biofilm formation, and killing bacteria.

1.4 Superparamagnetic iron oxide nanoparticles (SPION) for comprehensive infection control

1.4.1 There is a need for the development of novel SPION

An ideal antibacterial entity for treating infection would be delivered with high efficiency to the site of infection and selectively target bacteria over other cells; the therapeutic effectiveness of the entity should also be able to be ascertained. An appropriate target mechanism would direct the antibacterial treatment to the site of infection. Antibacterial activity would remove and inhibit those organisms relevant to infection and would be useful against all virulent strains. Finally, therapeutic feedback would provide information about the effectiveness of the treatment, location of infection, and delivery efficiency. SPION could achieve all of these goals, and some of the studies which lay the foundation for these concepts will be described below.

1.4.2 Potential of SPION as a multi-use tissue therapeutic

To date, no nanomaterials, or otherwise, have been designed to decrease biofilm formation, or alleviate many of the problems with antibiotics when attempting to prevent or treat biofilm mediated device related infections, while simultaneously improving tissue growth. On the other hand, superparamagnetic iron oxide nanoparticles (SPION,) a type of naturally occurring nanoparticle, have been recognized as a promising tool for the site-specific delivery of drugs, as diagnostic agents, and as promising agents to improve tissue growth, when engineered specifically for these applications (**Figure 1.13**).[205,206]

Moreover, the application of small iron oxide particles during *in vitro* diagnostics has been practiced for 55 years.[207] Specifically, studies have included mostly maghemite, γ-Fe_2O_3, or magnetite, Fe_3O_4, single particles about 5–20 nm in diameter, as these are very promising candidates due to their biocompatibility and relative ease to functionalize for a wide range of applications. [208-210] In particular, the application of these iron oxide nanoparticles in drug delivery has been well addressed for non-bone applications.[211] Briefly, Superparamagnetic iron oxide nanoparticles with tailored surface chemistry have been widely used experimentally for numerous *in vivo* applications such as magnetic resonance imaging contrast enhancements, tissue repair, immunoassays, detoxification of biological fluids, hyperthermia, drug delivery and in cell separation.[205,212-214]

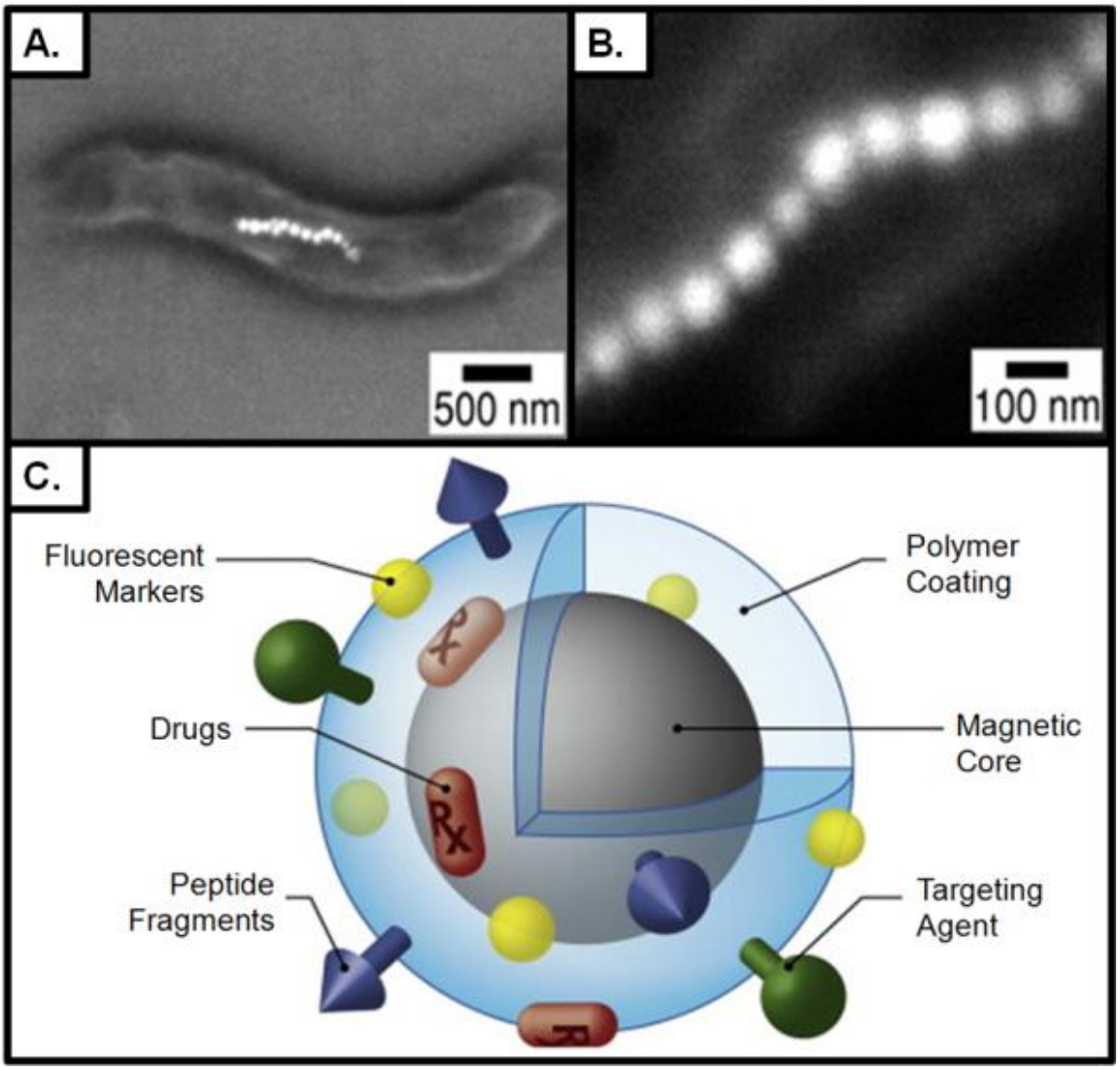

Figure 1.13 SPION are naturally produced, such as by *magnetospirillum magnetotacticum* (**A.**), a type of bacteria that synthesizes a chain of intracellular single-domain SPION within a magnetic organelle called a magnetosome (**B.**; images from reference).[215] SPION can also be engineered for control of the magnetic core size, along with a polymer coating, targeting agents, peptide fragments, drugs, and fluorescent markers expanding the biomedical uses of SPION to many (**C.**; image from reference).[216]

The use of iron oxide nanoparticles in orthopedic applications is promising, because of the potential of iron and iron oxide to increase bone health. For example, it has previously been shown that iron restriction can have an inhibitory effect on the mineralization of osteoblasts *in vitro*.[217] The beneficial link between iron and bone density has been demonstrated *in vivo* by the association of dietary iron and a healthy bone mineral density.[218,219] Moreover, experimental evidence also suggests that there may be some positive association between iron metabolism and the *in vitro* proliferation of non-bone cell lines such as fibroblasts.[220] Iron oxide nanoparticles can also aid in the site-specific generation of bone growth which can be accomplished by directing such magnetic nanoparticles to diseased bone under an external magnetic field, (such as in provided by magnetic resonance imaging; MRI) and the bioactivity could be further enhanced through coatings, such as calcium phosphate (CaP).[221]

The magnetic properties of SPION have also been used to generate mechanical forces, promoting the growth of bone and other mechanically sensitive tissues, towards tissue regeneration. Magnetic force has been used directly in combination with SPION to produce multilayer tissues *in vitro*. This has been demonstrated with a reconstruction of three-dimensional (3D) tissues, in which human mesenchymal stem cells (MSC) were labeled with cationic liposomes containing SPION and seeded under field strength of 4000 G.[222] Cellular sheets were then transplanted into nude rats and histological observation revealed that new bone surrounded by osteoblast-like cells was formed in the defect area 14 days after transplantation with MSC sheets, whereas no bone formation was observed in control rats without the transplant (**Figure 1.14).**[222] Yet, these studies relied on a development of transplant sheets outside of the body from cell isolates in a

culture tray, complicating the procedures in future applications.[222] Other studies have used magnetic fields to produce forces on magnetic particles resulting in enhanced bone tissue growth. For direct deformation or twisting of the cytoskeleton of cells, large particles ≥1 μm must be used to generate sufficient force.[223] It is also possible that SPION (~300 nm) could generate sufficient force if specifically targeted to mechanosensitive ion channels of bone and cartilage forming cells.[223,224] Yet, microparticles and large nanoparticles (≥300 nm) are limited by a short blood-circulation time, due to rapid clearing from the blood stream, either by mechanical trapping, or uptake into macrophages of the reticuloendothelial system, particularly in the liver and spleen;[118,225] thus for *in vivo* applications, this technology needs to be improved for smaller nanoparticles.

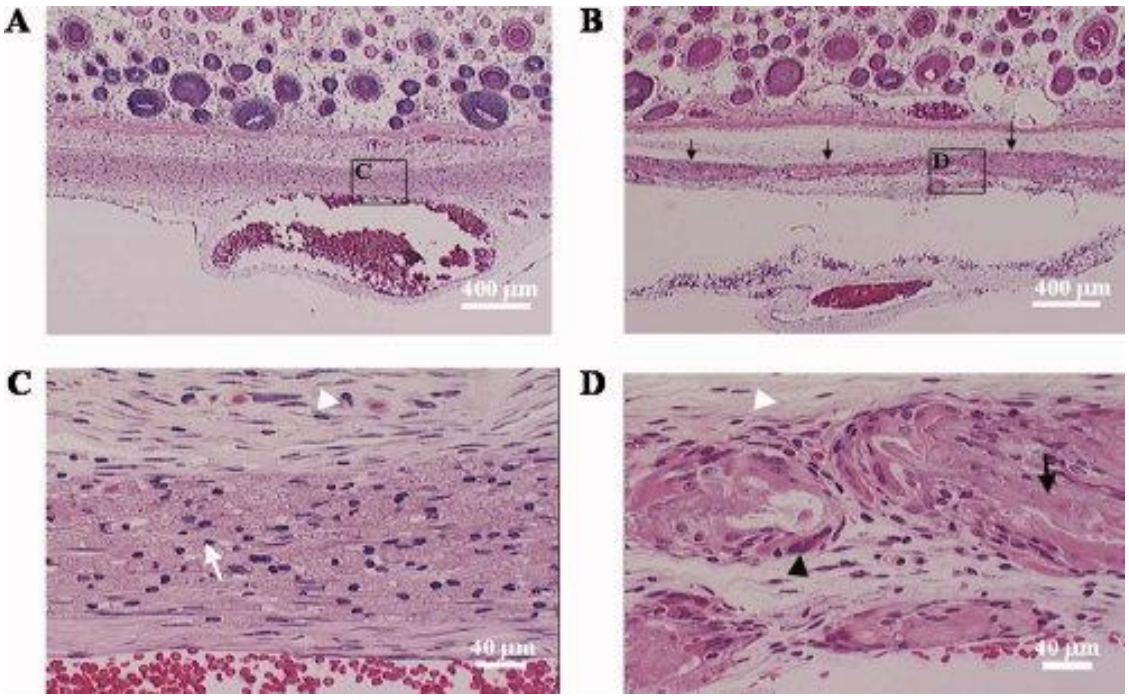

Figure 1.14 Histological analysis (hematoxylin and eosin staining) of *in vivo* bone formation by human mesenchymal stem cells (MSC) sheets on day 14 after transplantation. Low-power (A and B) and high- (C and D) power histology of defects without implanted MSC sheets (control; A and C) and with implanted MSC sheets (B and D). MSC sheets were apparently present throughout the defect site (black arrows in B). Numerous fibroblasts (white arrowhead in C) and adipocytes (white arrow in C) were observed in the control. When MSC sheets were transplanted, fibroblasts were observed (white arrowhead in D), but osteoblasts (black arrowhead in D) and new bone formation (black arrow in D) also were observed.[222]

1.4.3 Potential magnetically guided delivery of SPION to the site of infection

Magnetic nanoparticles can also be controlled and concentrated in the presence of a magnetic field. This opens up the possibility of magnetic antibiotic delivery to the site of an infection. Delivery to surface targets (such as the skin) can be achieved easily by the application of a strong magnetic field at that site. More complex strategies must be used

for the delivery of SPION to deep tissue targets (such as deep tissue infection). These deep tissue-targeting methods include regional targeting, sweeping, and magnetic implants. Combined approaches utilize MRI or other imaging modalities as feedback for magnetic drug delivery. Explanation of these potential deep tissue-targeting methods will be outlined below, and are further compared in **Table 1.5** at the end of this section.

Regional targeting and sweeping are two methods of magnetic drug delivery have been previously considered, although not for anti-infection applications. In regional targeting, a magnetic field is applied to a specific location to increase the local dosage. Regional targeting has been used to deliver magnetic nanoparticles into bone and cartilage tissues *in vitro* using a 10.15 mT magnetic field generated by a Polus-101 magnetic therapy device.[226] After only 20 minutes of exposure the tissues attained a significant increase in iron concentration (determined by histology sections) and reached saturation (compared to no field or 40 minutes exposure).[226] For *in vivo* applications, regional targeting could also be used to increase the location concentration of magnetic materials in one body compartment.[227] This method has the advantage of not requiring exact anatomical knowledge of delivery location, and only a general idea of deliver location (for example brain, upper body, or lower body), and yet is not very accurate. Another method which could be used for deep tissue targeting would be the application of magnetic sweeping. In sweeping, magnetizable objects are swept through a region or regions to better target hard to reach locations.[227] For example, even if a therapy could be confined to one region of the body it is still possible that the infection in this region would be hard to access and then therapeutic delivery to the site would be poor. Sweeping can overcome this problem to some extent by applying additional force which would move the magnetic materials

into the infection site. Both regional and sweeping methods need to be further tested using various sizes of magnetic materials, such as SPION, for determination of efficacy, and additionally the impact on the growth of tissues and infectious bacteria by such magnetic fields and particles must also be investigated.

Magnetic targeting methods combined with imaging can be used to further improve delivery efficacy. One such method is comprised of detecting one location of SPION within the patient, and using an externally applied magnetic field in response. This sensing and feedback allows better control of delivery to desired target volumes and more efficacious choice of magnetic field design. Chertok and collegues used this method to deliver 100 nm particles to brain tumors of mice under a 0.4T static magnetic field and MRI was used to determine delivery efficiency.[228] Using the method, the authors determined that a 5 fold increase in nanoparticles exposure over non-targeted tumors and a 3.6 fold enhancement of nanoparticles accumulation in tumors over normal brain tissues could be achieved.[228] In a similar method, Oh and others used ultrasound to visualize an intravenous injection of 20nm SPION.[229] Exciting results were obtained while using M-scan mode and color power Doppler which demonstrated SPION movement under focused magnetic fields.[229] The introduction of ultrasound as an imaging modality which can be used to visualize SPION opens up the possibility of bed-side application of feedback controlled magnetic drug delivery during the treatment of implant infections.

Finally, magnetic targeting could also be guided by a magnetic implant to deep tissue targets. It has been shown that 304-grade stainless steel has near superparamagnetic properties which were utilized to deliver cells loaded with SPION to the surface of

vascular stents.[230] Further investigation of 304-grade stainless steel must be carried out to determine if other metal devices such as prostheses could also maintain this useful magnetic property, if SPION formulations which could decrease infections could be guided to the implant, and infection models must be developed on such devices. Additionally, the impact of magnetic properties in a permanent implant must be considered for other practical reasons (for example, if the patient will be in danger upon entrance into an MRI, or in the presence of other devices that generate magnetic fields).

Table 1.5 Potential methods for deep tissue targeting of SPION to the site of an infection.

Method type	Description and advantages	Disadvantages
Regional targeting[226]	A magnetic field is applied to a specific region of the body to increase the local dosage	Targets a region of the body with low accuracy
Sweeping[227]	Magnetizable objects are swept through a region or regions of the body to improve tissue penetration	Improved penetration into a region of the body with low accuracy
Sensing and feedback with magnetic resonance imaging (MRI)[228]	Combination of other targeting methods with MRI imaging	MRI may interfere with drug delivery; this technology has not been fully developed
Sensing and feedback with ultrasound[229]	Combination of other targeting methods with ultrasound imaging; bedside imaging	Magnetic field and imaging must be provided by separate devices
Magnetic implants[230]	Implant activated by an external magnetic field	Implant interferes with MRI or other magnets

1.4.4 Good prospects of SPION in treatment of device related infections

Most importantly for the application of SPION being developed here, iron oxide nanoparticles may also provide an effective means for biofilm treatment on orthopedic implants, or other medical devices. The greatest numbers of bacteria in a biofilm are

present at a nominal depth of about 10 μm.[193,231] Penetration of a colloid to any depth in a biofilm is diffusion dependent with an inverse relationship to their size due to steric and mobility factors while plasma clearance plays a role in decreasing nanoparticle local concentration.[81] Nanoparticles are small enough to penetrate the biofilm, large enough to have a long plasma half-life, and additionally offer a surface to volume ratio optimized for mass loading of targeting moieties, drugs, and antibiotics.[193]

Iron nanoparticles may offer some additional benefits for biofilm treatment. Iron restriction is closely related to the physiological onset of biofilm formation for common pathogenic bacteria such as *Staphylococcus epidermidis*, *Staphylocccus aureus*, and *Pseudomonas aeruginosa*. Biofilm formation through polysaccharide intercellular adhesin (PIA) production by *Staphyloccus epidermidis* and *Staphyloccus aureus* is a stress response mechanism to conditions such as heat, anaerobic conditions, or iron-limited culture medium.[61] Iron-limited medium can cause gene transcription in *Staphyloccus epidermidis*, which results in the release of siderophores that mediate the covalent bonding of the bacterium to metal surfaces.[67,68] Biofilm pathogenesis of *Staphyloccus aureus* has been implicated by the expression of extracellular adherence protein (Eap) and extracellular matrix binding protein (Emp) which are induced by iron restriction.[69] Most profoundly, biofilms grown from *Pseudomonas aeruginosa* strains obtained in the sputum of cystic fibrosis patients have been disrupted and cleared by switching to iron-rich medium in flow chamber tests.[70]

To further explore the multifunctional use of SPION for orthopedic applications, and as a novel approach to prevent device related infections, a superparamagnetic nanoparticle platform is proposed here. Superparamagnetic nanoparticles are attractive for this

purpose because antibacterial drug delivery can be carried out in the presence of a magnetic field. Biofilm targeting for this purpose could be achieved through the development of magnetic fields,[226-229] or delivery to a magnetic implant.[230] Finally, detection of bacteria could also be provided by enhanced T2-weighted magnetic resonance image contrast offered by infection site targeted SPION, especially if the particles enter the bacteria.[232] However, as a first step in this direction, this study will explore the groundbreaking hypothesis that SPION prevent biofilm formation, and could potentially outperform antibiotics in the treatment of device related infections.

1.5 Future Directions

Tissue engineering with nanotechnology is no longer in its infancy; with the growing number of studies, we are beginning to understand its benefits. Specifically, nanotechnology offers the possible to improve stem cell differentiation,[101,102] increase bone growth,[91-94,96-98,103,104] improve bladder stent urothelialization,[105] decrease inflammation,[98,106] and increase vascular stent endothelialization[107] by increasing the nanoroughness of an implant material. More recently, researchers and doctors have switched focus towards the impact of nanotechnology on other important clinical problems, such as infections caused by implantation of numerous medical devices.[9-13,15,18,22-24] Here, it has been found that nanotechnology can provide some very innovative approaches towards simultaneously controlling bacterial growth, controlling the inflammatory response through decreased infection, and improving tissue growth. Yet, with nanomaterials developed to date, localization at the desire site, toxicity due to free radical release, simultaneous potent antimicrobial activity, and activity against biofilm resident bacteria have not been well controlled or understood. In particular, SPION show promise in each desirable category due ease of magnetic localization, biodegradation and low toxicity, and potential for antimicrobial activity or delivery.[205-211,222-224,226-230,232] Despite the promise of this nanomaterial, new formulations must be generated to further improve applications of SPION for decreased infection. Moreover, with the growing applications of nanomedicine throughout the body, future studies must also consider the long-term impacts of implanted nanomaterials. Specifically, toxicity of nanomaterials is still not well understood. Therefore, studies which consider the various components

individually, in terms of biocompatibility, and together as parts of the whole nanomaterial, which enables unique properties in the biological setting, will better guide the future impacts of nanomaterials and biomaterials in general to improve medicine.

1.6 Contributions to the Field

While numerous investigators have been creating different implant chemistries or designing new drugs, nanotechnology, or the science that deals with technologies on the scale of one billionth of a meter (10^{-9} m = 1 nm), is only recently being investigated as a means for infection control on medical devices, and is the focus of this thesis.[4-7] Additionally, superparamagnetic iron oxide nanoparticles are investigated in detail towards providing a novel material to decrease biofilm formation, to increase tissue growth, and towards potentially outperforming antibiotics during the treatment of device related infections clinically. Finally, this thesis has the focus of developing basic methods to compare nanomaterials to conventional therapies, such as antibiotics, through a biofilm model, a standard which has not been well developed to date in the nanomaterial field.

2. Materials and Methods

2.1 Nanoparticle synthesis, coating, and conjugations

2.1.1 Magnetite (Fe_3O_4) SPION synthesis

Magnetite (Fe_3O_4) SPION were synthesized by a wet chemistry method under high pH as previously reported.[233] Here, iron(II) chloride (Sigma Aldrich, Saint Louis, MO, USA) and iron(III) chloride (Riedel-de Haen, Seelze, Germany) were dissolved in 25 ml of nitrogen (N_2) gas purged ultrapure water (filtered with a Milli-Q Advantage system from Millipore, Billerica, MA) in the presence of 0.4 M hydrochloric acid. This solution was added dropwise at 0.5 ml/min to a 250 ml solution of 1.5 M sodium hydroxide under nitrogen gas flow. This solution was centrifuged at 5000 rpm and the supernatant decanted. The particles were dispersed in ultrapure water while vortexing, followed by sonication. This was repeated three times whereby a black solution of Fe_3O_4 SPION was obtained. The particles were sterilized through dispersion in ethanol once, centrifuged at 5000 rpm, and decanted before suspension in ultrapure water. When a magnet was available, the Fe_3O_4 SPION were instead collected in a magnetic field, decanted, and dispersed in 100% ethanol several times. Three aliquots were taken from the solution, dried, and weighed to determine particle concentration.

2.1.2 Maghemite (γ-Fe_2O_3) SPION synthesis.

The oxidation of the cleaned Fe_3O_4 SPION was carried out under low pH and high temperature. Fe_3O_4 SPION were sonicated and vortexed. The pH of the nanoparticle solution was adjusted to 3.5 using 0.1 M hydrochloric acid. This solution was then heated to 100ºC in oxygenated water while vigorously magnetically stirring for 30 min. The resulting solution was a reddish-brown suspension of maghemite (γ-Fe_2O_3) SPION. This solution was centrifuged and decanted, whereby it was sterilized in ethanol as described above. The cleaned solution was then resuspended in double deionized water.

2.1.3 Calcium phosphate (CaP) coating on SPION

Calcium phosphate (CaP) coatings were produced on magnetic nanoparticles in the presence of bovine serum albumin (BSA) or citric acid (CA) capping agents (Sigma Aldrich). Surfactants have been shown to have a stabilizing effect on SPION.[234] BSA and CA were used with the motive to disperse SPION so that an effective CaP coating could be created. Calcium nitrate and monopotassium phosphate (Sigma Aldrich) were used at a molar ratio of 1.67, which is the ratio of calcium to phosphate for the natural hydroxyapatite phase of bone.[235] Into a 150 ml solution of double deionized water, 60 mmol of calcium nitrate was added. This solution was dissolved while magnetically stirring and the pH was adjusted to 10 by the addition of ammonium hydroxide. SPION at 13.33 mg/ml and respective capping agents (BSA and CA) at 1.9 mg/ml were added to the calcium solution. Separately, a 150 ml solution was prepared using 36 mmol of monopotassium phosphate whereby the pH was adjusted to 10 using ammonium hydroxide. This solution was added dropwise to the calcium solution. Then, the mixture

was moved to a PTFE hydrothermal unit and heated for 9 h at 70ºC. After cooling, particles were centrifuged (5000 rpm) and the aqueous component was decanted for dispersion in ethanol for sterilization purposes as described above. After subsequent sonication, the coated SPION were again centrifuged and the solvent decanted. This was repeated for a total of three times before their dispersion in double deionized water.

2.1.4 Monodisperse SPION synthesis and dimeraptosuccinic acid (DMSA) coating

To produce monodisperse SPION, synthesis was carried out using a variation of a high temperature synthesis method in triethylene glycol.[236-238] During this process, 2 mmol of Iron(III) acetylacetonate (Strem Chemicals, Newburyport, MA) was dissolved in 25 ml of triethylene glycol (Alfa Aesar, Ward Hill, MA) in a round bottom boiling flask with magnetic stirring (**Figure 2.1.A**). This solution was heated gradually to 278°C (and held at this temperature for 30 minutes) whereby gentle refluxing occurred, and was then cooled to room temperature. From this point, a conjugation method was carried out using 4 mmol dimercaptosuccinic acid (DMSA; Acros Organics, Geel, Belgium) as a capping agent, and was allowed to react overnight. The SPION produced during this process were precipitated in 200 ml absolute ethanol saturated with ammonium sulfate (Sigma Aldrich) and subsequently isolated in the presence of a strong magnetic field (**Figure 2.1.B**) produced by two DZX08-N52 neodymium magnets (4" diameter x 1/2" thick magnet, 1795 Gauss; K&J Magnetics, Jamison, PA). Small nanoparticles do not easily separate from solution; therefore, this isolation process is thought to take place through aggregation of SPION under applied magnetic fields, which is then reversible once the field is removed, thus enabling magnetic collectability under a reasonable field

gradient.[239,240] The entire process was completed over a two day period; on the first day nanoparticles were redispersed 3 times (every ~8 hours) into the solution phase by mixing; on the second day the supernatant clarified and was decanted. Particles were then transferred into a 50 ml centrifuge tube, rinsed twice in 100% ethanol using a BZXOXOXO neodymium block magnet (4" x 1" x 1", 4871 Gauss; K&J magnetics, Jamison, PA), dried, and weighed to determine the SPION stock solution dry mass concentration (combined weight of DMSA and SPION). SPION could be stored under refrigeration (4°C) in the ethanol solution, and no changes were observable for at least one month (oxidation of SPION when stored in water or on the countertop results in a detectable color change of dark black, to brown, and finally to brownish red).

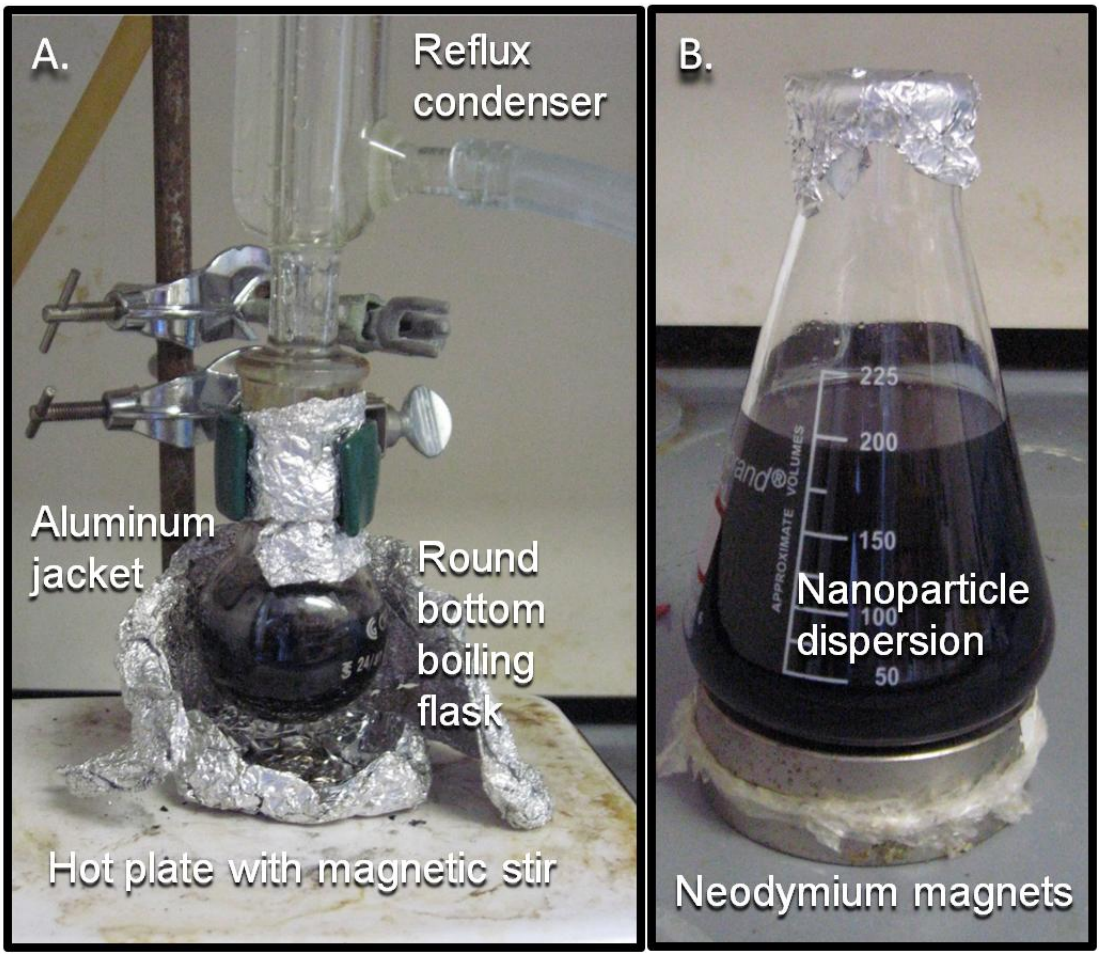

Figure 2.1 Methods used for the synthesis and isolation of superparamagnetic iron oxide nanoparticles (SPION). SPION were prepared by high temperature reflux of Iron(III) acetylacetonate in triethylene glycol (**A.**) in a round bottom boiling flask under magnetic stir while outfitted with a reflux condenser. SPION were isolated in a strong magnetic field (**B.**) produced by two DZX08-N52 neodymium magnets (4" diameter x 1/2" thick magnet, 1795 Gauss; K&J Magnetics, Jamison, PA).

2.1.5 Conjugation of antibacterial metals to SPION via DMSA

Fabrication of SPION bound to a variety of metals with well documented antibacterial and antibiofilm activity, including Fe, Zn, and Ag, was next carried

out.[63,67,69,70,124,155,172,241] SPION prepared up to this point were conjugated with the chelator molecule, DMSA (referred to here as chelated SPION); this coupling process is known improve the water solubility of SPION, and to leave free thiols on the surface useful in further biomedical conjugation applications.[242-244] Moreover, it is known that chelated SPION with DMSA retains the chelation functionality, enabling binding to a variety of metals.[239]

In line with prior studies,[63,67,69,70,124,155,172,239,241-244] SPION were conjugated with antibacterial metals including silver, zinc, and iron to enhance antibacterial activity in a novel way **(Figure 2.2)**. During this process, 10 mg/ml of the SPION stock solution was placed in a 15 ml centrifuge tube (15 ml high-clarity polypropylene conical tubes; 17 mm diameter X 120 mm length; BD Falcon; Franklin Lakes, NJ) and diluted into 100% ethanol with metal salts including $AgNO_3$ (Sigma Aldrich), $ZnCl_2$ (Fisher Scientific Inc, Waltham, MA) and $FeCl_3$ (Riedel de Haen) at a concentration of 100 µmol or 400 µmol per final volume of 10 ml ethanol (these are denoted as 1 mmol or 4 mmol for the amount of salts added to each). Solutions were then placed on a shaker overnight (~12 hours) at 88 RPM. Vortex mixing and water bath sonication before and after shaking was also used to increase the dissolution of large salt crystals in the mixture (especially for the solution containing 4 mmol $AgNO_3$; this, the only salt that did not completely dissolve after the procedure). After this process was completed, purification was repeated in triplicate by placing the mixture next to a BZXOXOXO neodymium block magnet. This magnetic field allowed purification of magnetic components, while non-magnetic components of the mixture were decanted; this procedure was also used for the sterilization procedure with the entire process completed under sterile air in a Forma

1400 series biological safety cabinet (Thermo Scientific, Waltham, MA) and with sterilized equipment. For all bacterial procedures, this same method was used only on the final rinse, the samples were transferred to a sterile 15 ml centrifuge tube (BD Falcon) and redispersed into sterile tryptic soy broth (TSB; 15 g per liter double distilled water; MP Biomedical, Solon, OH).

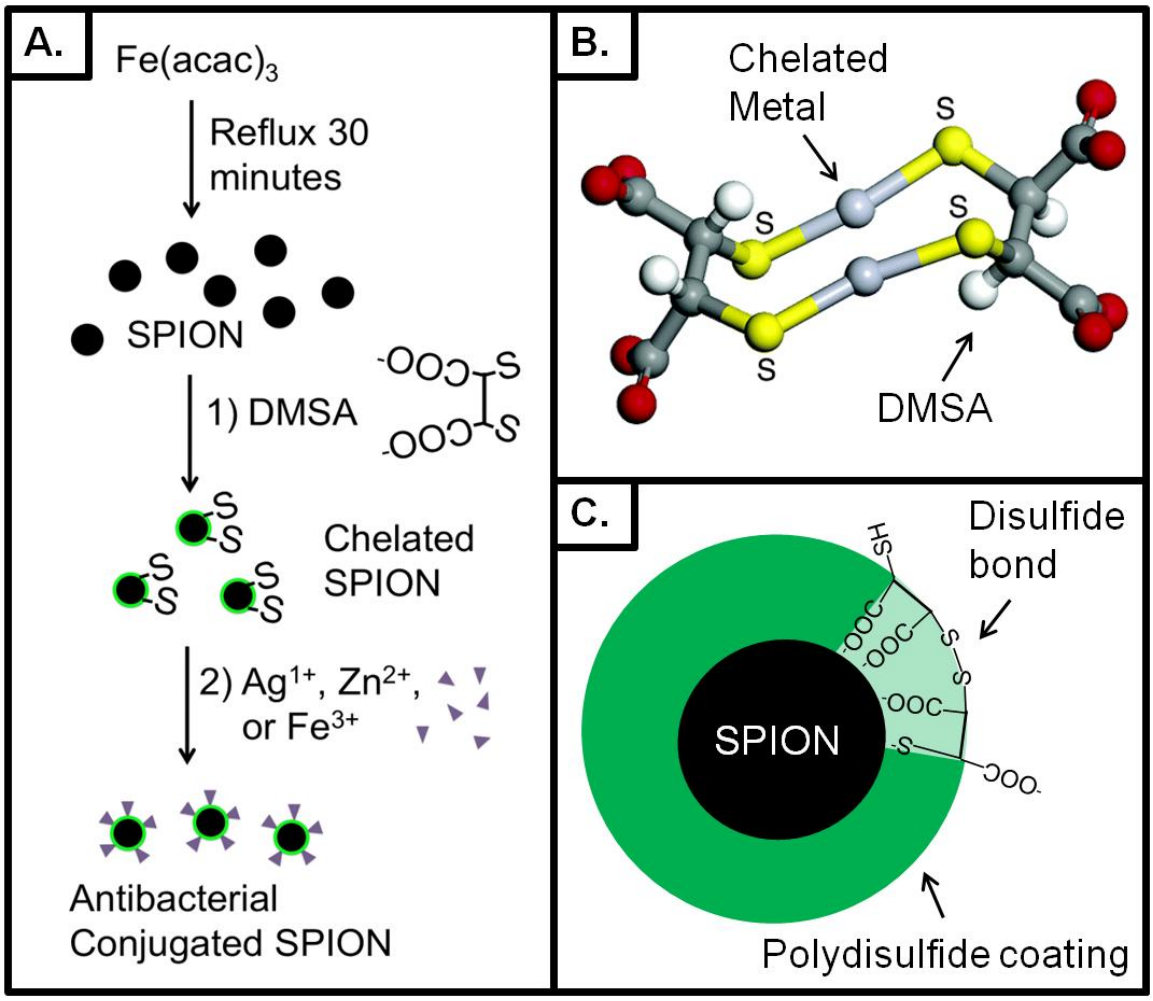

Figure 2.2 Conjugation of antibacterial metals to superparamagnetic iron oxide nanoparticles (SPION) via dimercaptosuccinic acid (DMSA) after synthesis via high temperature reflux of Iron (III) acetylacetonate in triethylene glycol for 30 minutes. **A.** Two-step synthesis scheme required addition of DMSA to the reaction mixture to produce chelated SPION, followed by a further reaction with metal ions from $FeCl_3$, $ZnCl_2$, and $AgNO_3$ to produce iron, zinc, and silver conjugated SPION respectively. Each of these products was isolated in a magnetic field in triplicate under sterile conditions. **B.** DMSA is U.S. food and drug administration (FDA) approved for metal chelation therapy to remove heavy metals from the body (e.g. for treatment of lead poisoning).[245] **C.** Oxidation of DMSA by SPION yields a polydisulfide coating.[242]

2.1.6 Conjugation of gentamycin and vancomycin to SPION via DMSA

In a separate procedure, the DMSA capping agent was conjugated with antibiotics gentamycin and vancomycin (Sigma Aldrich) to enhance antibacterial activity. During this process, 10 mg of SPION in 100% ethanol were placed in a centrifuge tube and centrifuged at 10,000 rpm. Phosphate buffered saline (PBS) at pH of 7.4 was then added into the tube and the SPION were dispersed by a water bath sonicator followed by vortex mixing. To this solution was added 5 mg of antibiotics (either gentamycin or vancomycin) and a Sulpho-SMCC (Pierce, Rockford, IL) cross-linker was added which bonded sulfur groups of DMSA to the amine groups of the antibiotics. The solution was diluted to a final volume of 6 ml and placed on a shaker at 88 RPM for 30 minutes. After this process was completed, purification was carried out by a strong magnetic field placed parallel to the beaker. The magnetic field allowed purification of magnetic components, while non-magnetic components of the mixture were decanted. The precipitate was then rinsed once with ethanol, centrifuged from this solution, and placed into phosphate buffered saline with the SPION diluted to 1 mg/ml.

2.2 Characterization of nanoparticles

2.2.1 X-ray diffraction (XRD) to determine crystal structure

Fe_2O_3, γ-Fe_2O_3, and CaP coated magnetic nanoparticles, along with chelated SPION were characterized with x-ray diffraction (XRD) to verify the various phases present. Prior to analysis, coated samples were dried from as-prepared solutions in 100% ethanol, and obtained as a powder. The samples were then pressed into a glass crucible for analysis. Alternatively, to reduce background noise, samples were analyzed after direct drying onto a 24.6 mm diameter X 1.0 mm thick zero diffraction plate made of single crystal silicon (MTI, Richmond, CA).

XRD utilized Cu Kα radiation (Siemens Diffractometer D5000 Kristalloflex; Bruker AXS Inc; Chicago, IL, USA), where the 2θ angle was varied from 20º to 70º at 10º min^{-1}. Diffraction signal intensity was recorded and processed using DiffracPlus: TexEval (Bruker AXS, Inc; Palo Alto, CA, USA) software. Peak search was used to determine the phases present. Crystallite size analysis was also carried out using the Scherrer Equation, which can be written as:

$$D = 57.3 \cdot k \cdot \lambda / \beta \cdot \cos(\theta) \qquad \textbf{(2.1)}$$

In **equation 2.1**, D = mean diameter, k = shape factor, λ = wavelength, β = the full-width at half maximum, and θ = Bragg angle.[246] The factor 57.3 is used for conversion of β from degree to radians.[246] Here, scherrer constant K was set to 0.94 with the assumption of round nanoparticles, and λ to 0.15418 nm as produced by Cu Kα X-ray radiation.[246]

2.2.2 Transmission electron microscopy (TEM)

Transmission electron microscopy (TEM) was used to visualize the morphology of the SPION. The dispersion of nanoparticles in deionized water was allowed to slowly dry on a formvar-coated copper grid (Electron Microscopy Sciences, Chicago, IL). All imaging was carried out using a Philips JOEL 140 kV TEM (Philips, New York, NY) and size calculations were carried out using Image J version 1.41 (National Institutes of Health, Bethesda, MD) or a manual method with the scale bar as a unit of reference.

2.2.3 Vibrating sample magnetometry (VSM) for magnetic properties

The magnetic properties (hysteresis loop) of the dried nanoparticles were assessed using vibrating sample magnetometry (VSM, LakeShore 7400; Chicago, IL, USA) at 300 K. Briefly, for VSM, samples were centrifuged and the supernatant decanted. Nanoparticles were then dispersed in ethanol, centrifuged and the supernatant decanted. These nanoparticles were then allowed to dry at room temperature for several days. Powders were weighed and then placed in a capsule for magnetic readings.

2.2.4 Fourier transform infrared spectroscopy (FTIR) for chemical analysis

The success of conjugation between SPION and antibiotics were analyzed using Fourier Transform Infrared Spectroscopy (FTIR). For this, samples were centrifuged and the ethanol supernatant decanted. Powders were obtained at room temperature under vacuum, and refrigerated when not in use. Powders were weighed and then placed in a capsule for analysis by the Nexus 870 FTIR (Thermo Scientific, Waltham, MA).

2.2.5 Zeta potential for surface charge

The physical properties of SPION were determined using zeta potential measurements. For zeta potential measurements, particles were precipitated from Tryptic Soy Broth (formulation described below) in a magnetic field and dispersed in DI water. Zeta potential measurements were repeated 5 times for each sample and in triplicate using a Zetasizer Nano ZS (Malvern Instruments, Worcestershire, UK).

2.2.6 Inductively coupled plasma atomic emission spectroscopy (ICP-AES)

ICP-AES was used to quantitatively confirm the presence of metals in the SPION after purification (**Figure 2.3**). This technique uses argon plasma to excite metal ions, which can then be analyzed spectrophotometrically. Standard solutions containing iron, zinc, silver, and sulfur ions were first prepared in a 2% solution of nitric acid at 100 parts per million (ppm) which produces a standard curve giving quantitative data. A small volume of SPION (50 µL) was then dissolved by aqua regia (nitric acid and hydrochloric acid at a volumetric ratio of 1:3). This was evaporated to completely dissolve nanoparticles and all metal salts. One additional drop of aqua regia was then added, and 5 ml of 2% nitric acid was added as a matrix before analysis. All volumes were weighed to ensure accuracy, with adjustments made based on mass.

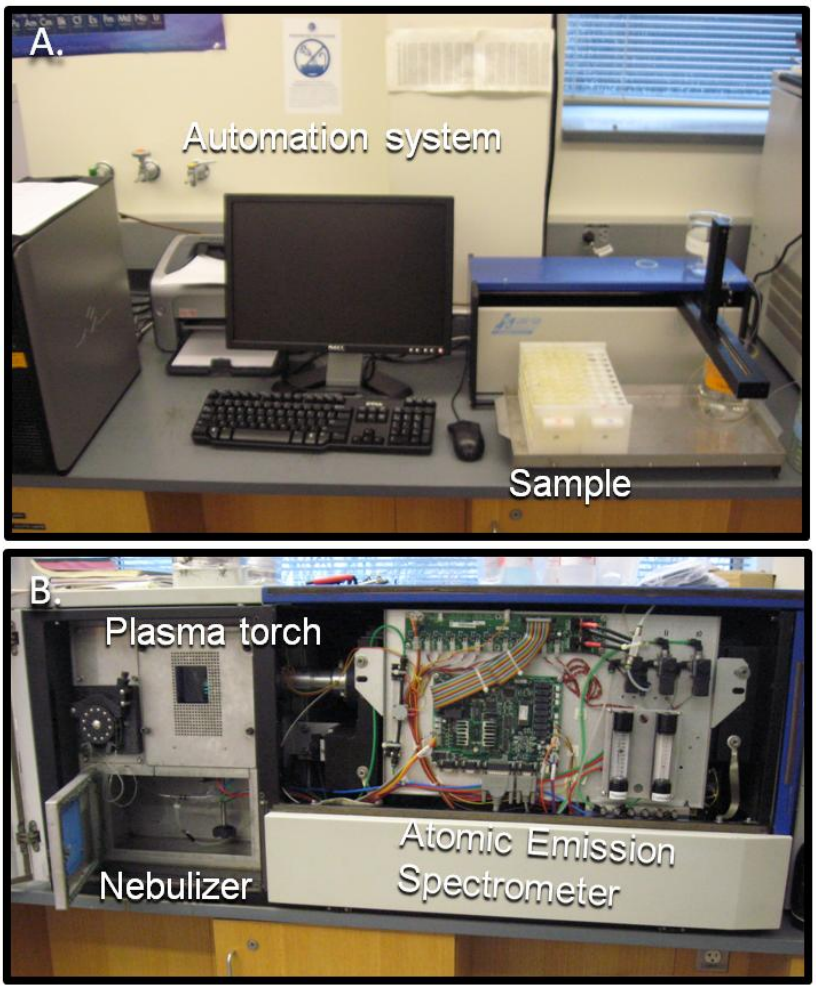

Figure 2.3 Inductively coupled plasma atomic emission spectroscopy (ICP-AES) was carried out on a Jobin Yvon model JY2000 (HORIBA; Kyoto, Japan). The automation system (**A.)** is used to transfer sample into the nebulizer (**B.**), where it is sprayed into the plasma torch, and analyzed by the atomic emission spectrometer.

ICP-AES was also used to determine the concentration of zinc ions released from SPION conjugates or chelated SPION. For this study, 200 µL aliquots of solutions containing SPION dispersed in TSB in a 96 well plate were incubated at 37 °C, 5% CO_2, and humidified conditions for up to 48 hours. At time points of 1, 4, 12, 24, and 48 hours, an entire SPION aliquot was collected, placed into 800 µL of 100% ethanol, and centrifuged

at 13,000 RPM for 5 minutes. During this process, the supernatant was collected containing released zinc ions separate from the pellet containing proteins and SPION. This supernatant was placed into a sealed microcentrifuge tube, and refrigerated at 4 °C until analysis. During analysis, 500 µL of each solution was diluted into 4.5 ml of 2% nitric acid, for a final ethanol content of about 10%. Standards were also established with 10% ethanol for consistency, and used during this analysis procedure.

2.2.7 Dynamic light scattering (DLS) for particle sizing

Chelated SPION, or with iron, zinc, and silver conjugated SPION at 1 mmol or 4 mmol added, were prepared in sterile TSB. TSB alone with also maintained as a control, and treated the same as the other SPION solutions. Prior to readings, samples were diluted by placing 100 µl of each solution into 0.9 ml double deionized water (prepared from a milli-Q system; Millipore) either directly as prepared, or after sterile filtration using a 0.2 µm filter (Corning; low protein binding #431219). For DLS readings, a Zetasizer Nano ZS (Malvern Instruments) was used set to high resolution mode to search for peaks in the Dispersion Technology software (**Figure 2.4**). Samples were repeated in 5 replicates for each reading.

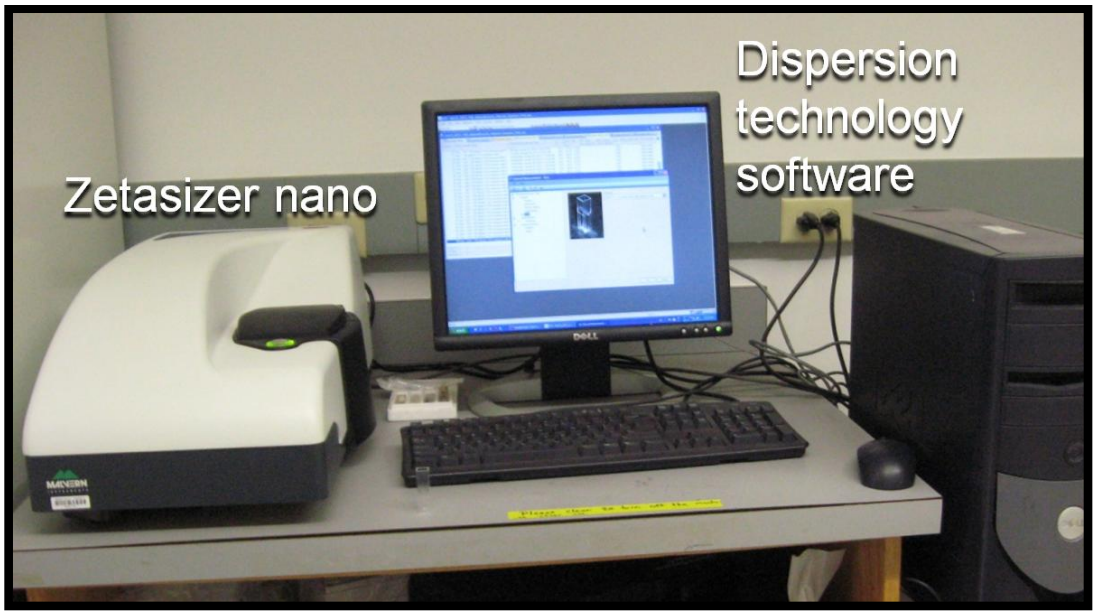

Figure 2.4 Zetasizer nano and dispersion technology software (Malvern Instruments) uses dynamic light scattering to determine particle sizes (0.3 nm diameter to 10 µm) and samples dilute to 100 µg/ml (determined for proteins). The same apparatus can also be used for zeta potential measurements if also equipped with laser doppler microelectrophoresis.

2.3 Osteoblasts methods

2.3.1 Osteoblast culture

Human osteoblasts (HOB, CRL-11372, ATCC, population numbers 8–10; Bethesda, MD, USA) were cultured under standard cell culture conditions (i.e. a 37 ºC, humidified, 5% CO_2, 95% air environment) in Dulbecco's modified eagle medium (DMEM, Gibco; Tampa, FL, USA), supplemented with 10% fetal bovine serum (FBS, Hyclone; Boston, MA, USA) and 1% penicillin/streptomycin (P/S, Hyclone), under standard cell culture conditions. Previous studies have characterized the phenotype of these osteoblasts at these population numbers by measuring alkaline phosphatase activity and deposition of calcium containing mineral.[247]

2.3.2 Osteoblast proliferation in the presence of uncoated SPION

Osteoblasts were grown in DMEM supplemented with 10% FBS and 1% P/S on the bottom of a 96-well polystyrene plate at a seeding density of 3000 cell/cm^2 with or without the presence of either magnetite (Fe_3O_4) or maghemite (γ-Fe_2O_3) uncoated SPION for 1, 5 and 8 days. Nanoparticles were dispersed by sonication and were vortexed before their immediate addition (at a constant volume of 20 μl and at a concentration of 4.25 mg/ml for both Fe_3O_4 and γ-Fe_2O_3 SPION) to the cells. This was replicated three times with two repeats each time per plate for both SPION solutions and the control (no particles). The cell culture medium was not changed throughout the experiment. Cell counts were performed using the CellTiter96 assay (Promega, Boston, MA, USA). Briefly, during a reading interval, CellTiter96 was added at 20 μl to all wells

of the 96-well plate, after which the plate was incubated for 3 h. After this time, the plate was analyzed using a microplate reader (SpectraMax 340PC, Molecular Devices; Chicago, IL, USA) at 490 nm for absorbance and the creation of a standard curve.

2.3.3 Osteoblast proliferation in the presence of calcium phosphate coated SPION

Similar to the above, a single plate was prepared for experiments with SPION and CaP-coated SPION. 20 µl of these nanoparticles (4.25 mg/ml) were added to 200 µl of a DMEM solution (supplemented with 10% FBS and 1% P/S) containing osteoblasts seeded at a density of 3000 cell/cm^2. Cells were allowed to grow for 1 day. A control containing cells with no nanoparticles was also utilized. Each trial was replicated three times with two repeats each time. The CellTiter96 assay was also used as described above.

2.4 Bacteria methods

2.4.1 Preparation of *Staphylococcus epidermidis* frozen stock

Bacteria used were *Staphylococcus epidermidis* #35984 obtained in freeze-dried form (American Type Culture Collection, Manassas, VA). The dry pellet was rehydrated in 6 ml Luria broth (LB) consisting of 10 g tryptone, 5 g yeast extract, 5 g NaCl (all obtained from Sigma, St. Louis, MO) per liter double distilled water with pH adjusted to 7.4. The solution was incubated (37 °C, 5% CO_2, humidified environment) and agitated until the bacteria reached late stationary phase (about 24 hours). The second passage was diluted at a ratio of 1:200 into fresh LB and incubated until late stationary phase whereby it was mixed with equal proportions of 50% glycerol (Sigma Aldrich) and frozen at -18 °C.

2.4.2 Bacteria propagation in the presence of uncoated Fe_3O_4 SPION

Centrifuge tubes were prepared with 3 ml LB and inoculated with a sterile 10 µL (Sigma) loop followed by agitation at 250 revolutions per minute (rpm) until the bacteria culture reached stationary phase (about 18 hours). At that point, cells were diluted in LB to an optical density of 0.52 at 562 nm using a microplate reader. This value is equivalent to 30% absorbance correlating to a three on the McFarland Scale, or 9×10^8 bacteria per ml. Bacteria were further diluted and inoculated at 3×10^6 cells per well into 96 well flat-bottom culture plates.

SPION solutions in ethanol were centrifuged for 10 minutes at 13,000 rpm. The supernatant was decanted and SPION were redispersed in LB. Solutions were serially

diluted to achieve concentrations of 2 mg/mL, 1 mg/mL, 100 μg/mL, and 10 μg/mL while 50 μL of the decanted supernatant solution possibly containing iron salt and ethanol or LB only (0 mg/ml) served as supernatant controls during each 48 hour experiment. Optical density readings were taken using a microplate reader to determine bacteria number at 12-, 24-, and 48-hour time points.

2.4.3 Bacteria live/dead staining

After 48 hours of culture, plated bacteria were dispersed into culture media and transferred into microcentrifuge tubes. Bacteria were centrifuged at 10,000 rpm for two minutes after which the supernatant was discarded. Cell pellets were redispersed into 300 μL tris buffer solution containing the BacLight Live/Dead solution (Life Technologies Corporation; Carlsbad, CA) at the concentration recommended by the manufacturer and placed onto microscope slides at a volume of 200 μL before cover slips were applied for microscopy purposes. Prepared slides were allowed to dry for at least 24 hours before visualization.

2.4.4 Bacteria viability and image analysis *in situ*

After 48 hours of culture, *in situ* fluorescent images were taken to assess bacteria cluster formation and biofilm formation. Image-Pro Analyzer version 6.2 (Media Cybernetics; Bethesda, MD) was used to quantify either total fluorescent area (TFA) of live or dead bacteria or bacteria colonies. Bacteria colonies were counted as any object larger than a single cell. Similar to the above, red and green fluorescent stains corresponded to live or

dead bacteria clusters, respectively.

2.4.5 Duel screening for biofilm and planktonic inhibitory action

Staphylococcus aureus was obtained in freeze-dried form (#25923; American Type Culture Collection; Manassas, VA). The dry pellet was rehydrated in 6 ml tryptic soy broth (TSB; 15 g per liter double distilled water; MP Biomedical). All further experiments with bacteria were carried out in TSB. The solution was incubated (37 °C, 5% CO_2, humidified environment) and agitated until the bacteria reached late stationary phase (about 24 hours). The second passage was diluted at a ratio of 1:200 into fresh TSB and incubated until late stationary phase whereby it was mixed with equal proportions of 15% glycerol (Sigma Aldrich) and frozen at −80 °C.

Sterile TSB agar plates (TSB-agar) were streaked with frozen bacteria stock, and incubated for 24 hours (ensuring culture purity). Centrifuge tubes were inoculated directly from one colony on TSB-agar prepared with 3 ml of TSB and inoculated with a sterile 10 µL loop (Sigma Aldrich) followed by agitation at 200 revolutions per minute (rpm) until the bacteria culture reached stationary phase at 18 hours. For each experiment, seeding densities were calculated using optical density measurements, after which bacteria were diluted at a ratio of 1:100 in TSB and seeded onto 96-well plates for 24 hours to allow for the formation of a biofilm. At this time, metal conjugated SPION at 1 mg/ml were added or serially diluted to 1:10 or 1:100 before addition. After an additional 24 hours, the average bacteria density was calculated by reading the optical density at 562 nm, and also biofilm density was analyzed using a 0.1% crystal violet solution in water. This solution was added to the biofilms at 175µL, rinsed three times in

PBS, dissolved in 100% ethanol, and analyzed by a spectrophotometer at 562 nm (a schematic of this method is shown in **Figure 2.5**). Control solutions with SPION, but without bacteria, were also included and subtracted from each optical reading. To compare the inhibitory properties of synthesis components or a panel of five antibiotics including penicillin, oxacillin, gentamycin, streptomycin, and vancomycin to SPION, the components were tested under the same conditions after passing through a 0.2 μm sterile filter (Fisher Scientific, Pittsburgh, PA).

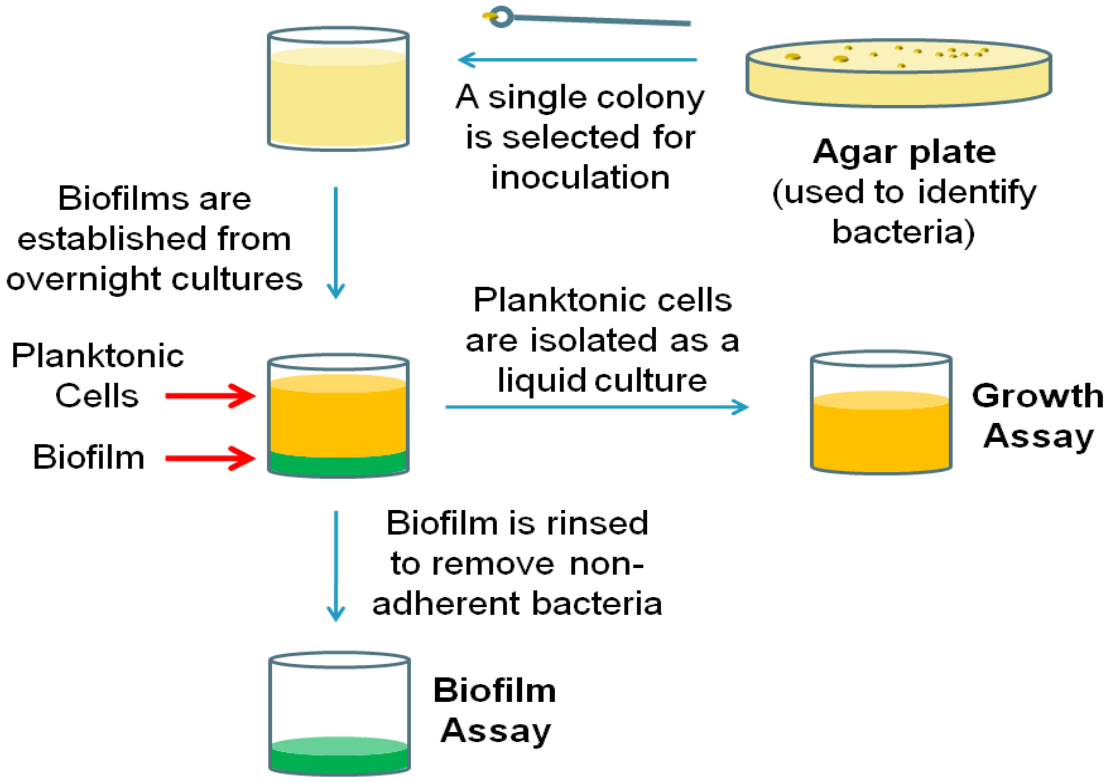

Figure 2.5 This *in vitro* duel screening assay was used to differentiate between planktonic (free floating) and biofilm bacteria. Specifically, bacteria are identified using agar plates, whereby a single colony obtained from a frozen stock, consisting of genetically identical bacteria clones, is used to inoculate an overnight culture (18 hours, 200 revolutions per minute, 37°C) in nutrient rich broth (such as tryptic soy broth; TSB). Biofilms are then established using a high seeding density (~10^7 bacteria colonies per ml), whereby a portion of the bacteria adhere to a given surface upon incubation in standard culture conditions (37°C, 100% humidity, 5% CO_2). Biofilm formation occurs during the 24 hours prior to treatment, and thus planktonic bacteria can be separated and quantified independent to biofilm bacteria. In this method, experimental treatments were applied to this 24-hour biofilm, and planktonic growth and biofilm formation after an additional 24 hours were analyzed using optical density and crystal violet respectively.

2.4.6 Continuous monitoring of antibacterial activity via optical density

Bacteria used were *S. aureus* (#25923) and *S. epidermidis* (#35984) grown for 18 hours streak onto TSB-agar were diluted at a ratio of 1:100 in PBS and seeded onto a 96-well plate for 24 hours (to allow for the formation of a biofilm). At this time, SPION (1 mg/ml) with various antibiotic coatings (estimated at 0.5 mg/ml) were added. For a period of 24 hours, the average bacteria density was calculated every four minutes by reading the optical density using a Spectromax 340PC (Molecular Devices).

2.4.7 Fluorometric determination of intracellular bacillithiol (BSH)

Intracellular bacillithiol (BSH) was determined using a fluorometric method with monochlorobimane as the probe. Monochlorobimane is non-fluorescent, but freely passes through cell membranes, forming a fluorescent adduct in the presence of bacillithiol.[186,187] Importantly, unlike other bimanes such as monobromobimane, monochlorobimane forms fluorescent adducts exclusively with glutathione[184] or bacillithiol,[186,187] and not with other LMW thiols. In particular, bacillithiol is a LMW thiol present in many bacteria species in the Bacilli class of bacteria (the Bacilli class defines many bacteria including the Staphylococcus genus of bacteria, including *Staphylococcus aureus*, and the Bacillus genus, including the common bacteria *Bacillus subtilis*), while glutathione is absent.[186,187] During detection, a 125 ml glass bottle was filled with 100 ml of tryptic soy broth, autoclaved for 15 minutes at 120 °C, and then inoculated with *Staphylococcus aureus*. Centrifuge tubes (15 ml) were filled with 10 ml of bacteria, and centrifuged at 5,000 RPMs for 5 minutes, and the media was discarded. A pellet was collected with about 100 μL of bacteria per centrifuge tube, and redispersed

into 4 ml solutions containing either iron, silver, and zinc conjugated SPION, chelated SPION, or TSB alone. Incubation was then carried out for 24 hours at 37 °C and 200 RPM. At the end of this time period, the bacteria were collected through centrifugation, rinsed with 1 ml PBS, transferred into microcentrifuge tubes, and centrifuged again. At this step 150 µL of 1X lysis buffer (#L6168; Sigma Aldrich) was added to each sample, incubated at 4 °C for 15 minutes, centrifuged at 13,000 RPM for 10 minutes, and finally frozen overnight at -20 °C. To begin the next step, a spectrofluorometer was first turned on with excitation of 390 nm, emission of 500 nm, and allowed to warm up for at least 30-45 minutes (Jobin-Yvon Horiba Fluoromax with a xenon arc lamp). Next, frozen samples in microcentrifuge tubes were allowed to thaw, while a glutathione detection kit from sigma Aldrich was modified for detection of bacillithiol (Kit # CS1020). For this, each microcentrifuge tube containing one sample was treated with the provided assay buffer (825 µL) combined with Glutathione S-Transferase (20 µL) and the substrate solution (10 µL) containing monochlorobimane. The solution was incubated for 1 hour at 37 °C, before analysis by the spectrofluorometer. For estimation of concentration of bacillithiol, reduced glutathione was used, and a standard curve was developed for this using the same parameters as above.

2.4.8 Bacterial transmission electron microscopy

Transmission electron microscopy was used to visualize the interactions of bacteria with SPION. For this, biofilms were grown *in vitro* for 48 hours using overnight inoculums diluted at 1:100 in a 12 well plate on glass slides. SPION (1 mg/ml) were applied for two hours, and the supernatant was collected. The biofilm was then rinsed with 1 ml of

phosphate buffered saline, and the supernatant collected. The collected supernatants were centrifuged at 5000 revolutions per minute (RPM) for 5 minutes, and fixed with 2.5% glutaraldehyde in 0.1M sodium cacoadylate buffer at pH 7.4 with 0.1M sucrose, then gently agitated, and resuspended for 1 hour. The preparation was made into a pellet and rinsed three times with the buffer solution, followed by resuspension in 1% osmium tetraoxide as a contrast agent in buffer. A firm pellet was formed at this stage using 10,000 RPM for 5 minutes, rinsed in deionized water three times, suspended in 2% agar, and water was removed by successive ethanol rinses of 25%, 50%, 75%, 95%, 100%, 100%, and 100%, allowing between 20-40 minutes for each stage. Finally, the pellet was fixed with resin using successive curing stages in ethanol of 1:2, 1:1, 3:1, and finally 100% resin which was cured for 18 hours at 60°C (buffer, osmium tetraoxide, and resin were all purchased from Electron Microscopy Sciences, Hatfield, PA).

2.4.9 Magnetic iron uptake assay into biofilm

Prussian Blue (a histology stain creating a blue by-product in the presence of iron) was carried out to qualitatively determine the amount of iron deposited into biofilms (**Figure 2.6**). For this, biofilms were grown *in vitro* for 48 hours using overnight inoculums diluted at 1:100 in a 12 well plate on glass slides. SPION (100 μg/ml) were applied for a constant time of 60 minutes with a magnetic field (12.6mm dia. X 5mm thick magnet, 3761 Gauss, and Neodymium; K&J magnetics) exposure of 0, 20, 40, or 60 min. Prussian blue staining was carried out using a 10% solution of potassium ferricyanide mixed just prior to staining with an equal proportion of 10% hydrochloric acid (this combination reacts with Fe(II) to produce a blue colored precipitate), and was then

applied to the biofilm and allowed to react with the *S. aureus* biofilms for 15 minutes. Iron deposition was analyzed based on the amount of blue staining, and documentation was carried out using a digital camera (Powershot A570 IS; Canon, Lake Success, NY).

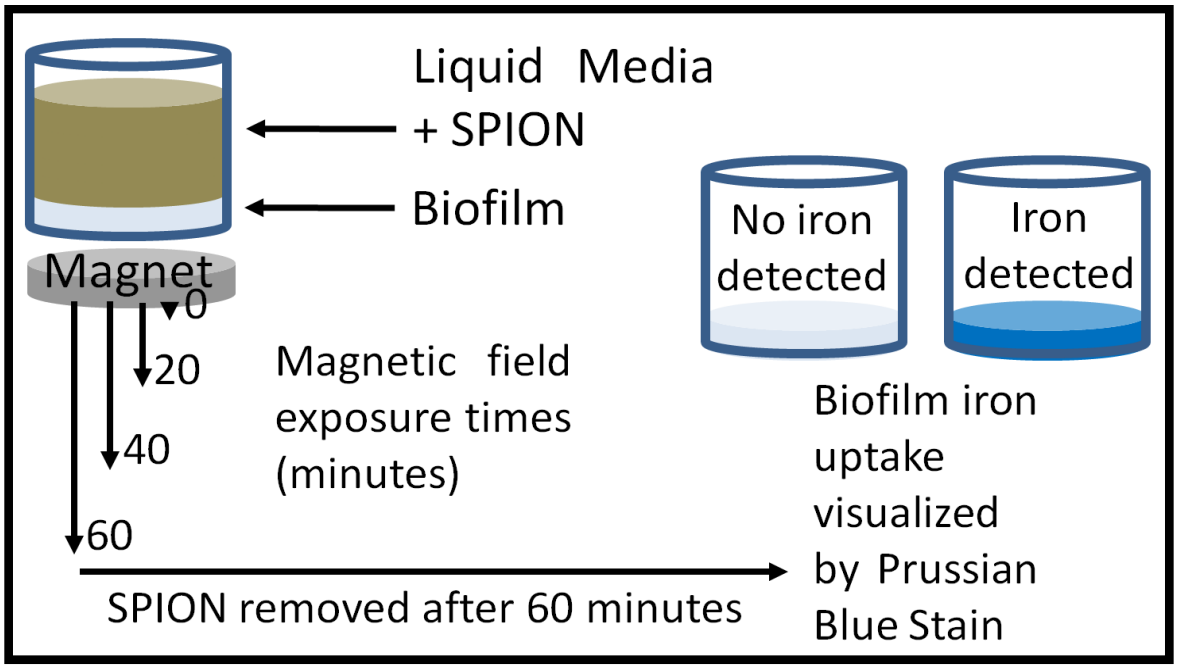

Figure 2.6 Workflow for detection of SPION biofilm uptake in the presence of a magnetic field. Biofilms were grown in 12 well plates on glass slides for 48 hours, and then exposed to SPION in liquid media (TSB). A magnetic field (generated by a 12.6mm dia. X 5mm thick magnet, 3761 Gauss, and Neodymium; K&J magnetics) was applied for a duration of either 0, 20, 40, or 60 minutes, and after 60 minutes, SPION were removed from all wells, and Prussian Blue staining was carried out. Using this method, deposits of blue staining material indicates the presence of iron, whereas no staining indicates that no iron was detected.

2.4.10 Magnetic bacteria separation

Overnight cultures of bacteria were centrifuged, re-dispersed into phosphate buffered saline, and diluted 1:10. SPION were added at a concentration of 1 mg/ml, and mixed well with the solution, and allowed two hours prior to magnetic field exposure with a BZXOXOXO neodymium block magnet (4" x 1" x 1", 4871 Gauss, and Neodymium; K&J magnetics, Jamison, PA).

2.5 Statistical analysis

All experiments were conducted in triplicate and repeated at three different times. Experimental data were analyzed statistically using a Student *T*-test, to determine statistical differences between the mean, *F-test*, to determine if the variance was equal between data sets, and commercially available programs (Excel, Microsoft; Seattle, WA, USA).

3. Results

3.1 Characterization of nanoparticles

3.1.1 Uncoated and CaP coated SPION

3.1.1.1 X-ray diffraction

For calcium phosphate coated nanoparticles, the first goal of this study was to determine the crystal structure of either calcium phosphate (CaP) coated or uncoated SPION. **Figure 3.1** shows the XRD pattern for the uncoated and Calcium Phosphate (CaP)-coated magnetite (Fe_3O_4) SPION. The peaks for the nanoparticle samples were matched with the pattern for Fe_3O_4 and hydroxyapatite (a crystalline type of CaP found in bone) standards. The Fe_3O_4 SPION sample XRD peaks matched those of the bulk Fe_3O_4 standard and so did the CaP coated Fe_3O_4 SPION formulated in the presence of CA, but the peaks for the CaP-coated Fe_3O_4 SPION formulated in the presence of BSA did not match those of bulk Fe_3O_4. Also, only CaP-coated Fe_3O_4 SPION formulated in the presence of BSA showed an exact match for the hydroxyapatite standard while CaP-coated Fe_3O_4 SPION formulated in the presence of CA displayed other phases of CaP. Uncoated and CaP-coated maghemite (γ-Fe_2O_3) SPION XRD diffraction patterns are shown in **Figure 3.2.** All three samples matched the bulk γ-Fe_2O_3 standard and both CaP-coated γ-Fe_2O_3 SPION also matched the hydroxyapatite standard.

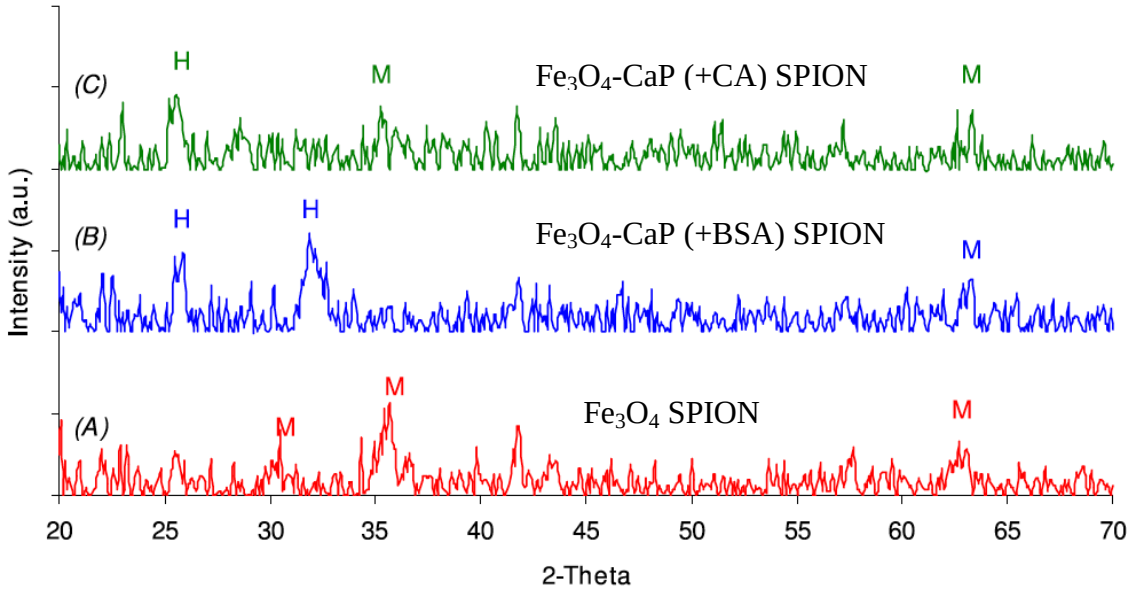

Figure 3.1 X-ray diffraction patterns for (A) magnetite (Fe_3O_4) SPION, (B) Fe_3O_4 SPION coated with CaP in the presence of BSA, and (C) Fe_3O_4 SPION coated with CaP in the presence of CA. BSA = bovine serum albumin; CA = citric acid; H = hydroxyapatite peak; M = magnetite peak.

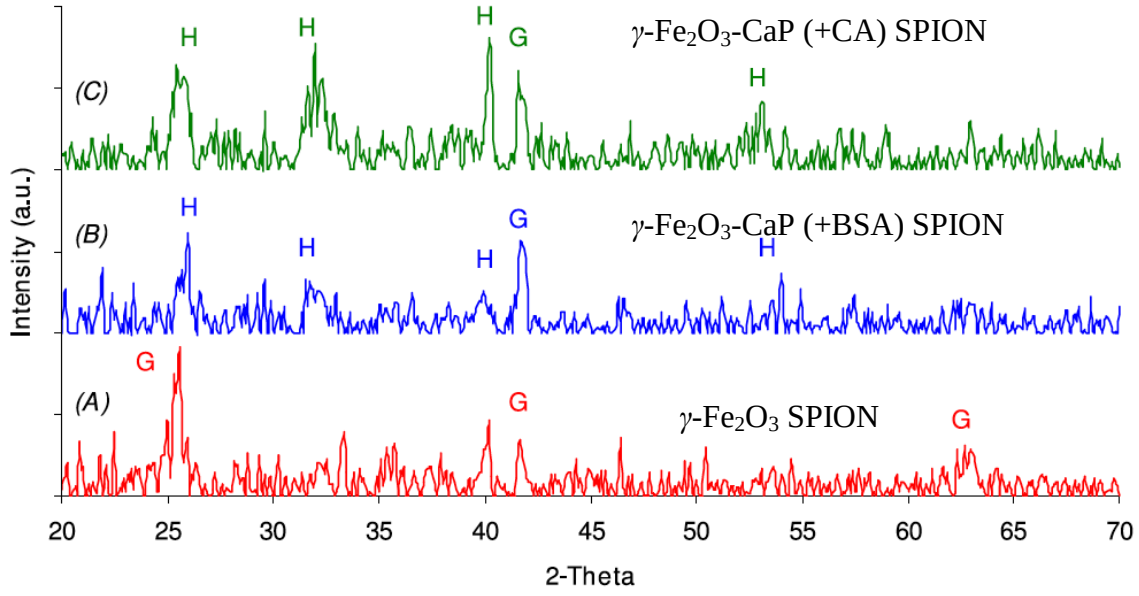

Figure 3.2 X-ray diffraction patterns for (A) maghemite (γ-Fe_2O_3) SPION, (B) γ-Fe_2O_3 SPION coated with CaP in the presence of BSA, and (C) γ-Fe_2O_3 SPION coated with CaP + CA. BSA = bovine serum albumin; CA = citric acid; H = hydroxyapatite peak; G = maghemite peak.

3.1.1.2 Characterization of magnetic properties

VSM measurements were taken for all the dry powdered SPION samples, showing that each sample possessed magnetic properties. The maximum electromagnetic unit (emu) per gram for each sample is shown in **Table 3.1**. γ-Fe_2O_3 SPION had higher magnetic saturations compared to Fe_3O_4 SPION (this was also true for the CaP-coated γ-Fe_2O_3 SPION). As expected, because of the higher magnetic crystal content, uncoated SPION had higher magnetic properties than CaP-coated SPION. Between CaP-coated SPION, those synthesized in the presence of CA had higher magnetic saturations compared to those synthesized in the presence of BSA. **Figure 3.3** compares the normalized magnetization curves (hysteresis loop) of the uncoated and CaP-coated Fe_3O_4 SPION formulated in the presence of BSA and CA. **Figure 3.4** compares the normalized magnetization curves (hysteresis loop) of uncoated and CaP-coated γ-Fe_2O_3 SPION formulated in the presence of BSA and CA.

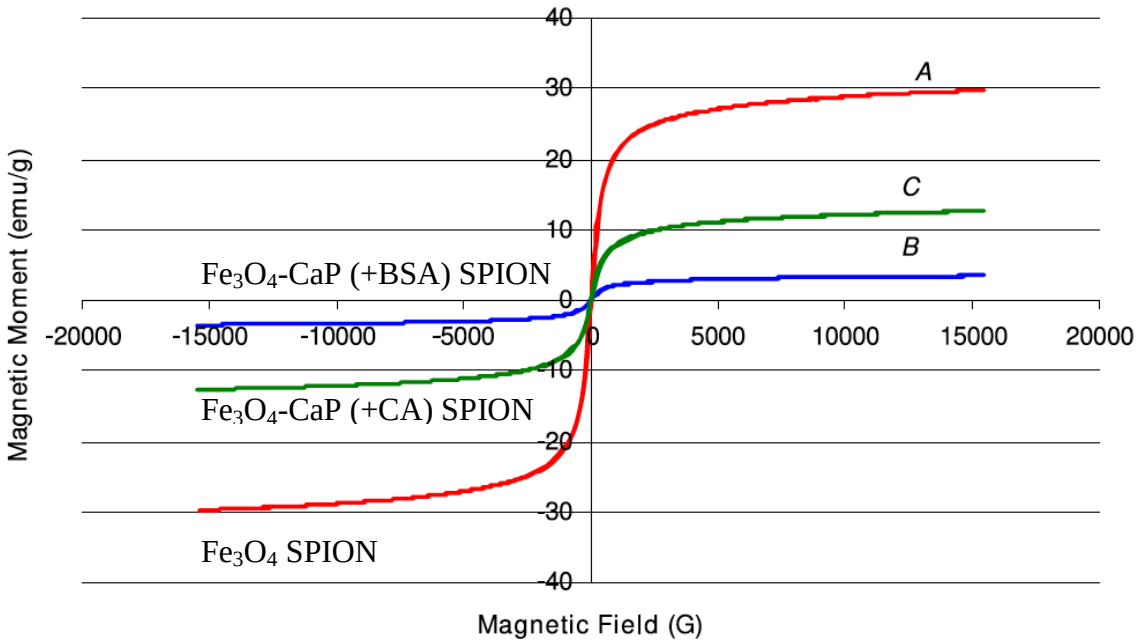

Figure 3.3 Normalized magnetization curves of (A) uncoated and CaP-coated Fe_3O_4 SPION in the presence of either (B) BSA or (C) CA as measured by VSM at room temperature. BSA = bovine serum albumin; CA = citric acid.

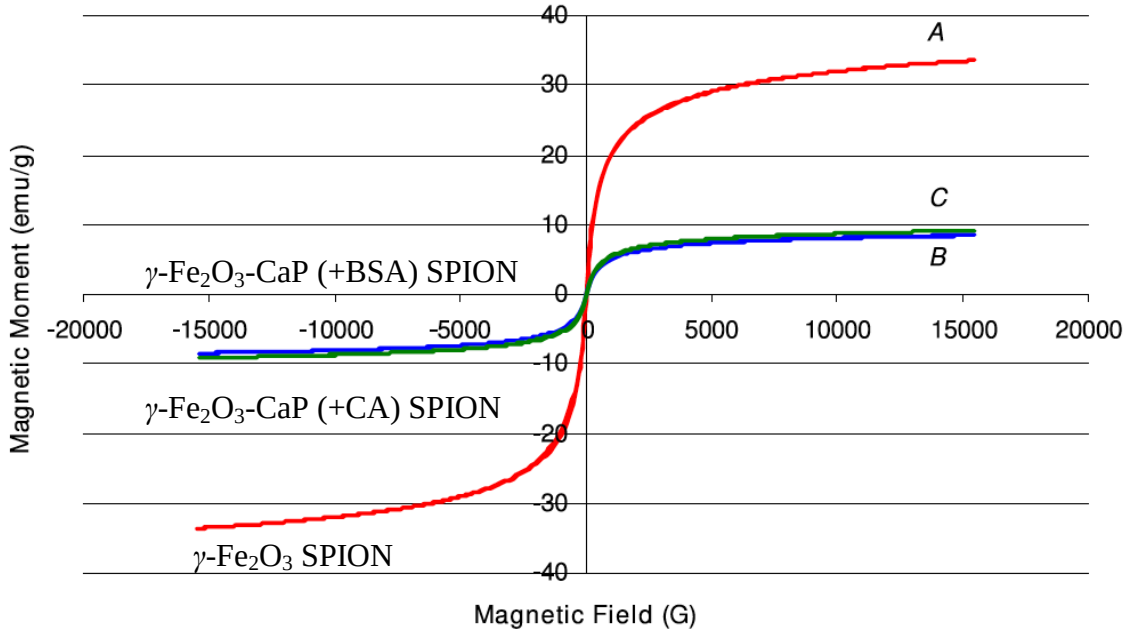

Figure 3.4 Normalized magnetization curves of (A) uncoated and CaP-coated γ-Fe_2O_3 SPION in the presence of (B) BSA or (C) CA as measured by VSM at room temperature. BSA = bovine serum albumin; CA = citric acid.

Table 3.1 Vibrating sample magnetometery (VSM) readings of dried samples.

Sample	**emu/g**
Fe_3O_4	29.77
Fe_3O_4-CaP (+BSA)	3.47
Fe_3O_4-CaP (+CA)	12.67
γ -Fe_2O_3	33.58
γ -Fe_2O_3-CaP (+BSA)	8.48
γ -Fe_2O_3-CaP (+CA)	9.12

The electromagnetic unit (emu) maximum per gram is shown for each sample. BSA = bovine serum albumin and CA = citric acid.

3.1.1.3 Characterization of morphology

TEM was used to characterize the morphologies of the various SPION. The uncoated samples are shown in **Figure 3.5**. The as prepared Fe_3O_4 SPION displayed a cubic structure with only one phase visible and diameters less than 10 nm. γ-Fe_2O_3 SPION were very similar in shape and size (~15 nm) but seemed more agglomerated, possibly due to higher emu/g as shown in **Table 3.1** and the lack of any surfactant. The γ-Fe_2O_3 SPION also appeared finer than Fe_3O_4 SPION, possible due to a lower standard deviation of particle size (**Figure 3.5**). With the CaP-coated SPION, two different phases were observed (**Figure 3.6**). The iron oxide particles were seen as dark cubes and spheres, and the CaP coatings as an amorphous surrounding. The iron oxide particles could be seen encapsulated within the needle-like arrays of the CaP sheath. The SPION were less agglomerated after CaP coating, and in the presence of both BSA and CA. **Table 3.2** gives an estimation of SPION sizes as measured by TEM micrographs.

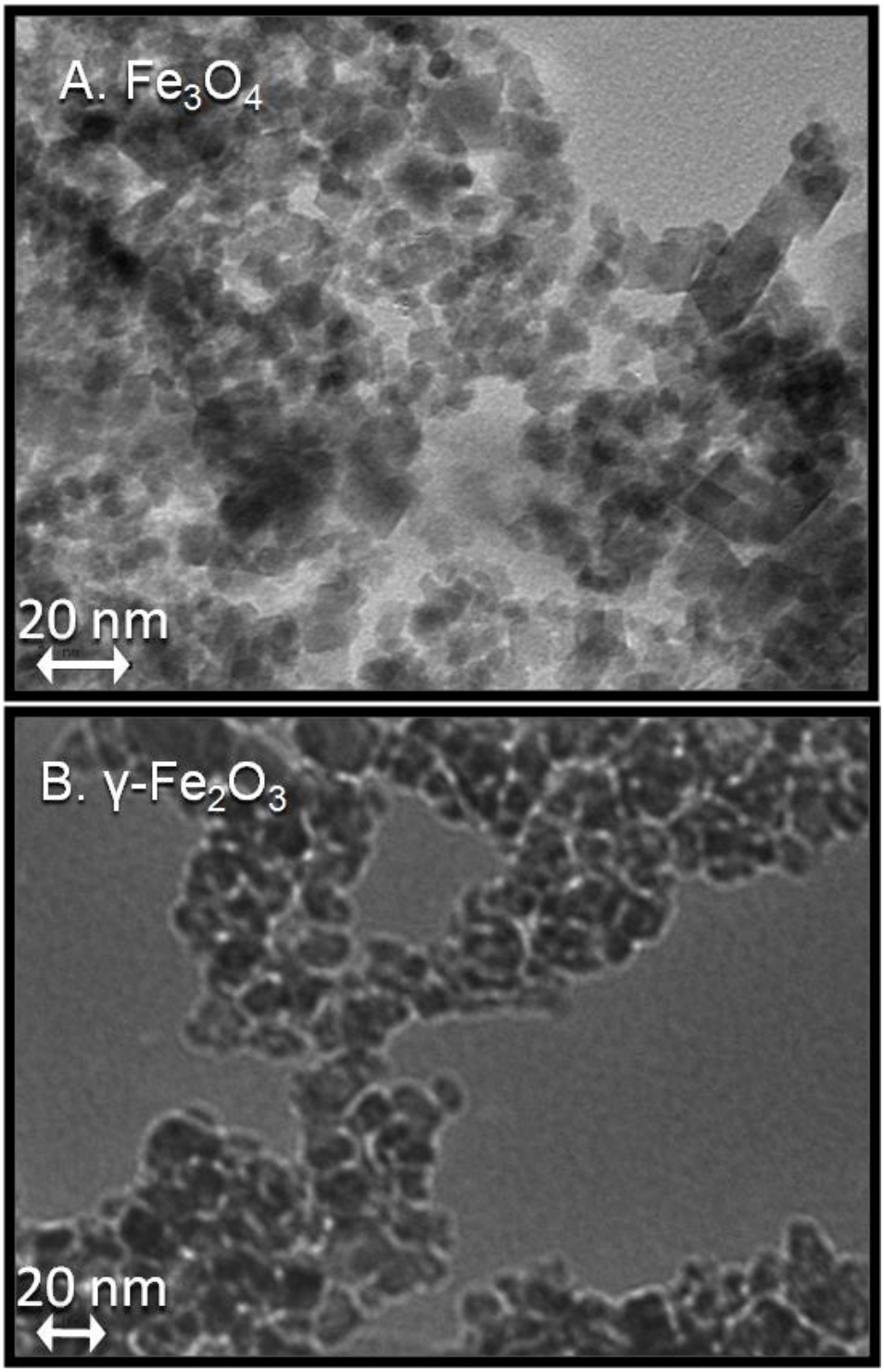

Figure 3.5 TEM images of (**A**) magnetite (Fe_3O_4) nanoparticles, and (**B**) maghemite (γ -Fe_2O_3) SPION. The images were collected on a Philips JEOL at an operating voltage of 120 kV.

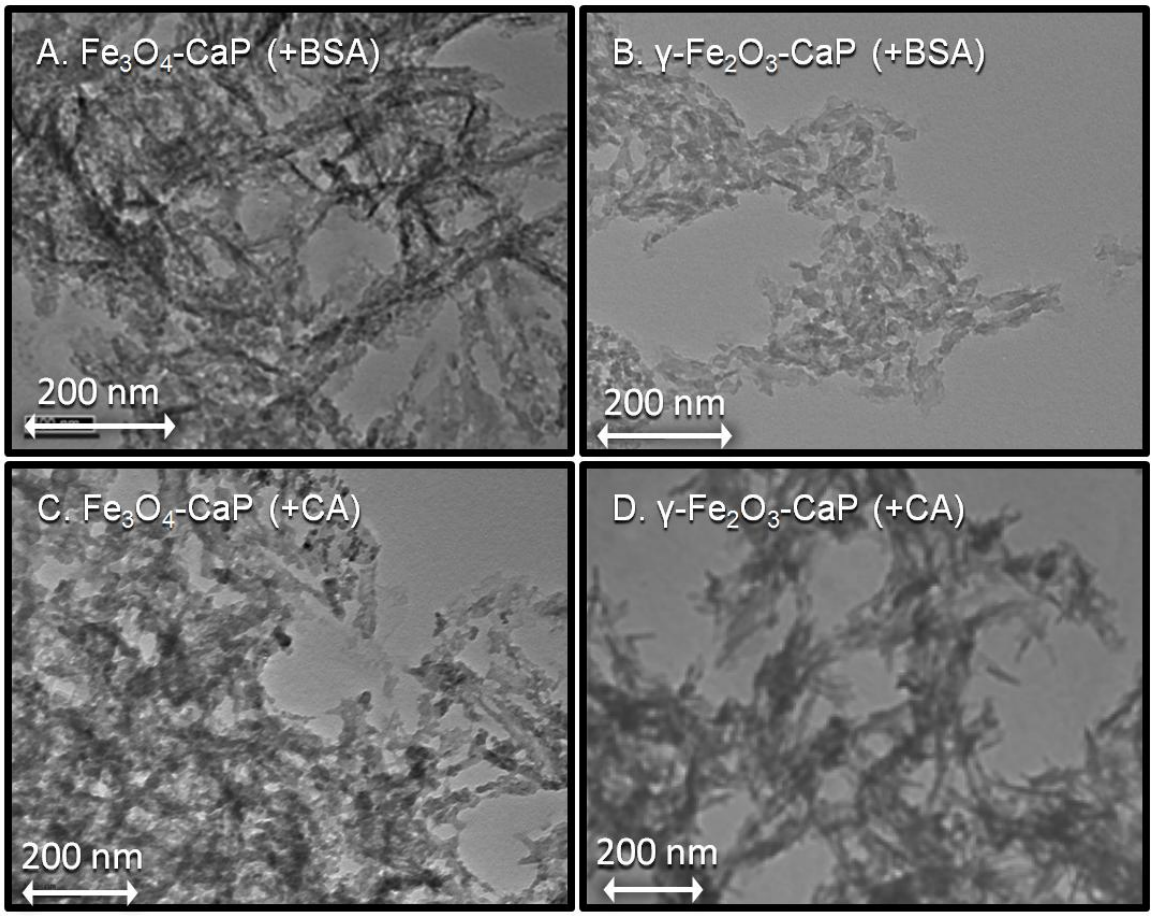

Figure 3.6 SPION formulations coated with calcium phosphate in the presence of surfactants including (**A**) CaP-coated Fe_3O_4 SPION dispersed in BSA, (**B**) CaP-coated γ-Fe_2O_3 SPION dispersed in BSA, (**C**) CaP-coated Fe_3O_4 SPION dispersed in CA, and (**D**) CaP-coated γ-Fe_2O_3 SPION dispersed in CA. The images were collected on a Philips JEOL at an operating voltage of 120 kV. BSA = bovine serum albumin; CA = citric acid.

Table 3.2 Particle size analysis of magnetic nanoparticles, uncoated and coated.

Sample	**Size (nm) ± standard deviation**
Fe_3O_4	11.5 ± 3.5
Fe_3O_4-CaP (+BSA)	125 ± 25 long, 50 ± 10 wide
Fe_3O_4-CaP (+CA)	125 ± 25 long, 50 ± 10 wide
γ -Fe_2O_3	12.5 ± 2.5
γ -Fe_2O_3-CaP (+BSA)	125 ± 25 long, 50 ± 10 wide
γ -Fe_2O_3-CaP (+CA)	175 ± 25 long, 65 ± 15 wide

3.1.2 Chelated SPION and conjugations of metal ions

SPION were successfully synthesized using high temperature reflux of Iron(III) acetylacetonate in triethylene glycol and were chelated with dimercaptosuccinic acid (DMSA), then conjugated via a two-step process to produce iron, zinc, and silver conjugated SPION. The physical and chemical properties of these preparations were characterized using transmission electron microscopy (TEM), vibrating sample magnetometry (VSM), zeta potential measurements, and inductively coupled plasma atomic emission spectroscopy (ICP-AES).

3.1.2.1 TEM analysis of chelated SPION

SPION as produced could not be separated from solution with a magnet because of their small size and because they did not form agglomerates, so 175 mL of 100% ethanol saturated with ammonium sulfate was added, producing larger agglomerates which could then be isolated. DMSA is also known to form disulfide bonds, so SPION were

refrigerated and stored in 100% ethanol to prevent oxidation. These SPION prior to coating were well dispersed in various media (tryptic soy broth, PBS, and 0.85% NaCl), and had an average size of about 9.92 +/- 3.14 nm as determined by manual measurement of SPION size **(Figure 3.7)**.

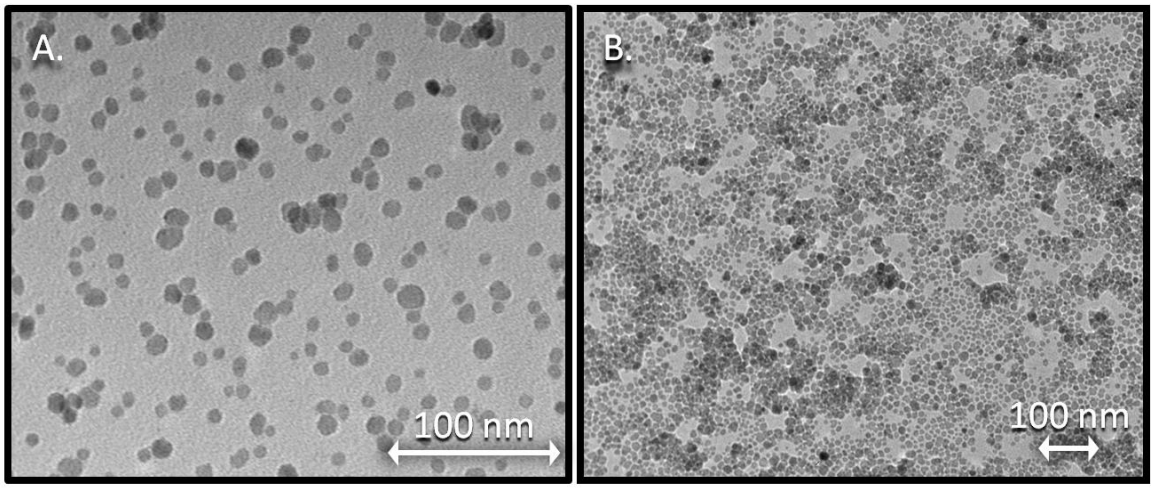

Figure 3.7 SPION prepared by refluxing iron (III) acetylacetone in triethylene glycol (TREG) analyzed by transmission electron microscopy (TEM). These representative images demonstrate the uniform quality of nanoparticles prepared here after drying onto a formvar coated copper TEM grid (magnification of A. 112K and B. 350K; scale bars = 100nm).

3.1.2.2 X-ray diffraction (XRD) to determine crystal structure of chelated SPION

XRD was carried out and compared to patterns obtained from the bulk magnetite crystal phase reference Joint Committee on Powder Diffraction Standard (JCPDS) card #75-1609, indicating that this is the primary phase of iron oxide present (**Figure 3.8**). Using the Scherrer formula shown in **equation 2.1** where $\beta = 1.05° +/- 0.05$ and $2\theta = 35.4, 30.1, 43, 57$, and 62.5 (then converted to radians) with the mean diameter of SPION crystallites

estimated from averaging of the fives peaks to be 8.65 +/- 0.24 nm.

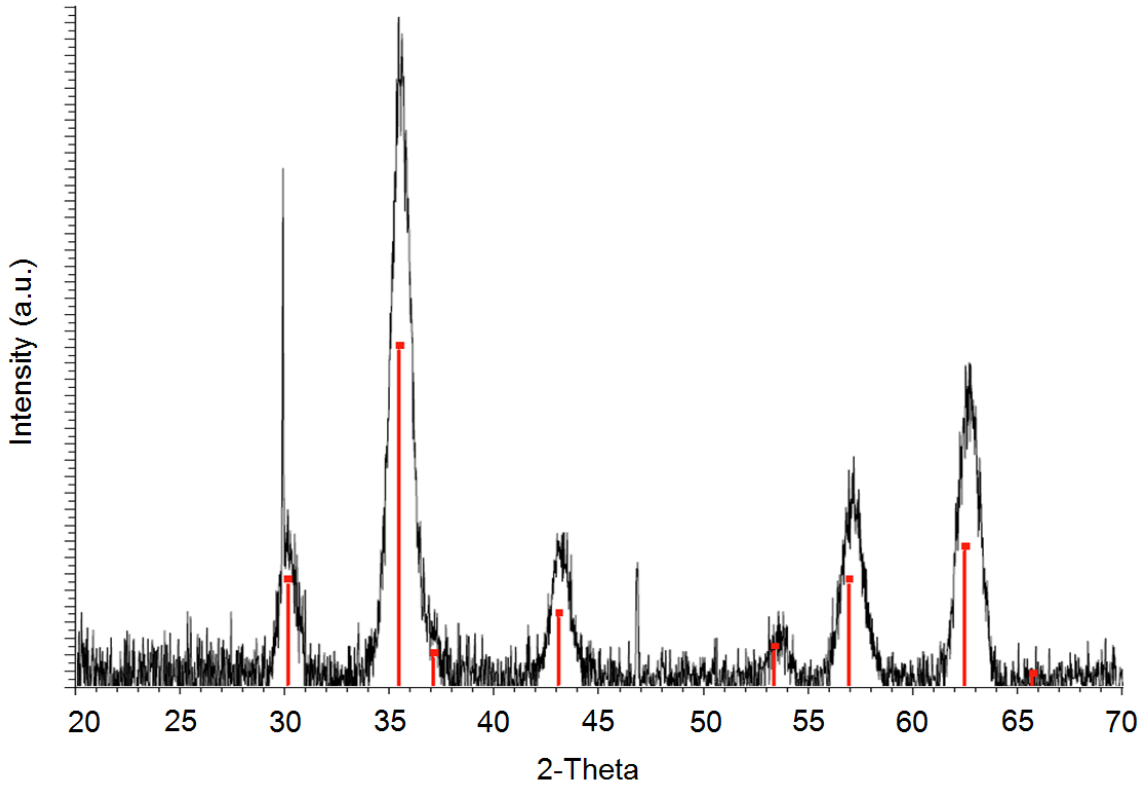

Figure 3.8 XRD pattern of SPION prepared by loading onto a glass crucible. Matching peaks (shown as red lines) indicate magnetite crystal phase from bulk reference JCPDS card #75-1609.

3.1.2.3 VSM for magnetic properties of chelated SPION

VSM was used to determine the saturation magnetization of chelated SPION, and metal conjugates (emu/g; **Table 3.3**). Uncoated SPION had a saturation magnetization of 58.625 emu/g, or 63.723% of bulk magnetite, which has a saturation magnetization of 92 emu/g.[248,249] Zinc and iron conjugated SPION had a lower value than uncoated SPION, with both about 25% of bulk magnetite, while silver coated SPION had higher magnetic properties, demonstrating a magnetic moment 99.497% of bulk magnetite.

Table 3.3 Characterization of chelated SPION, or metal conjugated SPION using vibrating sample magnetometry (VSM) demonstrating saturation magnetization.

Type of SPION	Magnetic moment (emu/g)	% bulk magnetite*
Iron conjugated	23.875	25.951%
Zinc conjugated	22.625	24.592%
Silver conjugated	91.537	99.497%
Chelated	58.625	63.723%

The magnetic moment of bulk magnetite is 92 emu/g.[248,249]

3.1.2.4 Zeta potential for surface charge of chelated SPION

Zeta potential was used to determine the surface charge of SPION after dispersal into TSB. Zeta potential experiments determined that all chelated or metal conjugated SPION have a negative surface charge and this charge further decreased with the zinc and silver conjugations, or increased after the iron conjugation **(Table 3.4)**.

Table 3.4 Characterization of metal conjugated SPION, or chelated SPION with no additional metal ion conjugate, using zeta potential (demonstrating surface charge).

Type of SPION	Zeta potential (mV)
Iron conjugated	-34.0
Zinc conjugated	-40.1
Silver conjugated	-43.2
Chelated	-35.5

3.1.2.5 Chemical Composition of Chelated SPION determined by ICP-AES

ICP-AES was used to quantify the chemical properties of the SPION produced here before and after metal conjugations**,** and these values were normalized to equivalents of Fe_3O_4 or DMSA (**Figure 3.9**). TSB normally contains iron (~0.938 +/- 0.230 µg/ml), sulphur (~110.313 +/- 2.104 µg/ml), and zinc (~1.288 +/- 0.018 µg/ml) which were subtracted from these readings, but does not normally contain silver. Some of the sulfur present in TSB is contributed from amino acids cysteine and methionine in addition to sulfate added during digestion of the 17g casein (milk protein) digest and 3g soybean meal (a dry soybean product) digest (as determined from the manufacturer on a per liter basis). Reacting chelated SPION with zinc increase the quantity to 147.213 +/- 91.535 µg/ml zinc, or reacting chelated SPION with silver increased the quantity to 183.100 +/- 28.310 µg/ml silver.

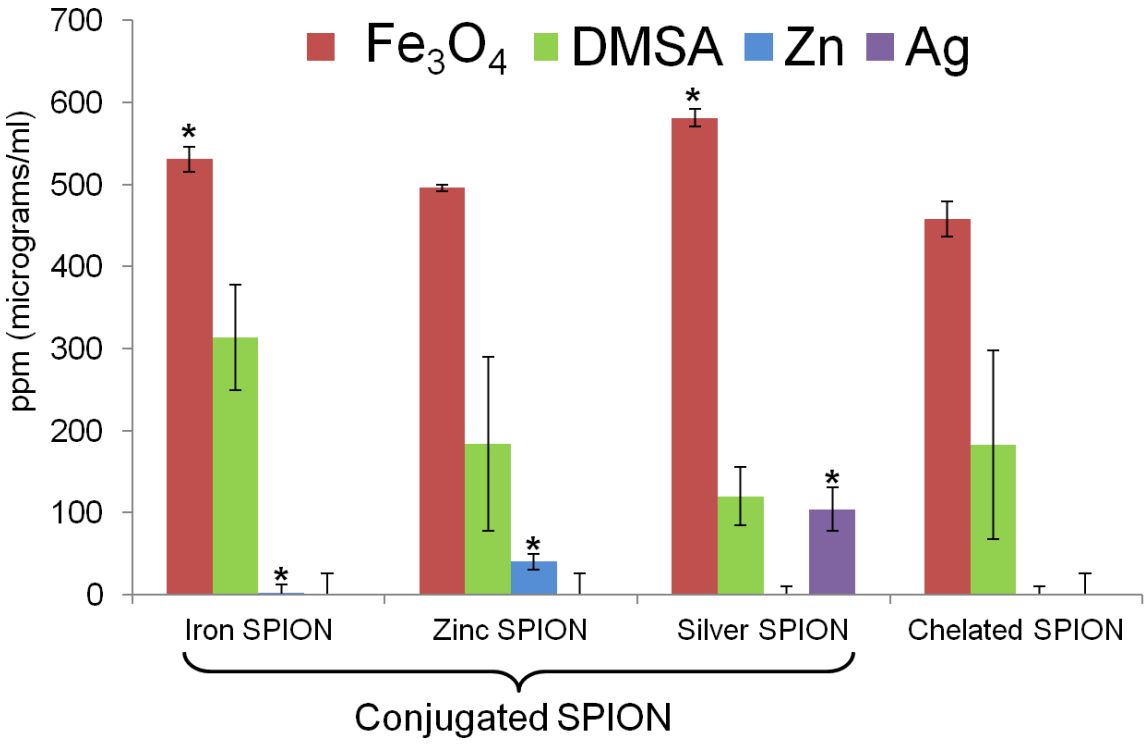

Figure 3.9 Elemental composition of metal conjugated SPION, or chelated SPION, as determined by inductively coupled plasma atomic emission spectroscopy (ICP-AES) after digestion of respective nanomaterials in hot aqua regia, followed by dilution into 2% nitric acid for analysis. The concentration of iron and sulfur were normalized to give the equivalent concentrations of Fe_3O_4 and DMSA, and the contents of TSB including iron (~0.938 +/- 0.230 µg/ml), sulphur (~110.313 +/- 2.104 µg/ml), and zinc (~1.288 +/- 0.018 µg/ml) were subtracted. A increase in the concentration of Fe_3O_4, silver, and zinc were observed in coated SPION with *P value is significant at 5% compared to control (data = mean +/- standard error, N=3).

Furthermore, increasing concentrations of metals added to SPION was also tested, with either 1 mmol (the same concentration shown in **Figure 3.9**) or 4 mmol of metal added (a comparison of both shown in **Figure 3.10**). It was determined that by increasing the concentration of metals, an increase was found in either silver (when $AgNO_3$ salt was

added) or zinc (when any other metal salt was added; the concentration of zinc in $FeCl_3$ salt is ~0.002% as a trace contaminate, contributing 0.541 mg or 2.162 mg total to the 1 mmol or 4 mmol iron formulations, respectively).

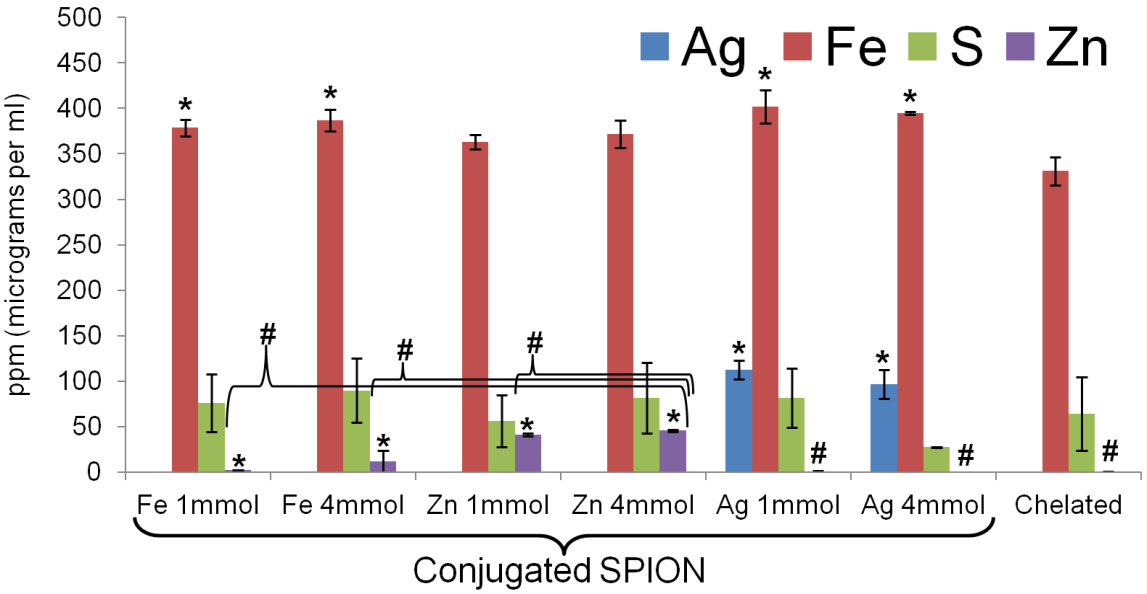

Figure 3.10 Elemental composition of increasing concentration of metal with conjugated SPION, or chelated SPION, as determined by inductively coupled plasma atomic emission spectroscopy (ICP-AES) after digestion of respective nanomaterials in hot aqua regia, followed by dilution into 2% nitric acid for analysis. The contents of TSB including iron (~0.938 +/- 0.230 µg/ml), sulfur (~110.313 +/- 2.104 µg/ml), and zinc (~1.288 +/- 0.018 µg/ml) were subtracted. Significance was observed in concentration of iron, zinc, and silver with *P values compared to chelated SPION and #P values compared to zinc 4 mmol, both at the 5% level. Importantly, zinc 4 mmol SPION contained the highest concentration of zinc (45.738 +/- 1.301 µg/ml) compared to other formulations (0.163 +/- 0.020 in silver 1 mmol SPION to 40.163 +/- 0.765 µg/ml in zinc 1 mmol SPION; data = mean +/- standard error, N=3).

ICP-AES was also used to quantify the concentration free metal ions in solution as released from SPION (**Figure 3.11**). The zinc 4 mmol SPION formulations contained 45.738+/- 1.301 ppm zinc (= µg/ml zinc), and released about 10.790 ppm after 4 hours as free ions, whereas other formulations released between 0.922 – 2.256 ppm at same time point (**Figure 3.11**). These later values were comparable to TSB, which normally contains 1.29 ppm of zinc, whereas with Zn 4 mmol SPION formulation, 836% of this amount of zinc was released at 4 hours.

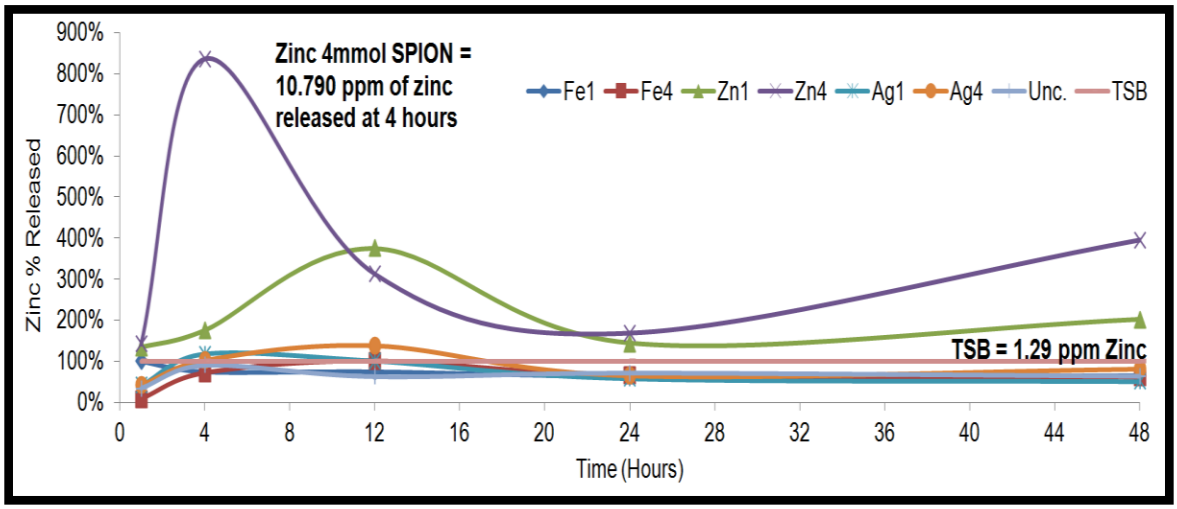

Figure 3.11 ICP-AES determined the release of free metal ions. At 4 hours, 10.790 ppm of zinc was released by zinc 4 mmol, whereas other formulations released 0.922 – 2.256 ppm zinc at the same time point (data = mean, normalized to the concentration of released elements from TSB; N=3).

3.1.2.6 DLS for particle sizing of chelated SPION

DLS readings were obtained after 1:10 dilution for all preparations of chelated SPION. Prior to sterile filtration, chelated, zinc conjugated, and iron conjugated SPION had

several detectable sizing peak ranges with one around 15 nm, one around 100 nm, and another around 1000 nm; while silver conjugated SPION only had the larger two peak ranges. TSB alone demonstrated peaks around 100 nm and 1000 nm. Some similarity between peaks in TSB could be seen between those found in other samples, making it difficult to distinguish between peaks present due to TSB and those due to nanoparticles, although the smaller peaks dominated in nanoparticle samples as shown by the averages (**Table 3.5;** unfiltered particle size). To remove background noise contributed from TSB, sterile filtration was used through a 0.2 µm filter, which was smaller than the average peak size in TSB of 479.25 +/- 67.85 nm. Using this method, smaller particle averages were obtained, whereas TSB gave no detectable background readings alone (**Table 3.5**; filtered particle size).

Table 3.5 Particle sizing of chelated SPION and iron, zinc, and silver conjugates using dynamic light scattering (DLS) before and after filtration through a 0.2 µm filter.

Type of SPION	**Unfiltered particle size (nm)**	**Filtered particle size (nm)**
Iron conjugated	82.84 +/- 16.58	23.32 +/- 1.17
Zinc conjugated	58.62 +/- 16.85	19.67 +/- 0.72
Silver conjugated	699.95 +/- 18.47	193.72 +/- 6.15
Chelated	167.98 +/- 43.62	19.93 +/- 1.31
TSB	479.25 +/- 67.85*	No Data**

*Unfiltered readings with TSB were carried out to determine background noise. **Filtered readings removed background noise from TSB to an undetectable level.

3.1.3 Conjugation of antibiotics to SPION

FTIR determined conjugation of antibiotics was successful **(Figure 3.12)**. It was found that after magnetically separating SPION, and decanting non-magnetic components, antibiotic conjugated SPION exhibited functional groups unique to the gentamicin coating found at 1690 cm^{-1} demonstrating a carboxylic acid associated with an amide (created by sulpho-SMCC conjugation) and other peaks that were apparent only after coating at 1195 and 1210 cm^{-1} demonstrating aliphatic nitro-compounds (amine are only found in the antibiotics, but not other components used to make SPION). Vancomycin coated SPION had similar amide (1635 cm^{-1}) and amine (1045, 1105, and 1165 cm^{-1}) peaks, along with an aromatic ether group (at 1290 cm^{-1}), although the magnitude of these characteristic peaks were smaller than found from the gentamicin coating indicating that a lower concentration of vancomycin was present at the surface.

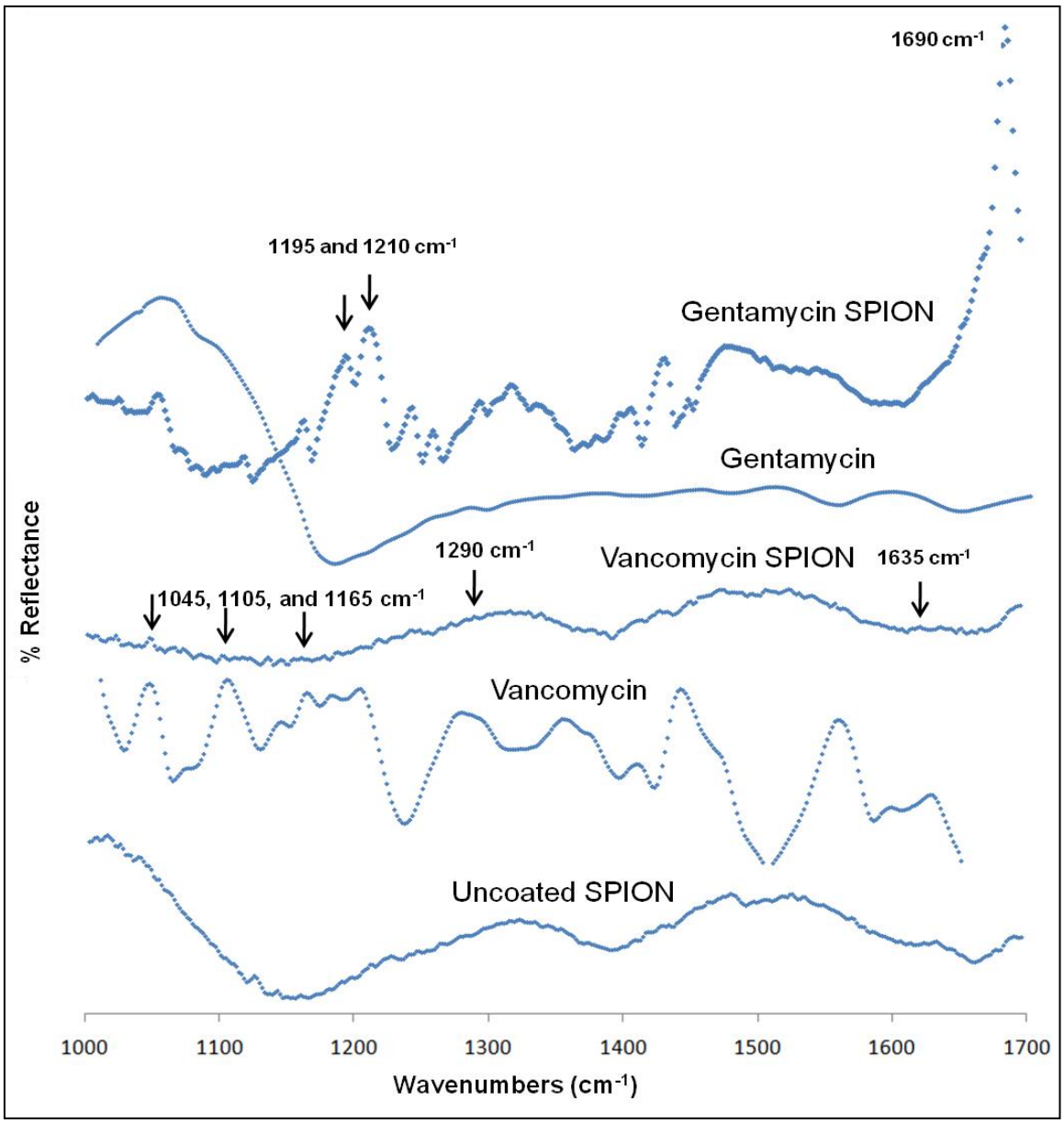

Figure 3.12 FTIR Spectra of antibiotic coated SPION compared to uncoated SPION, or vancomycin and gentamicin antibiotics alone. Matching functional groups are demonstrated and the peaks are provided. Gentamicin SPION characteristic peaks were larger than the vancomycin SPION characteristic peaks, indicating a higher coating concentration.

3.2 Osteoblasts Proliferation

3.2.1 Osteoblast proliferation in the presence of SPION

Preliminary data indicated that presently created SPION were non-toxic to bone cells, and some formulations even improved bone cell metabolic activity. Initial 1 day cell proliferation assays indicated that osteoblast density was similar in the presence of Fe_3O_4 and γ-Fe_2O_3 SPION when compared to the controls (i.e. osteoblasts grown on a polystyrene cell culture plate without nanoparticles; **Figure 3.13**). In contrast, after 5 and 8 days, osteoblast density in the presence of γ-Fe_2O_3 nanoparticles was significantly greater than controls while Fe_3O_4 was similar to the controls **(Figure 3.13)**.

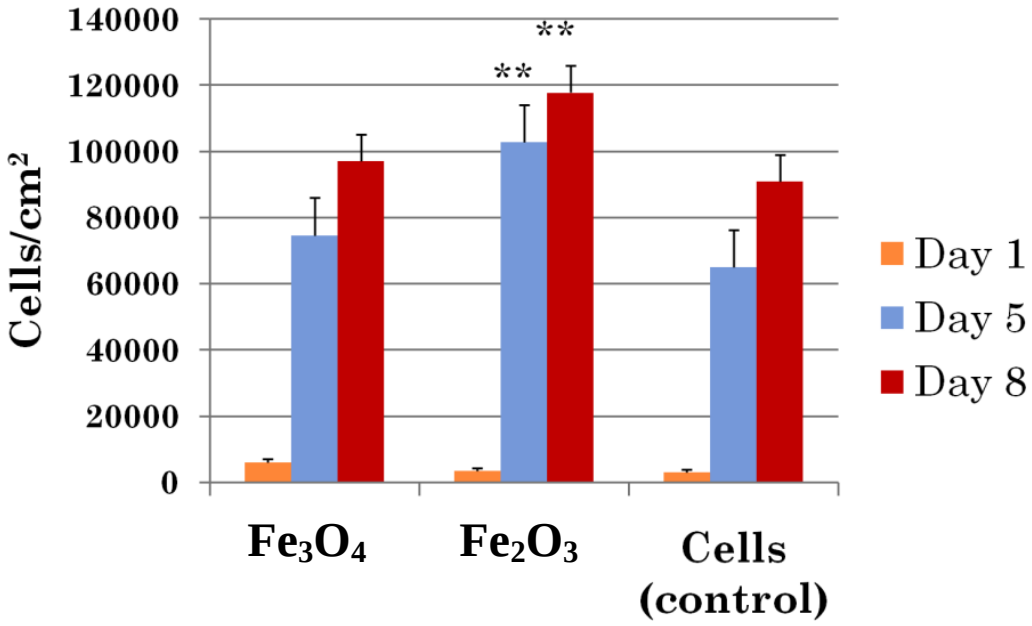

Figure 3.13 Enhanced osteoblast density in the presence of γ-Fe_2O_3 SPION. P values assessed at the 1% level are denoted ** and error bars indicate standard error (N=3).

3.2.2 Osteoblast proliferation in the presence of CaP coated SPION

Osteoblast density was also similar in the presence of CaP coated Fe_3O_4 nanoparticles (synthesized in the presence of both BSA and CA) compared to the controls **(Figure 3.14)**. Osteoblast density in the presence of the uncoated and CaP-coated γ-Fe_2O_3 synthesized with CA was similar to the controls, while for the CaP-coated γ-Fe_2O_3 synthesized with BSA, osteoblast density after 24 h was significantly higher ($p < 0.05$) than the controls as shown in **Figure 3.14**.

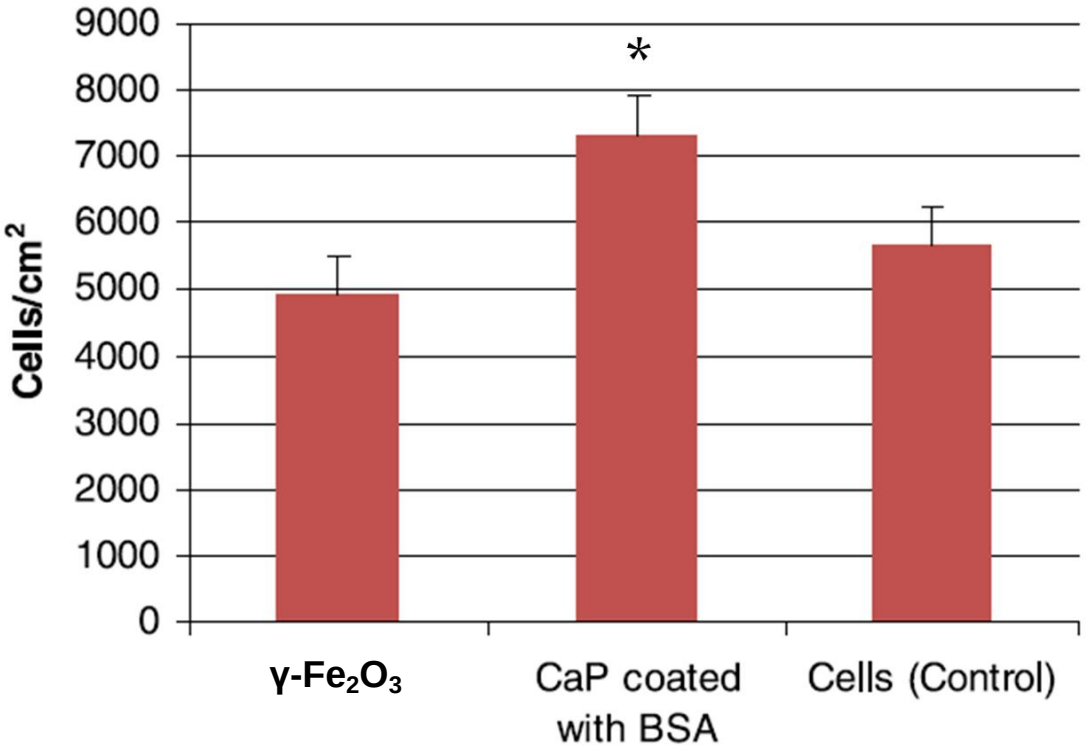

Figure 3.14 Calcium phosphate coated γ-Fe_2O_3 SPION further enhanced osteoblast function at day 1. P values assessed at the 1% level are denoted ** and error bars indicate standard error (N=3).

3.3 Inhibition of bacteria functions

3.3.1 Uncoated Fe_3O_4

3.3.1.1 Bacteria inhibition in the presence of uncoated Fe_3O_4

Next, bacteria studies were carried out to determine simultaneously if SPION could impact planktonic growth and/or biofilm growth. Optical density studies indicated progressively decreased *S. epidermidis* density at all time points (12, 24, and 48 hours) when cultured with 100 μg/mL, 1 mg/mL, and 2 mg/mL of SPION **(Figure 3.15)**. This is in contrast with the low SPION concentration of 10 μg/mL for which no significant difference was observed compared to controls (no particles). The SPION supernatant control (possibly containing ethanol and iron salt) did not cause a decrease in bacteria density compared to no particle controls, thus, providing evidence that the SPION (not other chemicals used/created when fabricating such particles) decreased bacteria number.

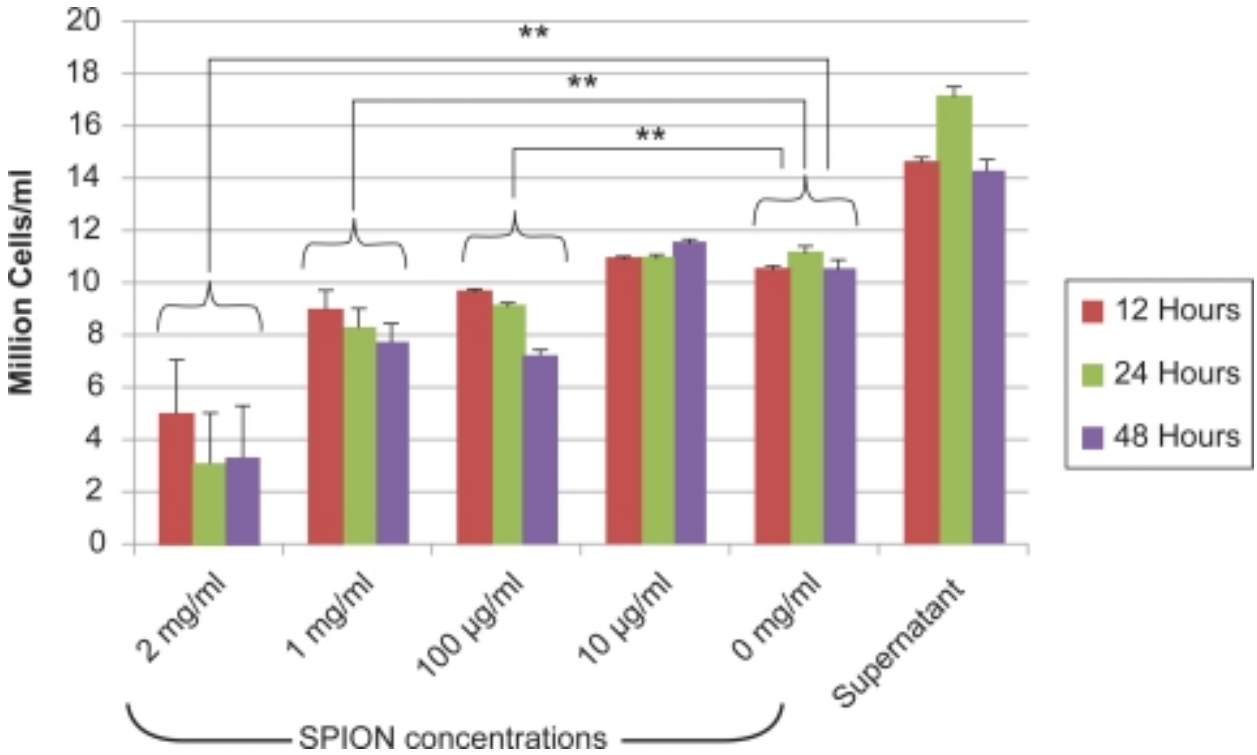

Figure 3.15 Decreased *S. epidermidis* numbers in the presence of SPION. Cells were inoculated at 3×10^6 cells per well and were cultured for up to 48 hours. Data was obtained using optical density readings and each bar represents the average of 24 readings. Bacteria density decreased for doses as low as 100 µg/ml compared to no particles (0 mg/ml) at all time points assessed. The lowest dose, 10 µg/ml, was not significantly different than controls (no particles). All P values assessed at the 1% level are denoted **and error bars indicate standard error of the mean (N = 3).

3.3.1.2 Bacteria live/dead staining

Moreover, fluorescence microscopy results demonstrated a higher percentage of dead bacteria when exposed to SPION after 48 hours **(Figures 3.16 and 3.17)**. Total fluorescent area (TFA) quantification data provided, for the first time, evidence that bacteria death increased in the presence of all SPION dosages of interest to this study **(Figure 3.16)**. A significant increase in bacteria death occurred at SPION concentrations of 2 mg/mL, 1 mg/mL, and 100 µg/mL compared to controls.

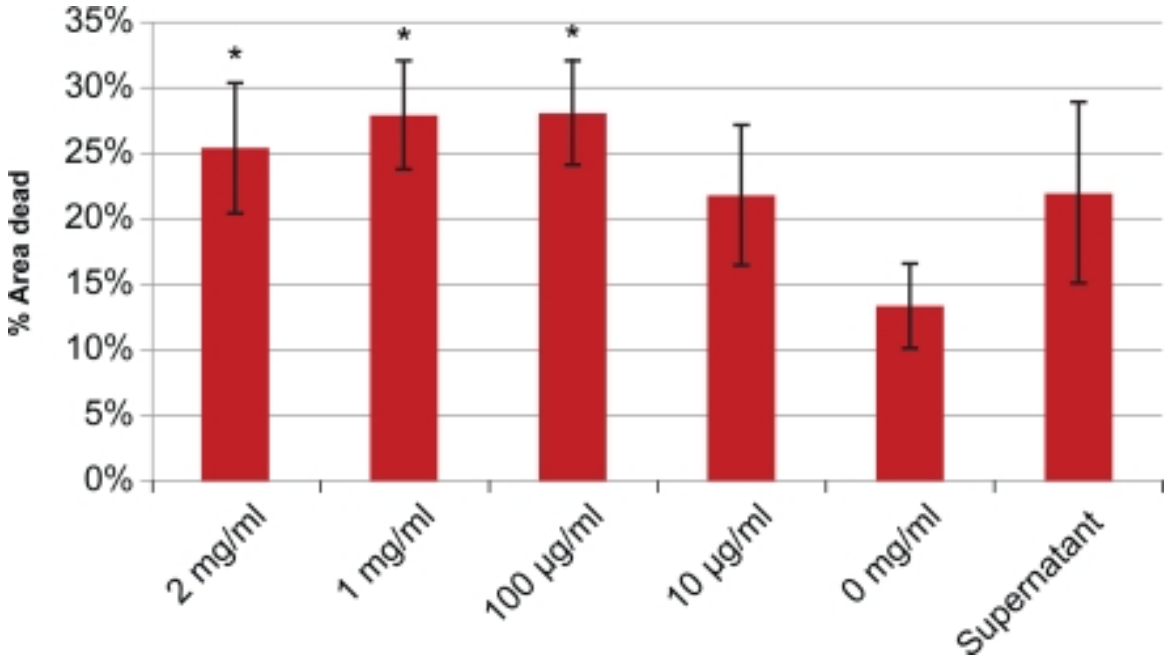

Figure 3.16 Percentage of dead bacteria quantified using fluorescence microscopy after 48 hours. Total fluorescent area (TFA) of bacteria cultures was determined for both green (live) and red (dead) regions and the average dead bacteria staining area for each is reported. A significant increase in dead cells was found for high SPION doses compared to controls (0 mg/ml), but not for the 10 µg/ml or supernatant alone conditions. All P values denoted with *are significant at the 5% level compared to controls and error bars are standard error of the mean (N = 3).

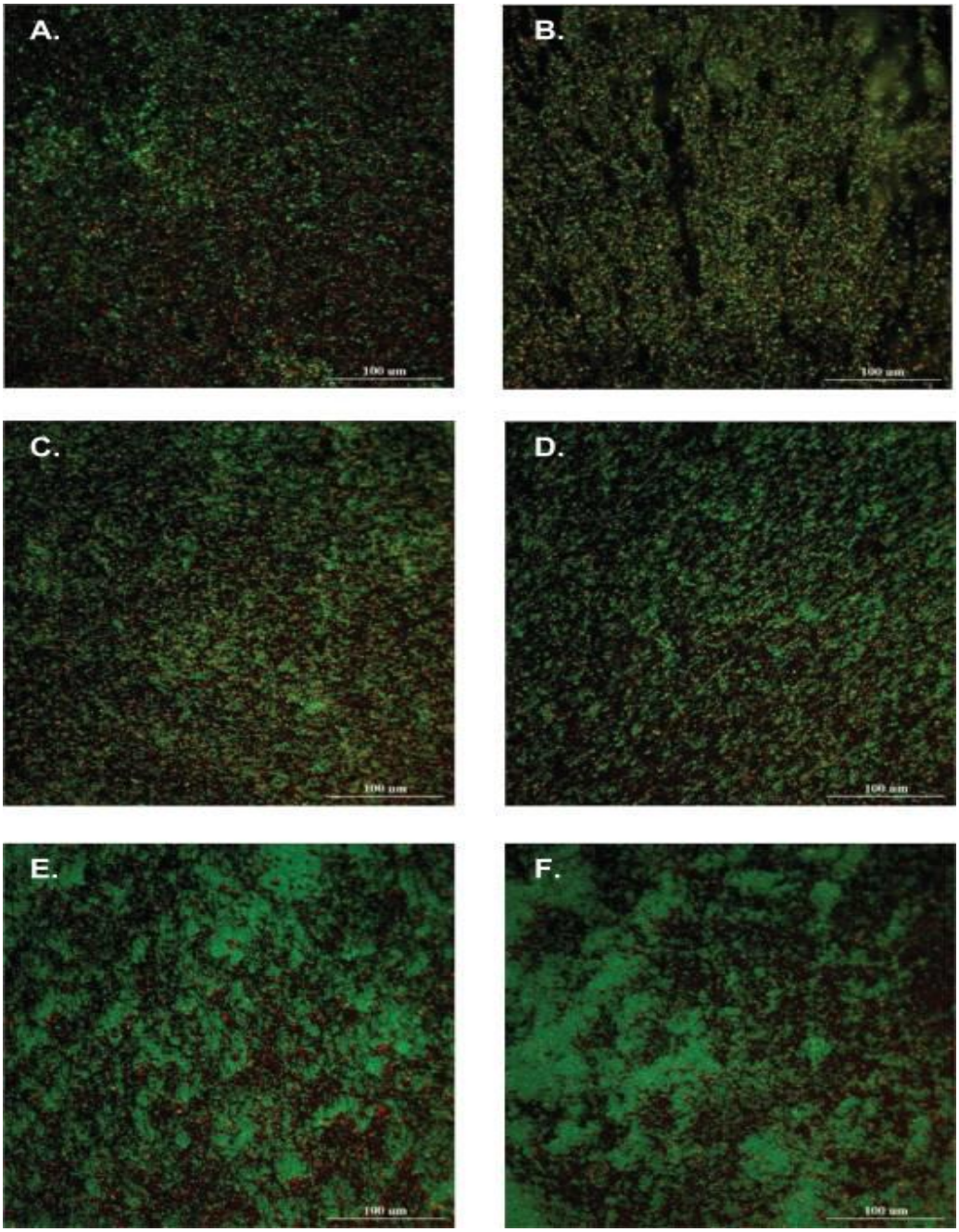

Figure 3.17 Fluorescently stained *in situ* bacteria colonies are inhibited as SPION concentration increased after 48 hours (living cells stained green and dead cells stained red). This was most obvious for the highest SPION concentrations of 2 mg/ml (**A**) and 1 mg/ml (**B**). This effect occurred in a dose-dependent manner with 100 μg/ml (**C**) and 10 μg/ml (**D**) causing an intermediate amount of disruption to bacteria growth. Normal bacterial growth was seen with controls (**E**) and the supernatant conditions (**F**).

3.3.2 Duel screening for biofilm and planktonic inhibitory action

3.3.2.1 Bacteria functions in the presence of synthesis chemicals (control readings)

Most importantly, *S. aureus* functions in the presence of SPION were determined using an *in vitro* infection model by isolating the activity of various compounds against free floating bacteria (planktonic), and surface adherent polysaccharide enclosed bacteria (biofilm) through analysis of the media optical density and crystal violet staining. For this study, DMSA coated SPION with metal coatings were used.

Initially, each metal salt, or other components used during SPION synthesis, were analyzed for antibacterial and anti-biofilm activity as controls **(Figure 3.18)**. Only $ZnCl_2$ and $AgNO_3$ controls (without SPION) demonstrated significant antibacterial activity **(Figure 3.18.A)**. Crystal violet staining (which stains extra-cellular polysaccharides in the bacterial cell-wall and the biofilm) determined that only DMSA controls had any significant biofilm inhibitory activity at 1 mg/ml, but not lower, whereas the $ZnCl_2$ salt increased biofilm formation **(Figure 3.18.B)**. These control studies showed that individual components used in SPION synthesis exhibited either antibacterial or antibiofilm activity, but not both.

A.

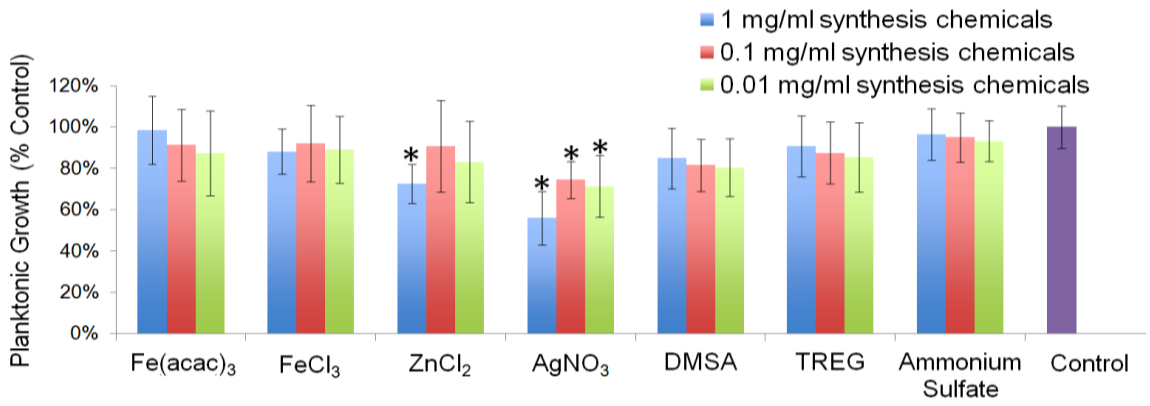

B.

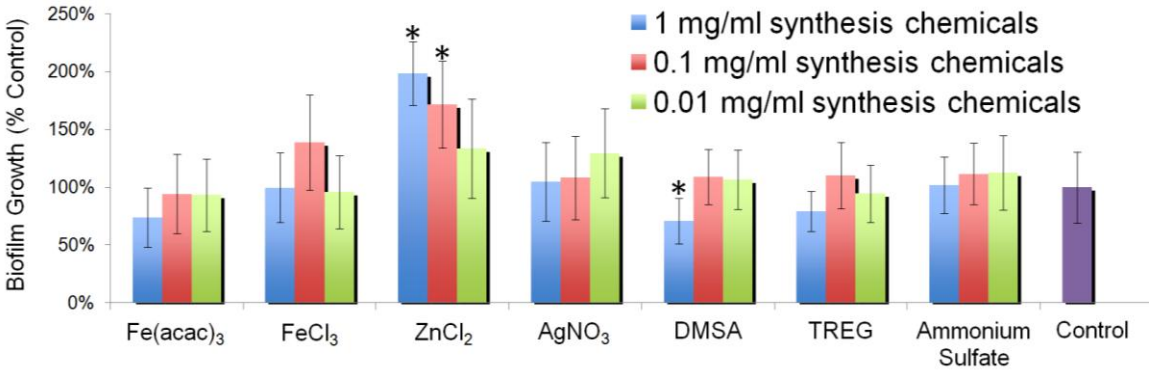

Figure 3.18 Growth of *S. aureus* cultured in the presence of SPION synthesis components quantified for planktonic growth by optical density (A.) and biofilm formation using crystal violet staining (B.). Each metal salt, or other components used during SPION synthesis was serially diluted to determine growth inhibitory action and used as controls versus SPION (DMSA= Dimercaptosuccinic acid; Triethylene glycol=TREG; Ammonium sulfate=AMS). Only $ZnCl_2$ and $AgNO_3$ controls (without SPION) had similar activity to the respectively conjugated SPION at 1 mg/ml or 0.01 mg/ml against planktonic growth (A.). Only DMSA controls (without SPION) had similar activity at 1 mg/ml, whereas $ZnCl_2$ at either 1 mg/ml or 0.1 mg/ml increased biofilm formation (B.). *P values are significant at the 5% level when compared to control values (mean +/- std.; N=3).

3.3.2.2 Bacteria functions in the presence of metal conjugated SPION

SPION were next analyzed for antibacterial and anti-biofilm activity against the *S. aureus* biofilm infection model **(Figure 3.19)**. Planktonic growth was inhibited by all SPION formulations at 1 mg/ml, with silver conjugated SPION inhibiting growth at a minimum concentration of 0.01 mg/ml **(Figure 3.19.A)**. It is important to note that these formulations contain ~370 µg/ml iron, while zinc conjugated SPION formulations contain ~40 µg/ml zinc, and silver conjugated SPION formulations contain about ~100 µg/ml silver depending on the amount of salt added (either 1 or 4 mmol were added) and the formulation. All conjugated SPION including iron, zinc, and silver inhibited biofilm formation at 1 mg/ml (corresponding to a iron concentration of 370 µg/ml; **Figure 3.19.B**), while 4 mmol iron conjugated SPION or 1 mmol zinc conjugated SPION blocked biofilm formation significantly at concentrations as low as 0.01 mg/ml (corresponding to a zinc concentration of 0.118 +/- 0.116 to 0.412 +/- .019 µg/ml). Biofilm recovery was observed with zinc 4 mmol (zinc concentration of 45.850 +/- 1.070 µg/ml). Therefore, metal conjugated SPION exhibited both antibacterial and antibiofilm activity as an emergent property not observed with the SPION synthesis components and metal salt controls, and this activity could be recovered by the addition of 4 mmol zinc conjugated SPION.

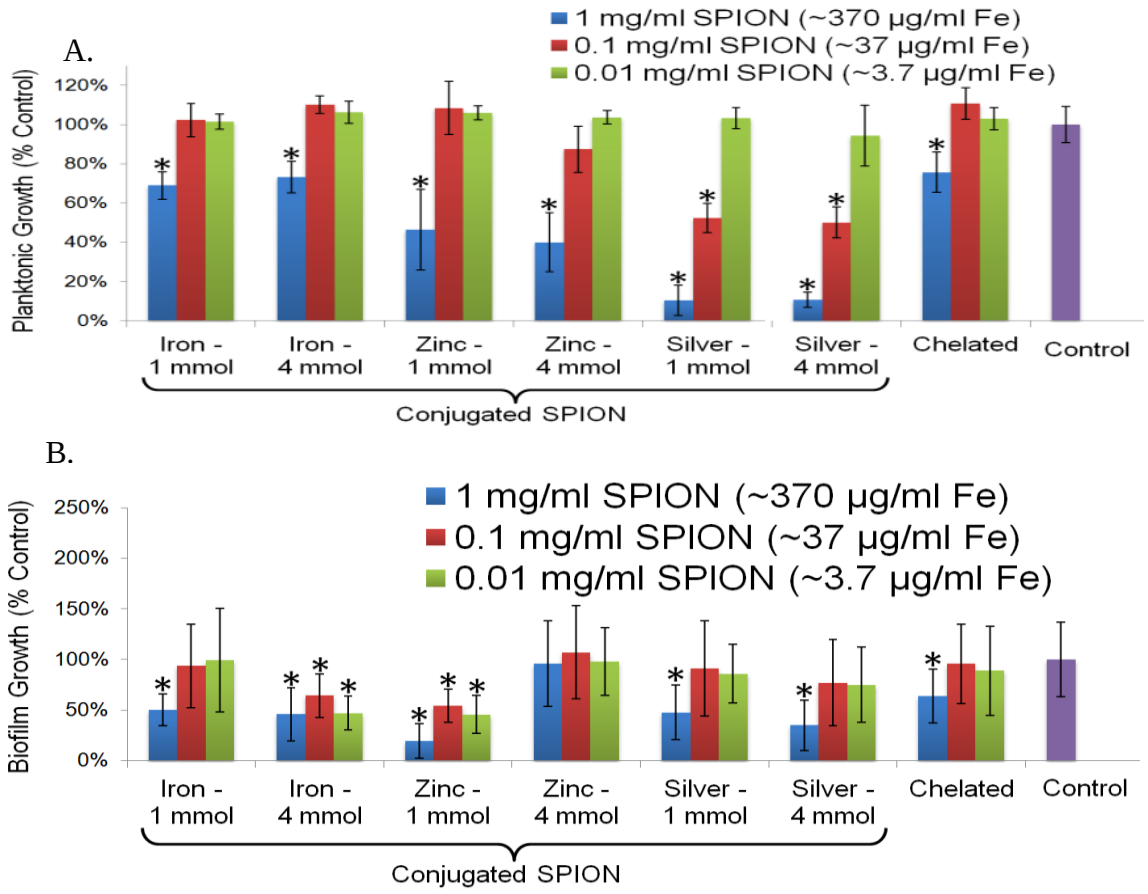

Figure 3.19 Growth of *Staphylococcus aureus* cultured in the presence of metal conjugated SPION quantified for planktonic growth by optical density (A.) and biofilm formation using crystal violet staining (B.). During the growth assay (A.), SPION were serially diluted to concentrations of 1, 0.1, and 0.01 mg/ml dry weight of SPION in tryptic soy broth (TSB). All SPION formulations inhibited growth at 1 mg/ml (dry weight corresponding to an iron concentration of ~370 µg/ml), while silver conjugated SPION formulations inhibited growth at 0.1 mg/ml (dry weight corresponding to a silver concentration of 11.257 +/- 1.0454 µg/ml). During biofilm growth in the presence SPION (B.), all metal conjugated SPION inhibited growth at 1 mg/ml, while iron 4 mmol or zinc 1 mmol conjugated SPION inhibited growth down to 0.01 mg/ml (corresponding to a zinc concentration of 0.118 +/- 0.116 to 0.412 +/- .019 µg/ml). Biofilm recovery was observed with zinc 4 mmol (zinc concentration of 45.850 +/- 1.070 µg/ml). *P values are significant at the 5% when compared to control values (mean +/- sterror.; N=3).

3.3.2.3 Bacteria functions in the presence of antibiotics

To compare the inhibitory properties of antibiotics to SPION, a panel of five antibiotics (including penicillin, oxacillin, gentamicin, streptomycin, and vancomycin) were then tested under the same conditions **(Figure 3.20)**. Using these methods, it was confirmed that the antibiotics were effective at inhibiting planktonic growth of *S. aureus* **(Figure 3.20.A)**. Strikingly, no inhibition of biofilm by any of the antibiotics tested here was observed; conversely, gentamicin, penicillin, and streptomycin at all concentrations actually increased biofilm formation while oxacillin caused an increase in biofilm formation at lower concentrations **(Figure 3.20.B)**.

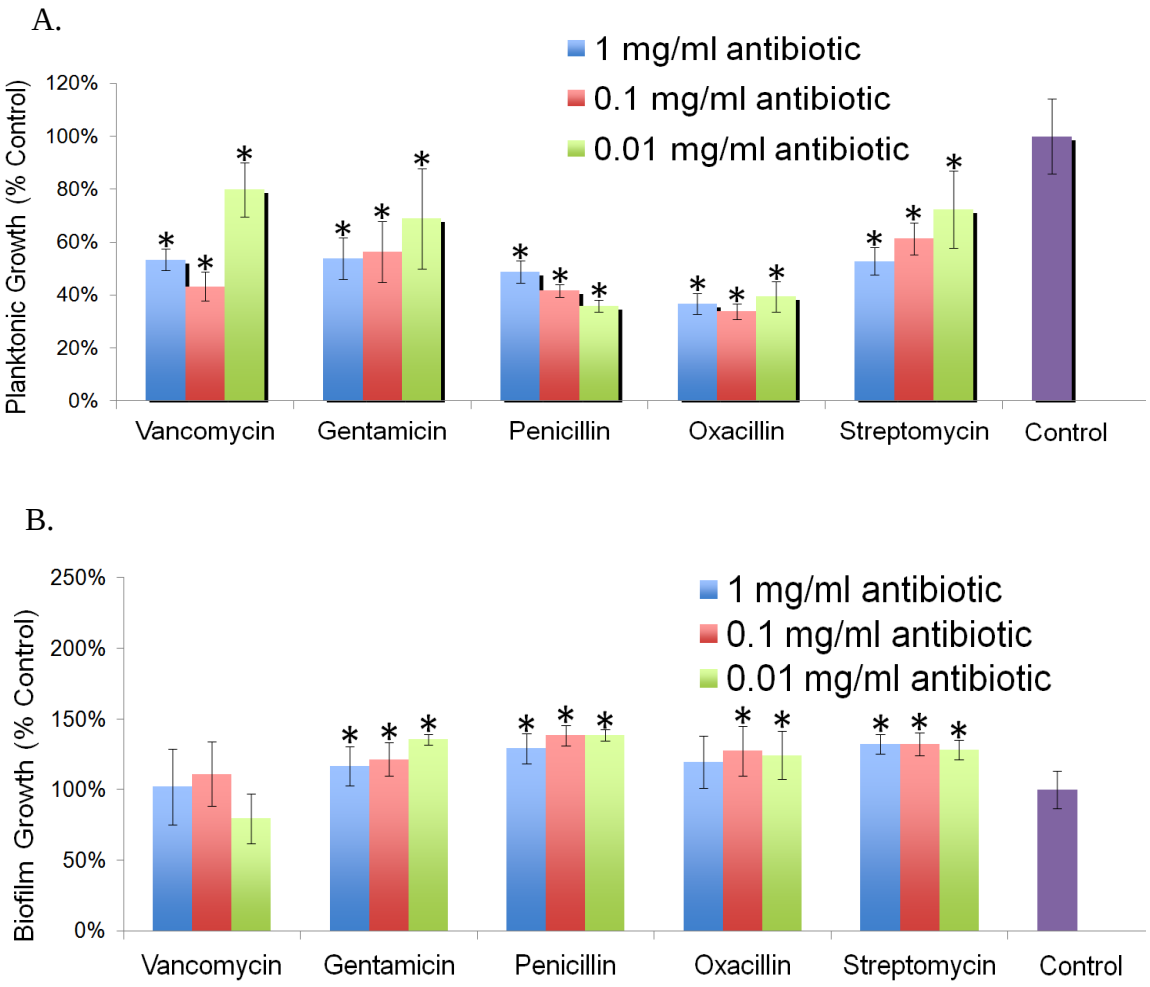

Figure 3.20 Growth of *S. aureus* cultured in the presence of antibiotics quantified for planktonic growth by optical density (A.) and biofilm formation using crystal violet staining (B.). Antibiotics at all concentrations decreased planktonic growth, yet did not decrease biofilm. Simultaneous increases in biofilm formation were observed for gentamicin, penicillin, and streptomycin at all concentrations, whereas oxacillin only increased biofilm at lower concentrations of 0.1 and 0.01 mg/ml. *P values are significant at the 5% level when compared to control values (mean +/- std; N=3).

3.3.2.4 Bacteria functions in the presence of antibiotic conjugated SPION

The goal of the next part of the study was to improve the antibacterial properties of SPION through the surface conjugation of antibiotics onto the surface of SPION. This is attractive because antibiotics can be selectively applied at the site of infection. For this, bacteria functions of planktonic growth and biofilm formation were assessed using the dual monitoring assay in the presence of antibiotic conjugated SPION. It was found that when conjugated to SPION, antibiotics had a tendency to decrease growth, and yet increase biofilm formation **(Figure 3.21)**. Interestingly, concentrations of vancomycin-SPION that decreased bacterial growth (0.5 mg/ml) did not increased biofilm, while concentrations of gentamicin that decreased growth (0.5 mg/ml or 0.05 mg/ml) did increase biofilm, possibly indicating a different mechanism of action both for antibiotic behavior and increased biofilm between the two antibiotic coated SPION formulations.

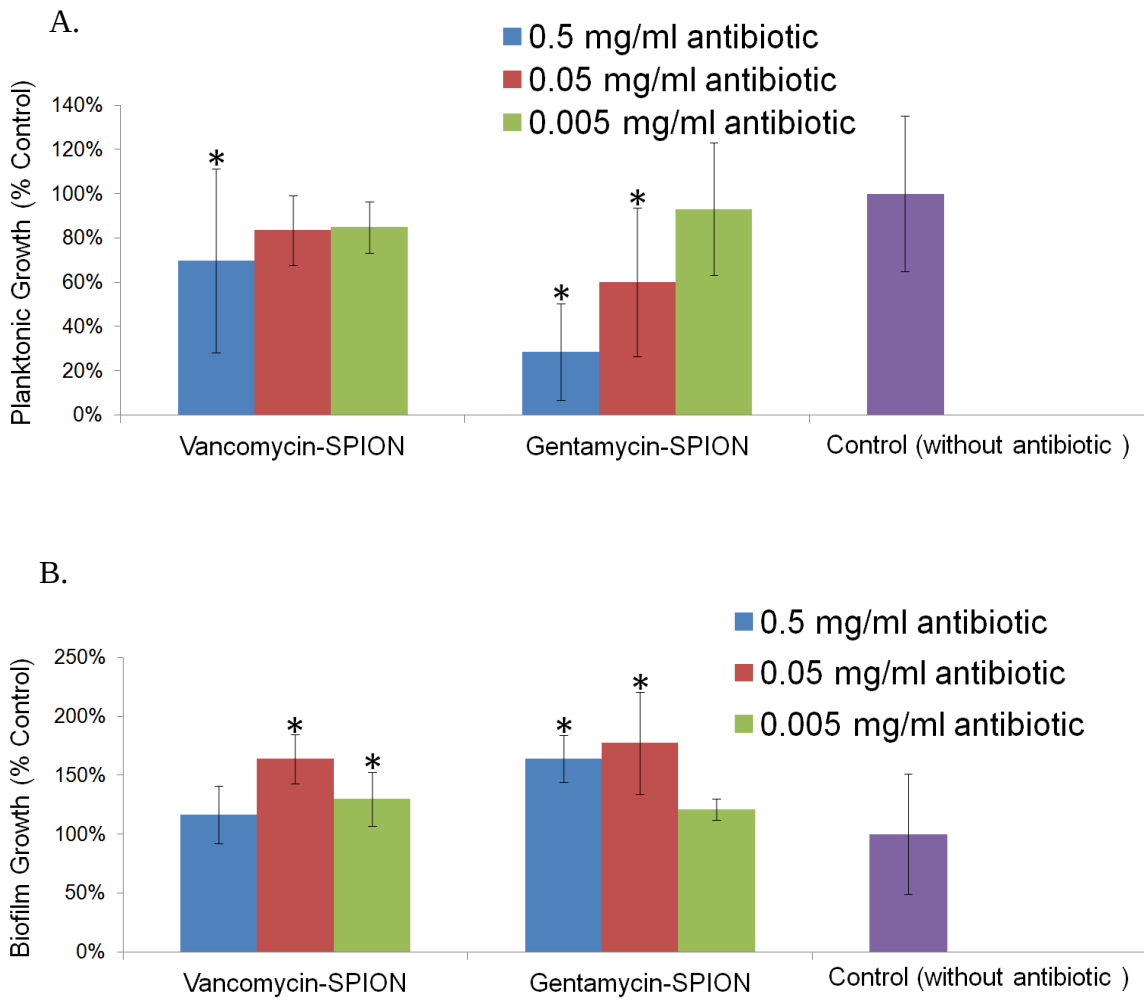

Figure 3.21 Bacterial growth (A., top) and biofilm formation (B., bottom) in the presence of antibiotic coated SPION. The concentration of SPION is 1 mg/ml at the 0.5 mg/ml antibiotic concentration. Vancomycin-SPION decrease growth at 0.5 mg/ml, and gentamicin-SPION decrease growth at either 0.5 or 0.05 mg/ml. Biofilm formation is increased by vancomycin SPION and gentamicin SPION, except at the highest concentration of vancomycin-SPION, or the lowest concentration of gentamicin-SPION.

3.3.3 Continuous monitoring of antibiotic coated SPION antibacterial activity

The antibacterial properties were demonstrated through culture of coated and uncoated SPION with *S. aureus*, monitored for 24 hours **(Figure 3.22)**. The antibiotic coated SPION were effective at reducing bacterial growth at the concentration tested (0.5 mg/ml antibiotic and 1 mg/ml SPION).

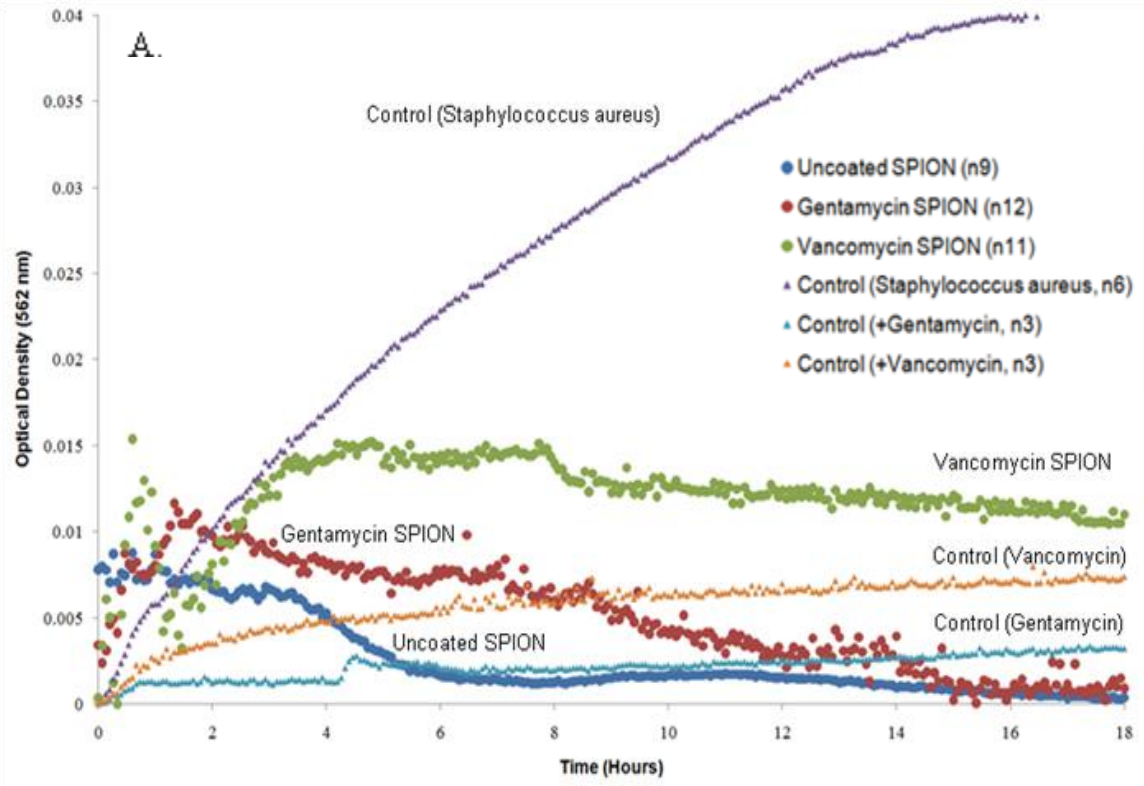

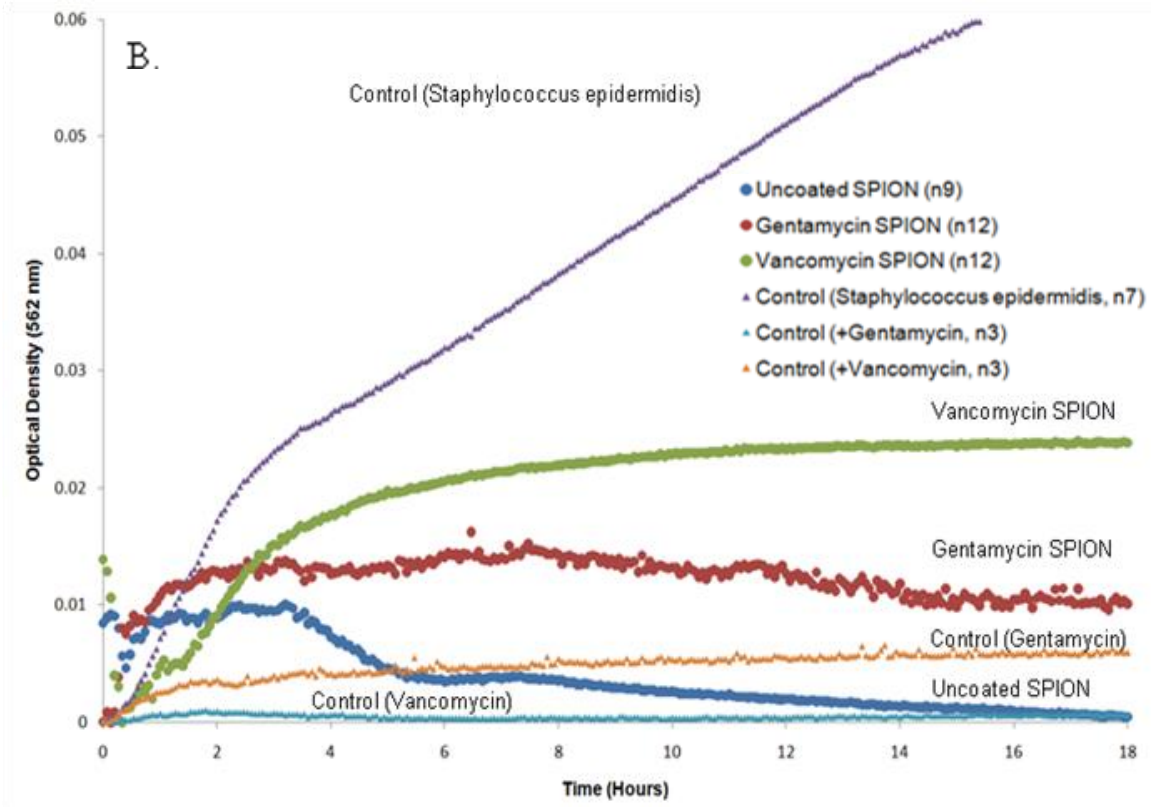

Figure 3.22 *Staphylococcus aureus* (A.) and *Staphylococcus epidermidis* (B.) growth inhibition in the presence of SPION coated antibiotics, or uncoated (no antibiotic). Control bacterial solutions continue to grow in solution for up to 18 hours, whereas growth in the presence of SPION is reduced during this period. Gentamicin coated SPION and uncoated SPION tended to have activity similar to antibiotics, whereas with vancomycin coating on SPION, activity was reduced (all solutions are 1 mg/ml of SPION). Each line represents the mean of several trials (number of trials is listed, n).

3.3.4 Mechanism of Action: Decreased Intracellular Bacillithiol (BSH)

Bacillithiol (BSH) was next probed using monochlorobimane for intracellular concentration. It was found that intracellular concentrations of BSH were decreased through the addition of SPION, compared to untreated bacteria. Specifically, iron, zinc

and silver SPION significantly decreased the concentration of intracellular bacillithiol to 0.170 +/- 1.037 µM, 0.864 +/- 0.654 µM, 0.465 +/- 0.647 µM, respectively. Chelated SPION also significantly decreased the concentration of intracellular bacillithiol to 1.593 +/- 0.568 µM versus 2.196 +/- 1.334 µM found in the control, which were cultured with tryptic soy broth under the same conditions.

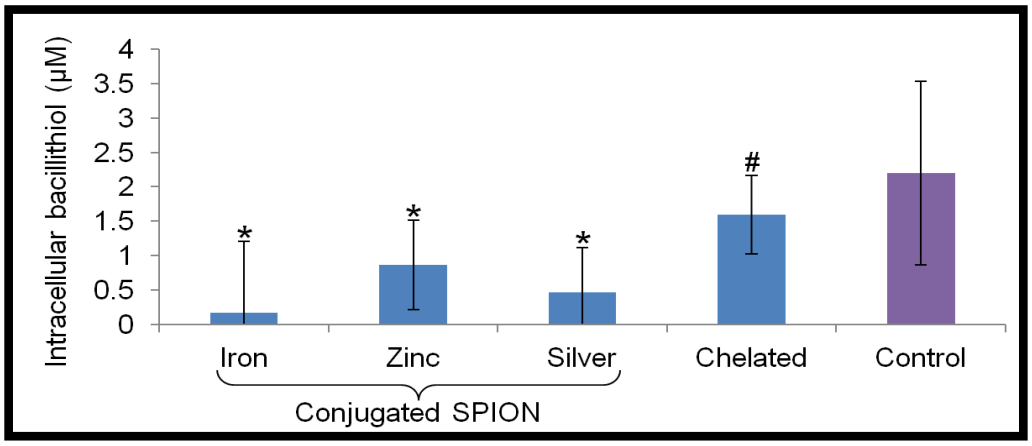

Figure 3.23 Intracellular bacillithiol, an antioxidant, is decreased by the addition of metal coated SPION, indicating that SPION penetrate bacteria, release metals, and thus reduce bacterial functions. *P values are significantly at 5% compared to control values or $^{\#}$P at 10% (data = mean +/- sterror; N=3).

3.3.4 Bacterial transmission electron microscopy

To gain further insights into the mechanism of biofilm inhibition and antibacterial activity by SPION, TEM was used to visualize the interaction between bacteria and SPION **(Figure 3.24)**. SPION, seen as dark particles under TEM, clustered at the bacterial membrane, which is visible through staining with osmium tetraoxide **(Figure**

3.24 A.-D) as compared to the no SPION controls (shown in **Figure 3.24.E**). It was apparent that SPION penetrated through the membrane, and either SPION aggregates or single particles could be found entering the bacteria (insets of **Figure 3.24.A-D**).

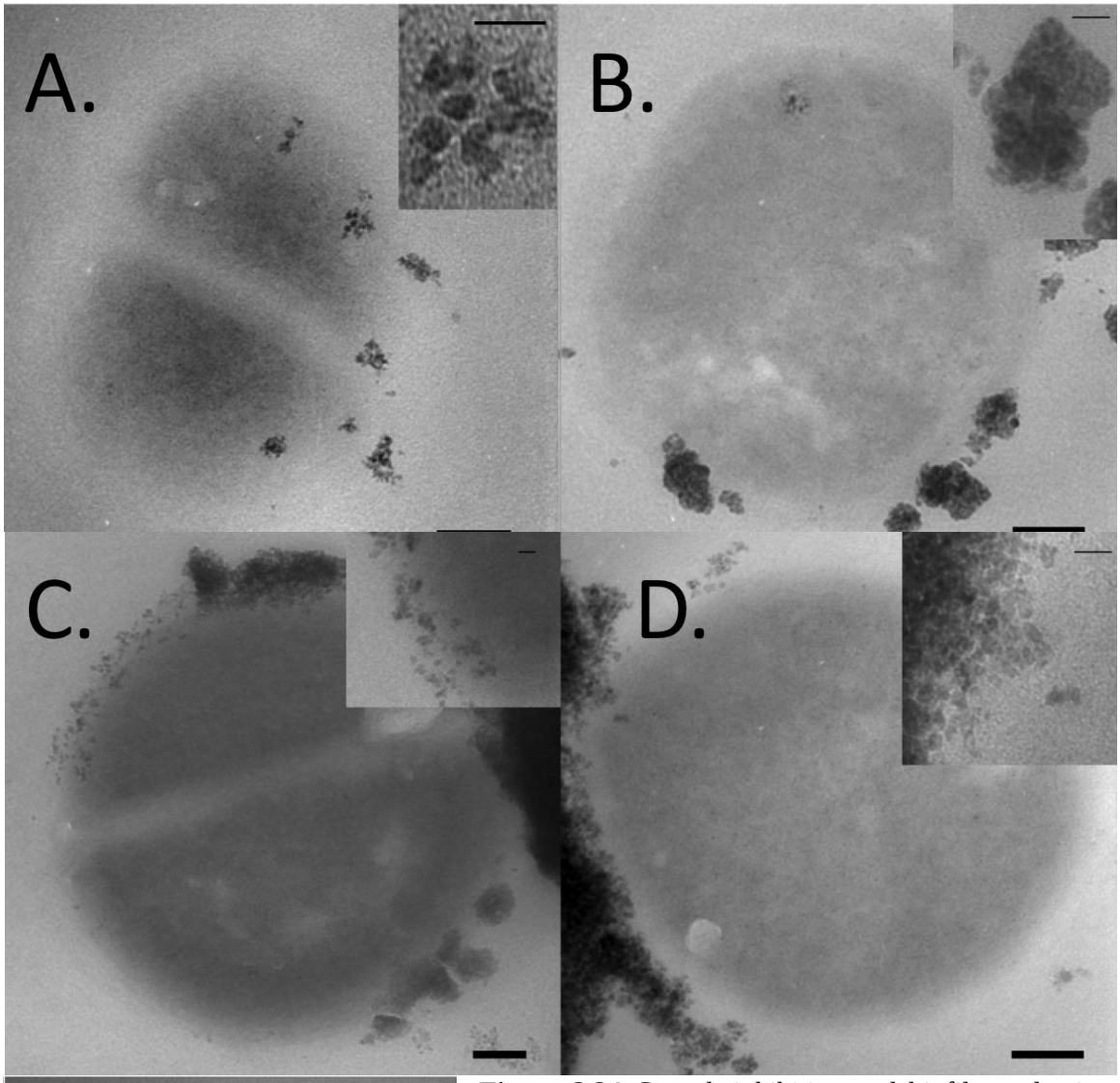

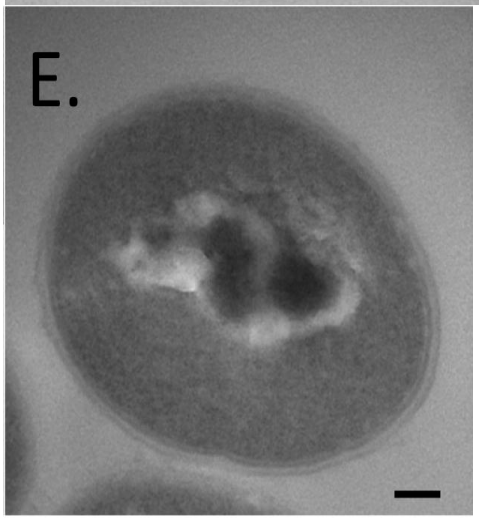

Figure 3.24 Growth inhibition and biofilm reduction by SPION is mediated by interactions with the *S. aureus* membrane surface. SPION including iron (A.), silver (B.), zinc (C.), and uncoated SPION (D.) adsorb to the surface of *S. aureus* (no SPION control shown in E.; scale bars = 100 nm in all images). SPION also penetrate the *S. aureus* membrane surface, as shown in insets (inset scale bars in A.-D. = 20 nm).

3.3.5 Multifunctional uses of SPION in the presence of a magnetic field

The final goal of this study was to determine the multifunctional uses of SPION which cannot be achieved with traditional antibiotics, and more specifically the applications of SPION for anti-infection applications in the presence of a magnetic field.

3.3.5.1 Magnetic biofilm uptake

In this study, evidence was provided that SPION could be used to penetrate *Staphylococcus aureus* biofilms with the aid of a magnet after a total exposure time of 60 minutes **(Figure 3.25)**. A magnet placed perpendicular to the biofilm was able to enhance the uptake of SPION after only 20, 40, or 60 minutes compared to no magnetic field (exposure time noted as t=0) as shown by Prussian Blue (a reaction with iron under acidic conditions used to form a highly insoluble and highly visible colored by-product) with the full 60 minutes of exposure providing the greatest amount of SPION biofilm penetration **(Figure 3.25)**.

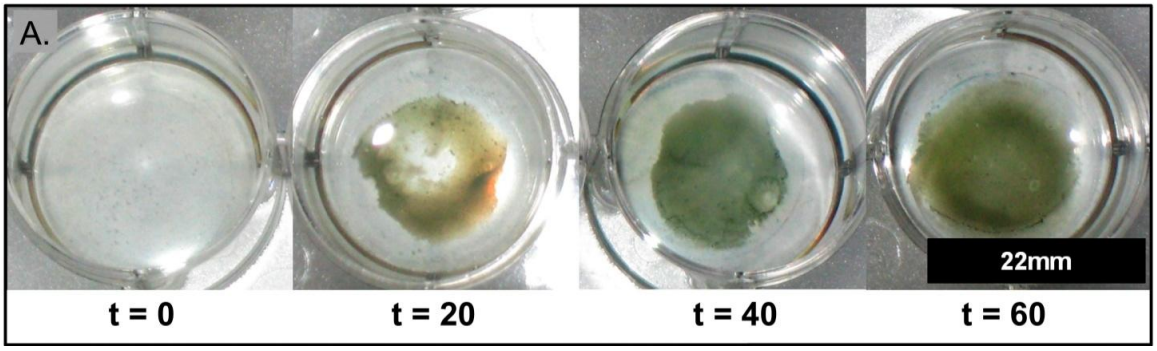

Figure 3.25 Uptake of SPION by biofilm in the presence of a magnetic field (12.6mm dia. X 5mm thick magnet, 3761 Gauss, and Neodymium). SPION (100 µg/ml) were applied to *S. aureus* biofilms (48 hour) for one hour. Magnetic field exposure was carried out for a 0, 20, 40, or 60 minute portion of the total 60 minutes of the assay. Prussian Blue staining was then used to detect iron deposition in biofilms.

3.3.5.2 Bacteria separation, quantification, and mechanism

After magnetic field application, bacteria could be separated from solution using uncoated or coated SPION **(Figure 3.26)**. It was found that bacteria exposed to SPION separated from solution through flocculation, and could subsequently be separated by a magnetic field **(Figure 3.27)**. Separation of bacteria by a magnet was analyzed further using TEM, which confirmed that SPION coated the bacterial surface resulting in bacterial clustering **(Figure 3.28)**.

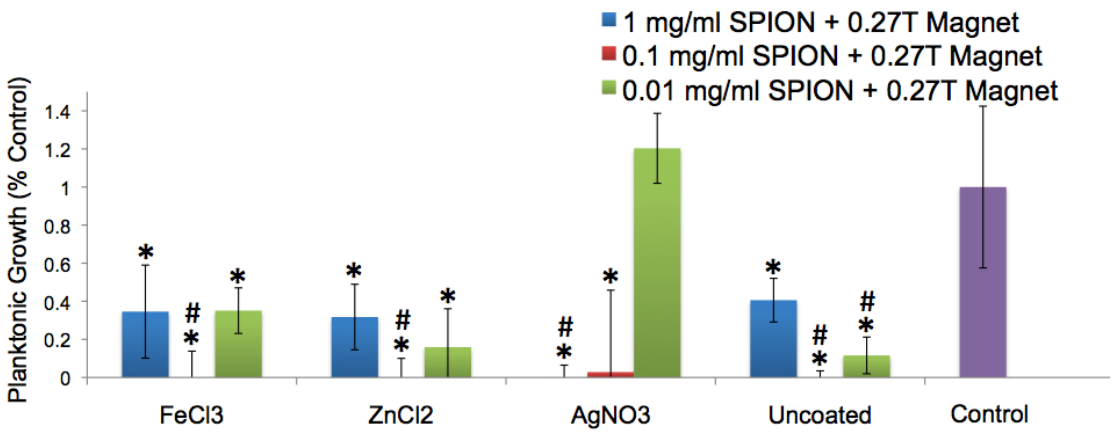

Figure 3.26 Inhibition of *Staphylococcus aureus* cultured in the presence of coated SPION quantified by optical density after magnetic field exposure. *P values are significant at the 5%, **P 1% level compared to control values, and #P value is significantly less at 5%, ##P 1% level when compared to 1 mg/ml uncoated nanoparticles (mean +/- standard error, N=3).

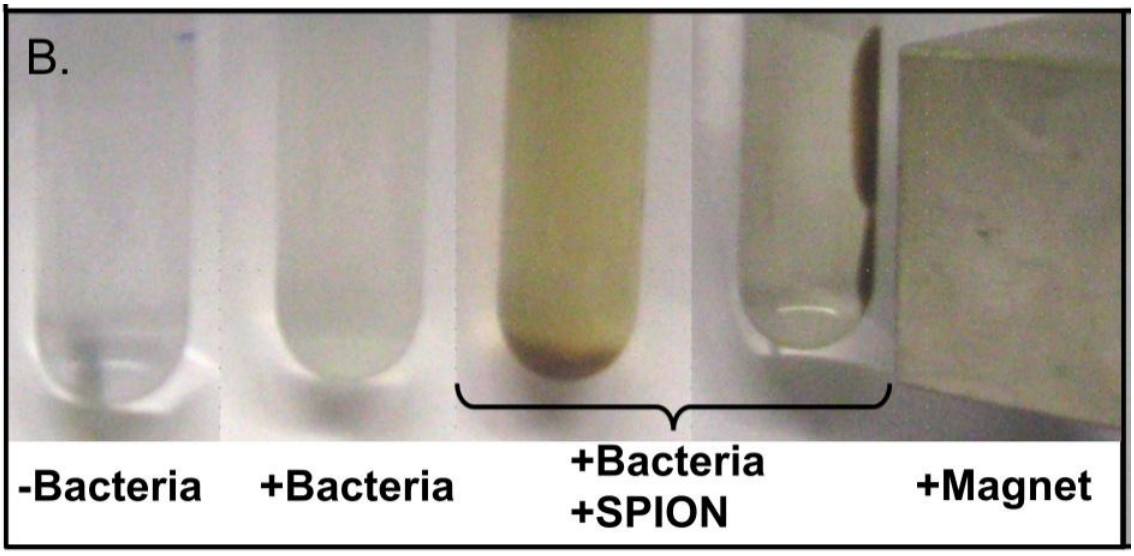

Figure 3.27 SPION mediated magnetic separation of planktonic bacteria. Image of phosphate buffered saline, bacteria control, SPION plus bacteria, and SPION plus bacteria next to a magnet, from left to right. In the presence of SPION, planktonic bacteria flocculate, resulting in settling (the brown precipitate is seen in the third test tube) and can be cleared by a magnetic field (the magnet used here is shown on the far right).

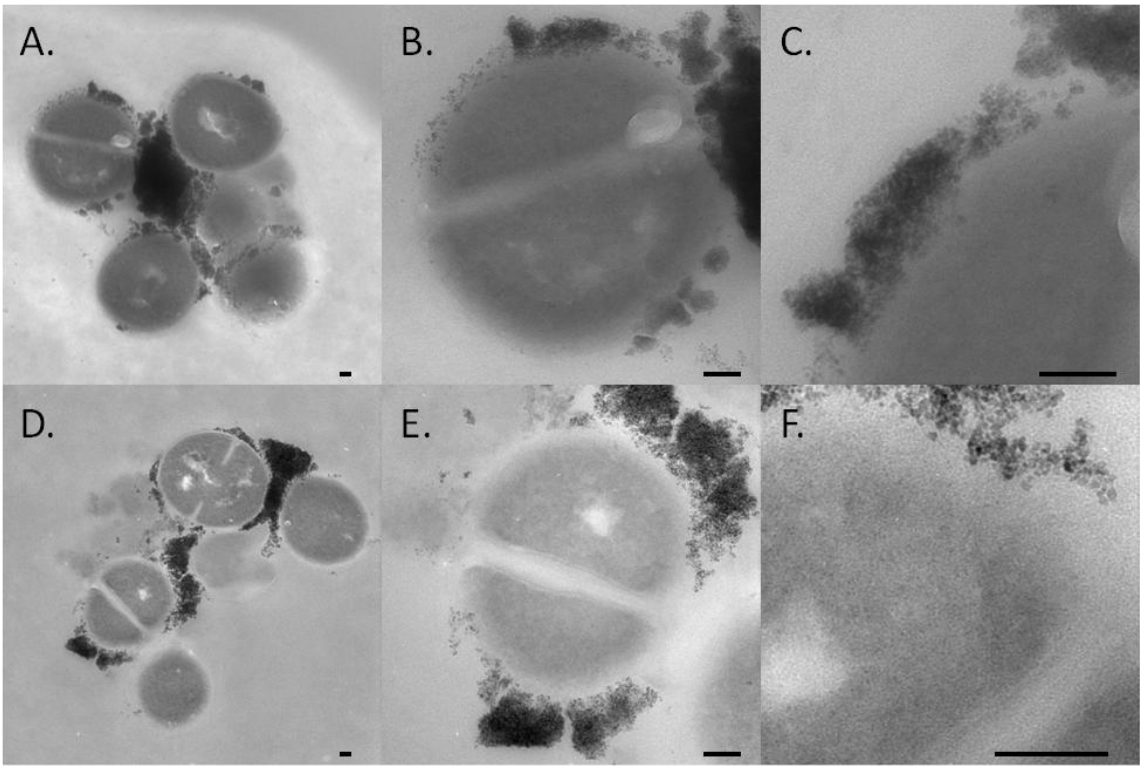

Figure 3.28 Clustering interactions between SPION and bacteria. Groups of bacteria interact with SPION resulting in clusters to form (A&D) mediated by SPION at the bacterial cell surface through aggregation (B&E) and surface coating (C&F). These representative images demonstrate a similar process with both metal coated SPION (zinc coated shown; A-C) and uncoated SPION (D-F).

4. Discussion and conclusions

4.1 Potential of SPION for bone regeneration

4.1.1 Uncoated SPION and CaP SPION characterization

To further enhance the compatibility of iron oxide nanoparticles with bone, SPION were coated with CaP in the presence of either BSA or CA in the present study. Since natural bone possesses numerous amorphous and crystalline phases of CaP-based materials, future studies should focus not just on the coatings formulated here but on a wide range of CaP-based coatings. Nevertheless, the CaP-coated magnetic nanoparticles were observed using TEM to have a core/shell structure. The magnetic particles were encapsulated within the spheres of CaP. Importantly, even after coating, each respective dried powder displayed magnetic properties.

Moreover, XRD diffraction characterization of the uncoated and CaP-coated magnetite nanoparticles indicated that there was a coating of hydroxyapatite around magnetite nanoparticles when synthesized in the presence of BSA. In contrast, coating in the presence of CA did not fully encapsulate the iron oxide nanoparticles as both phases were detected with XRD. In the case of the CaP-coated maghemite nanoparticles, both coatings (synthesized in the presence of BSA and CA) did not fully encapsulate the nanoparticles but the hydroxyapatite phase was observed in addition to other CaP phases. The incomplete coating of the iron oxide nanoparticles with CaP could be due to the

agglomeration of maghemite, which needs to be a focus of a future study.

The reduction of the saturation magnetization of the coated iron oxide nanoparticles could be largely due to the weight contribution from the CaP and surfactants.[250] But the hysteresis loop from the present study showed that the CaP-coated nanoparticles were still superparamagnetic. Clearly, this property can be utilized to direct such magnetic nanoparticles to a desirable bone site in the body to allow the magnetic nanoparticles to treat local bone disease. As an example, after such a magnetic field is removed, a functionalized version of the CaP-coated nanoparticles can attach themselves to osteoporotic bone, immediately building bone mass. Moreover, maghemite nanoparticles coated with hydroxyapatite in the presence of BSA were shown in this study to significantly increase the proliferation of bone cells. Thus, after such maghemite-coated nanoparticles attach, they may also increase bone formation.

This study also showed that the magnetite nanoparticles were better dispersed after early time points as compared to maghemite due to lower emu/g values. In the absence of any surface coating, magnetic iron oxide particles have relatively hydrophobic surfaces (compared with the cell culture media) with a large surface area to volume ratio. Due to hydrophobic interactions between the particles, these particles agglomerated and formed large clusters, resulting in increased particle size.

4.1.2 Cell studies with osteoblasts

When nanoparticles agglomerate, they decrease the effective surface area for protein, and subsequently, cell interactions. This is important as previous studies have demonstrated

greater vitronectin adsorption (a protein important for promoting osteoblast adhesion) on individual nanoparticles than when nanoparticles agglomerated into micron-sized particles.[251] In this manner, greater vitronectin adsorption on nanoparticles that do not agglomerate is a key design parameter for promoting osteoblast functions.

Most importantly, this study provided the first evidence of greater osteoblast densities in the presence of maghemite nanoparticles than magnetite nanoparticles and controls after 5 and 8 days. While further studies will be needed to determine why, it is known that magnetite is composed of two phases: FeO and Fe_2O_3. A likely explanation for this trend may be that, with time, the magnetite starts to agglomerate in the cell culture media and hence loses its bioactivity with respect to protein adsorption and subsequent osteoblast function. Nonetheless, this study showed that out of two iron oxide nanoparticles (magnetite and maghemite), maghemite is more inductive to osteoblast growth.

4.1.3 Conclusion

In performing this study, the possibility of applying magnetic nanoparticles for the treatment of osteoporosis was a focus. The promise of these particles (particularly maghemite) to immediately increase bone density at the site of disease was emphasized. Also, drug molecules can be attached and the magnetic properties of these nanoparticles can be utilized as they are guided under a magnetic field to desirable bone sites. Thus, the success of such a treatment requires that the particles are cytocompatible when in contact with osteoblasts. It is therefore beneficial that the results of the present study demonstrated that no iron oxide nanoparticle solution had anti-proliferative effects on

osteoblasts; they were all better or at least comparable to controls in which no particles were added. In summary, these results provided evidence that magnetic nanoparticles (particularly, maghemite) should be further studied and optimized for various bone disease applications.

4.2 Potential of SPION for treating orthopedic infections

4.2.1 Uncoated Fe_3O_4 interactions with bacteria

Proposed here is the hypothesis that iron oxide magnetic particles alone may prevent biofilm formation. Specifically, the antibacterial activity of magnetic nanoparticles was supported here by 48-hour live/dead bacteria studies showing significantly inhibited bacteria growth at 100 μg/mL or greater concentrations. Previous studies with metal oxides indicated that antibacterial activity could be mediated by hydrogen peroxide or superoxide anion free radical production.[124,126] Free radical production results from the use of metal oxides due to metal ion release or through their interaction with UV light.[124,175] Iron ions generate oxygen radicals by converting hydrogen peroxide to the more reactive hydroxyl radical via the fenton reaction.[175] Hydroxyl radicals generated by these iron ions can depolymerize polysaccharides, cause DNA strand breaks, inactivate enzymes, and initiate lipid peroxidation.[176] Moreover, nanoparticle binding to cell membrane or cell membrane proteins through electro-static interactions disrupting bacteria functions is another possible mechanism that may have caused bacterial death in this study.[129,157,252]

The adhesion of bacteria to iron oxide has been demonstrated for bulk iron oxide substrates in which greater bacterial adhesion has been observed to nonmetal surfaces such as glass.[113] It is thought that for negatively charged bacteria, adhesion on metal oxides increases due to a positively charged surface.[113] Yet, this conclusion lacks a consideration of the impact of greater surface energy on select protein and

macromolecule adsorption in relation to decreased particle size.[113,247] That is, the SPION fabricated here may have adsorbed proteins more favorable for binding to bacteria, further disrupting bacteria function leading to their death.[129,157]

The particles used in this present study had an average size of about 8 nm. To further improve the antibacterial function of the SPION formulated here, particles with an even lower average particle size should be fabricated as well as better dispersed particles. Lastly, results from this study indicated bacteria colony disruption for SPION dosages as low as 100 μg/mL. While this requires further investigation, this disruption of bacterial assembly may impact quorum sensing.

4.2.2 Conclusion

In summary, in this study a novel minimally invasive nanotechnology-based treatment for fighting orthopedic implant infection through the use of SPION was considered. Bacteria culture density decreased at SPION dosages of 100 μg/mL or greater added to cultures. Inhibition of bacteria colony formation even with the lowest SPION dosages used here, 10 μg/mL, was also found. These results indicated that when used alone, or coupled with other therapeutic agents, SPION could be useful to prevent biofilm formation.

This potential outcome provides a new paradigm for the treatment of persistent orthopedic implant infection using one multifunctional nanotechnology based platform. SPION can function as contrast agents allowing for the diagnoses of infection. Bacterial death caused by SPION alone or coupled with other antibiotics could decrease prosthesis infection. Decreased bacterial assembly could prevent biofilm formation and expansion.

Finally, positive interactions between bone resident cells could be promoted by SPION alone or by using a customized surface coating. Therefore, it may be possible to diagnose, treat, and promote bone tissue regeneration at the site of orthopedic prosthesis infection **(Figure 4.1)**.

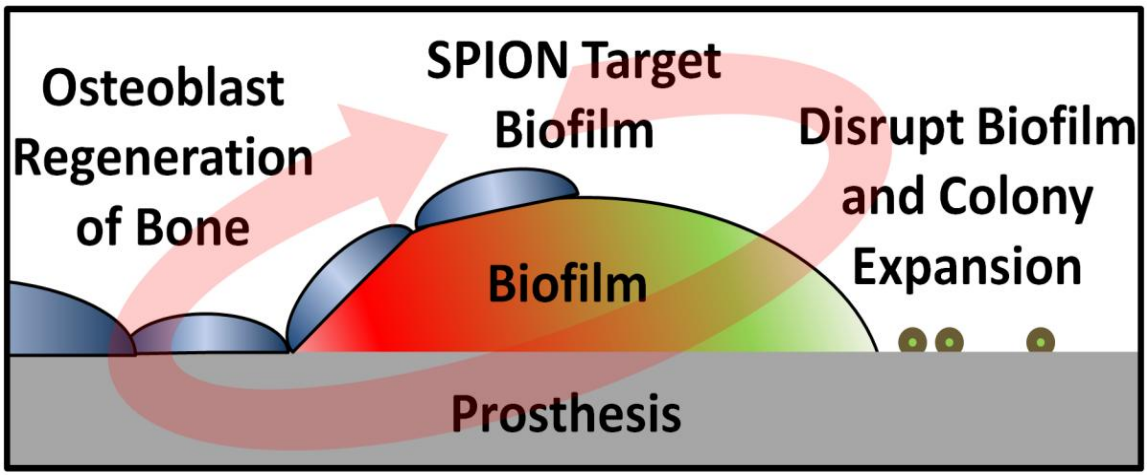

Figure 4.1 Schematic overview of multifunctional SPION applications used to treat orthopedic infections. First, SPION would be delivered to the site of infection via a magnetic field and receptor targeting. Once at the site, antibacterial SPION along with antibacterial agents (such as silver) would disrupt the biofilm and expansion of the bacteria colony. Finally, therapeutics, such as a calcium phosphates (CaP) or drugs adhering to the biofilm surface would promote osteoblast (bone forming cell) influx, and subsequent regeneration of bone at the infection site.

4.3 Antimicrobial conjugations to SPION via DMSA

4.3.1 Monodisperse nanoparticles coated with DMSA and metal ion conjugates

The next goal of this research was to further improve the antimicrobial behavior of SPION through increased water solubility and metal conjugation. It has been previously demonstrated that SPION coated with DMSA are well dispersed in water, cell media, or other cell or body fluids, and can bind to a variety of metals through the available DMSA chelator ligands or to the iron oxide lattice,[239] and moreover, the binding capability of DMSA includes iron, zinc, and silver.[239,253]

Chelated SPION synthesized here were first analyzed using the three methods of XRD, TEM, and DLS (**Table 4.1**). Using the three methods, it was found that XRD and TEM determined similar sizes, while the sizes from DLS were larger. XRD and TEM both measure crystallite size, and these two values matched, implying that nanoparticles are single crystalline and monodisperse (there are low variations in sizes of SPION).[246] Unlike the other two methods, DLS measures the effective size of a nanoparticle as determined by its diffusion coefficient in laser light, and this size is also referred to as the hydrodynamic diameter.[254] The hydrodynamic diameter takes into account nanoparticle agglomerations and coatings, and thus a higher value is expected since DMSA is on the surface of SPION. Moreover, the small size of SPION found by DLS indicates low nanoparticle agglomeration and a small size in liquid media.

Table 4.1 Comparison of chelated SPION* size by a three methods including X-ray diffraction (XRD), transmission electron microscopy (TEM), and dynamic light scattering (DLS).

Size from XRD	Size from TEM	Size from DLS
8.65 +/- 0.24 nm	9.92 +/- 3.14 nm	19.93 +/- 1.31 nm

*Chelated SPION = only DMSA was added after SPION synthesis.

In this study, it was demonstrated that chelated SPION could by synthesized with DMSA as a coating material, and furthermore, that metal salt conjugations were successful. An increased sulfur concentration demonstrated with ICP-AES indicated that DMSA chelated the SPION surface, and furthermore, increases in iron, zinc, and silver concentrations after purification from the free metal ions indicated that these metals were conjugated. These results were corroborated by the zeta potential results, where zinc and silver conjugated SPION demonstrated decreased zeta potentials of -43.2 mV and -40.1 mV compared to -35.5 mV for chelated SPION, while iron conjugated SPION increased the zeta potential to -34.0 mV. These variations in zeta potential also indicate that zinc and silver metals were incorporated into the DMSA polydisfulide layer, while iron associated with the surface (and thus increased the zeta potential compared to chelated SPION alone). This result is corroborated by DLS results, which shows that zinc conjugated SPION had a similar size to chelated SPION (19.67 +/- 0.72 nm versus 19.93 +/- 1.31 nm), while iron conjugated SPION were larger (23.32 +/- 1.17 nm). Moreover, silver is known to interact with thiol groups, and resulted in nanoparticle agglomerations, thus a larger particle size about 10X larger than chelated SPION was observed by DLS (193.72 +/- 6.15 nm).

SPION also exhibited magnetic properties both before and after metal conjugations, an

important property for the targeted delivery of magnetic SPION formulations to biofilms. Chelated SPION exhibited saturation magnetization of 58.625 emu/g, which is 63.723% of the magnetic moment for bulk magnetite (92 emu/g), and such a reduction in magnetic properties were expected, since these molecules contribute to a large proportion of SPION dry weight.[248,249] Metal conjugates decreased this value to ~25% of bulk magnetite due to the incorporation of additional non-magnetic metal components in the SPION preparations, with magnetic moments of 23.875 emu/g for iron conjugation SPION and 22.635 emu/g for zinc conjugated SPION, values which are consistent with the saturation magnetization of about 20-30 emu/g for many magnetic particles and beads based on SPION used in biomedical applications.[255] Exceptionally, silver conjugated SPION increased the value to 91.537 emu/g, or 99.497% of bulk magnetite, so it is possible that silver conjugation to SPION changed the crystal structure of the iron oxide, increasing the magnetic properties. Previous studies by Qiang et al. showed that core-shell SPION with nano-zero valence iron exhibited magnetic saturation values of 80 emu/g at a particle size of 10 nm, and as particle size increased to 100 nm, the magnetic moment increased up to 205 emu/g, which is close to the value for bulk Fe of 218 emu/g.[255] Silver conjugated SPION had an observed particle size of 193.72 +/- 6.15 as determined by DLS, and thus could have had magnetic properties closer to bulk Fe,[255] or 41.989% of the magnetic moment of this material.

4.3.2 Duel screening for biofilm and planktonic inhibitory action

4.3.2.1 Activity of antibiotics against planktonic and biofilm bacteria

A novel assay was developed here to simultaneously analyze the activity of a variety of antibiotics, chemicals, and nanoparticles against *Staphylococcus aureus* bacteria and biofilms. Here, antibiotics inhibited planktonic bacterial growth at a concentration range of 10 μg/ml to 1000 μg/ml, with a concentration range tested that is similar or higher than the typical minimum inhibitory concentration of these antibiotics against susceptible planktonic bacteria, with a lower limit of 0.5 μg/ml, for vancomycin, to 32 μg/ml, the upper limit of MICs observed for penicillin clinically against susceptible *Staphylococcus aureus*.[256] Importantly, these bacteria are free floating, non-adherent, non-biofilm associated, and moreover, non-resistant to antibiotics as shown here, and otherwise.[3,51,52,256] But, in contrast, antibiotics had little effect on biofilm formation, when exposed to biofilm that had already been established for 24 hours. Instead, these antibiotics frequently increased biofilm, with both gentamicin and streptomycin (aminoglycoside antibiotics) increasing biofilm at all concentrations, along with penicillin (a β-lactam). Oxacillin (also a β-lactam) increased biofilm at either 100 μg/ml or 10 μg/ml, with no effect at 1000 μg/ml; while vancomycin (the only glycopeptides tested) had no effect to either increase or decrease biofilm at any concentration tested. Therefore, these three major classes of antibiotics (aminoglycoside, β-lactam, and glycopeptides) frequently used to treat *Staphyloccus aureus* infections did not decrease biofilm formation, and instead had a tendency to increase it (for the aminoglycoside and β-lactam antibiotics tested).[256]

These findings coincide with the growing hypothesis that antibiotics frequently have no

effect on biofilm, or even increase biofilm formation, as has been observed for biofilm formation by pathogenic microorganisms including *Staphylococcus epidermidis* and *Staphylococcus aureus* at sub-lethal concentrations of antibiotics.[56-58] Rachid et al., found that tetracycline and quinupristin-dalfopristin antibiotics can lead to enhanced polysaccharide synthesis or biofilm formation,[58] while Kaplan et al. found another mechanism in RP62A *Staphylococcus epidermidis* using tigecycline and vancomycin related to the release and incorporation of extracellular DNA into biofilm.[56] These authors concluded that antibiotic induced biofilm formation is both strain and antibiotic dependent.[56-58] Other studies using *Staphylococcus aureus* biofilm grown on silk sutures found that gentamycin increased the amount of biomass at either sub-inhibitory or lethal (to planktonic bacteria) concentrations of gentamycin.[60] Perhaps such mechanisms are part of an evolutionary adaptation to defend against natural antibiotics produced by bacteria and fungus, but the problem needs to be alleviated by the design of novel drugs which can overcome such resistances.[59] Finally, these results help to corroborate the frequent clinical issue, that when a medical device (such as an orthopedic prosthesis) becomes infected with *Staphylococcus aureus*, or other similar pathogens, it becomes impossible to treat, and instead must be removed.[22,35,40,257] Therefore, a different treatment is desired, and thus SPION were developed here as a first step towards such a solution.

4.3.2.2 Activity of synthesis chemicals against planktonic and biofilm bacteria

All of the chemicals used to synthesize SPION were tested for antimicrobial activity and for their effect on biofilm formation. Antimicrobial activity was detected against

planktonic bacteria matching those expected for $ZnCl_2$ and $AgNO_3$, while other chemicals and salts used during SPION synthesis and preparation did not have antimicrobial activity.[155,258,259] Previous studies have shown that the MIC of $AgNO_3$ is about 12.5 μg/ml,[259] and the MIC of $ZnCl_2$ is about 136 μg/ml;[258] these values are similar to the concentrations determined to result in significant inhibition of planktonic growth, as was observed with either 10 μg/ml $AgNO_3$ or 1000 μg/ml $ZnCl_2$ (or great than 100 μg/ml tested here). Similar to antibiotics, biofilm response in the presence of metal ions caused either no effect (for most metals or salts), increased biofilm formation (for $ZnCl_2$), or with the exception of DMSA, decreased biofilm formation.

Biofilm response to metals ions in particular is different than free floating planktonic bacteria, because the bacteria in the biofilm have an opportunity to respond to antimicrobial ions, including Zn^{2+} and Ag^{+}.[155] In particular, it is known that biofilm bacteria can resist the antimicrobial activity of silver to some degree, through the generation of exopolymeric substances (EPS) that encapsulates the biofilm and can restrict the diffusion of silver ions, providing protection for the biofilm cells, explaining why silver ions had no effect on biofilm.[155,172,173] Unlike $AgNO_3$, $ZnCl_2$ exposure to biofilm resulted in a detectable increase in biofilm beyond the control. This response is most likely due to the presence of *Staphylococcus aureus* surface protein G (SasG;) this protein is a zinc dependent adhesion molecule, mediates bacterial cellular agglomeration, and subsequent formation of a protein rich biofilm.[50,241,260] Studies by Conrady et al. have also shown that biofilm formation can be blocked by chelation of zinc, explaining the activity of DMSA, although DMSA is novel for this purpose as shown here.[241]

4.3.2.3 Antimicrobial activity of metal ion conjugated SPION

Because of a lack of antibiotics or chemicals (such as metal salts) which can both decrease planktonic growth, and decrease biofilm formation, a novel SPION platform was developed here. Using this platform, all SPION showed antimicrobial activity and anti-biofilm activity at 1 mg/ml dry SPION weight. This dry weight corresponded to 457.871 +/- 21.064 μg/ml Fe_3O_4 after processing of the chelated SPION formulation, 530.796 +/- 15.241 μg/ml for iron conjugated SPION, 495.993 +/- 3.909 μg/ml for zinc conjugated SPION, or up to 581.353 +/- 10.26 ug/ml Fe_3O_4 in the silver SPION formulation (silver conjugated SPION formulations had the most Fe_3O_4, because the nanomaterial has a larger particle size and higher magnetic moment, and thus is more easily obtained during the magnetic separation process).

Antimicrobial activity was detected here with metal conjugations or chelated SPION. The silver SPION formulation was most effective against planktonic bacteria, with activity down to 100 μg/ml dry SPION weight (corresponding to 11.257 +/- 1.045 μg/ml silver), and had similar activity to $AgNO_3$ at this concentration. Interestingly, iron conjugated SPION and chelated SPION also showed antimicrobial activity without the presence of a known antimicrobial agent, and moreover, the zinc conjugated SPION formulation had activity at a concentration below that amount expected from studies with $ZnCl_2$ against planktonic bacteria (41.193 +/- 1.860 μg/ml zinc versus an MIC value of 136 μg/ml $ZnCl_2$ predicted from other studies).[258]

This study also showed that SPION produced antibiofilm activity, with all formulations showing activity at 1 mg/ml SPION dry weight. Moreover, zinc conjugated SPION inhibited biofilm formation down to 10 μg/ml SPION dry weight, or 0.415 +/- 0.0132

μg/ml of zinc. Higher concentrations of metals were also tested, where it was found that 4 mmol of iron added to SPION also inhibited biofilm formation down to 10 μg/ml SPION dry weight, or 0.169 +/- 0.131 μg/ml zinc. The presence of this zinc in iron conjugations, which was greater than the uncoated sample, is due to the $FeCl_3$ used in this study, which contained up to 0.002% zinc as contamination, and could account for 541 μg or up to 2,162 μg of zinc added (for 1 mmol or 4 mmol of $FeCl_3$ added, respectively) or less assuming a lower contamination level in this batch of salt. Furthermore, it was found that when 4 mmol of $ZnCl_2$ was added, biofilm recovery occurred in the presence of this SPION formulation. The zinc conjugated SPION formulated with 4 mmol of zinc contained 45.738 +/- 1.30 μg/ml zinc, more than any other formulation, but possibly more importantly, released a significant proportion (10.790 μg/ml) of this zinc at 4 hours, or 836% more zinc than TSB alone (which contained about 1.29 μg/ml zinc), where no nanoparticles were present. Comparatively, other formulations released 0.922 – 2.256 μg/ml zinc at the same time point.

In previous studies by Conrady and colleagues, it was determined that when a soluble G5 protein fragments of SaSG, an important receptor involved in biofilm formation and zinc chelation, biofilm was blocked in the presence of 136.315 μg/ml $ZnCl_2$. Under these conditions, the fragment inhibited biofilm at 10 μM, incorporating about 3 Zn^{2+} ions per molecule, or a loading capacity of about 9.489 μg/ml of zinc. Moreover, they showed that biofilm could be inhibited by chelation of zinc, specifically, addition of 30 μM of DPTA, and could be completely rescued by addition of about 6.326 μg/ml $ZnCl_2$ under these conditions. These results help to explain our own, that in the presence of SPION, or other macromolecules (such as the G5 protein fragment), that are able to chelate zinc and bind

to bacteria, biofilm is blocked, but when free zinc ions are present at a high concentration, or even released as observed here by zinc chelated SPION formulated with 4 mmol of $ZnCl_2$, biofilm growth resumes.

4.3.2.4 Antibiotic coated SPION

This study provided the first evidence that SPION would be useful for various infection related orthopedic applications. It was shown here that SPION could be produced with a coating of either vancomycin or gentamycin as confirmed by FTIR. Additionally, these materials retain antibacterial properties after the cross-linking. Importantly, it was found that antibiotics with magnetic properties (due to attachment to SPION) could be produced, as confirmed by VSM, and could also penetrate into a biofilm (as demonstrated by histology staining of iron). This research is promising, demonstrating the potential use of SPION for the magnetic delivery and concentration of antibiotics into infections such as those caused by bacterial biofilms. Yet, research still needs to be conducted before their application for infection treatment (such as the design of magnetic fields or magnetic implants for infection targeting). Another problem is that biofilm was increased by antibiotic coated SPION, and therefore other agents may be more promising (such as metal coated SPION or other combination treatments).

4.3.4 Mechanism of Action

It was shown here that antibiotics or antibacterial metal salts alone had a tendency to kill planktonic bacteria, but also had the propensity to increase biofilm formation. SPION

were explored as an alternative, and it was found that both antimicrobial activity and decreased biofilm could be achieved. Therefore, it was hypothesized that SPION acted by a unique mechanism compared to these other materials alone. Specifically, SPION formulated here could bind the 1) bacterial surface, and block biofilm formation, and/or 2) penetrate bacteria, releasing metals intracellularly, and thus kill bacteria (mechanisms 1 and 2 shown in **Figure 4.2**).

It was determined that for mechanism 1) SPION bind to the bacterial surface, specifically through chelation of zinc or other metal ions, that results in specific binding to the SasG surface receptor, in the range of ~15-40 μg/ml zinc. At higher concentrations zinc was released, and biofilm recovery occurred. Other formulations including silver, iron, and chelated SPION also blocked biofilm, and specifically these could be due to either lower concentration of zinc ions chelated from TSB, or present due to contaminates in iron salts (0.002% zinc contamination was in $FeCl_3$ salts used here), or due to mechanisms 2.

It was also determined that for mechanism 2) SPION penetrate bacteria, and thus can disrupt intracellular bacterial chemistry. It was found that SPION decreased intracellular bacillithiol (BSH) which protects cysteine from oxidation, and thus proteins from irreversible damage; can act as a buffer, or generate adducts to detoxify toxic challenges or antibiotics; and finally the thiols of BSH can avidly react with metals, and protect cytosolic chemistry from their harmful effects.[187,188] Bacillithiol is the only known low molecular weight (LMW) thiol present in *Staphylococcus aureus* devoted to protecting cytosolic chemistry; BSH- null bacteria are notably more sensitive to thiol-oxidizing reagents, reactive electrophiles, toxic metal ions and metalloids, and the antibiotic fosfomycin, and therefore BSH is of paramount importance for to ensure viability of

bacteria in the presence of such challenges.[186,188,261] In particular, it was found that for all free metal salts, including zinc, and iron, when applied to biofilms, these were not as effective (for zinc), or were not effective at all (for all iron salts) when used as antimicrobial alone compared to SPION (with the exception of silver, which showed similar activity against planktonic bacteria, but not against biofilm activity); this could be because the metal salts did not penetrate as well into the bacteria, and thus did not did not disrupt BSH chemistry. Importantly, in the presence of SPION, BSH could be oxidized directly, or alternatively, metal ions, such as silver, zinc, or iron, could be released directly by SPION, resulting in BSH depletion that leads to irreversible protein damage, compromised cytosolic chemistry, and subsequently cell death.[187,188]

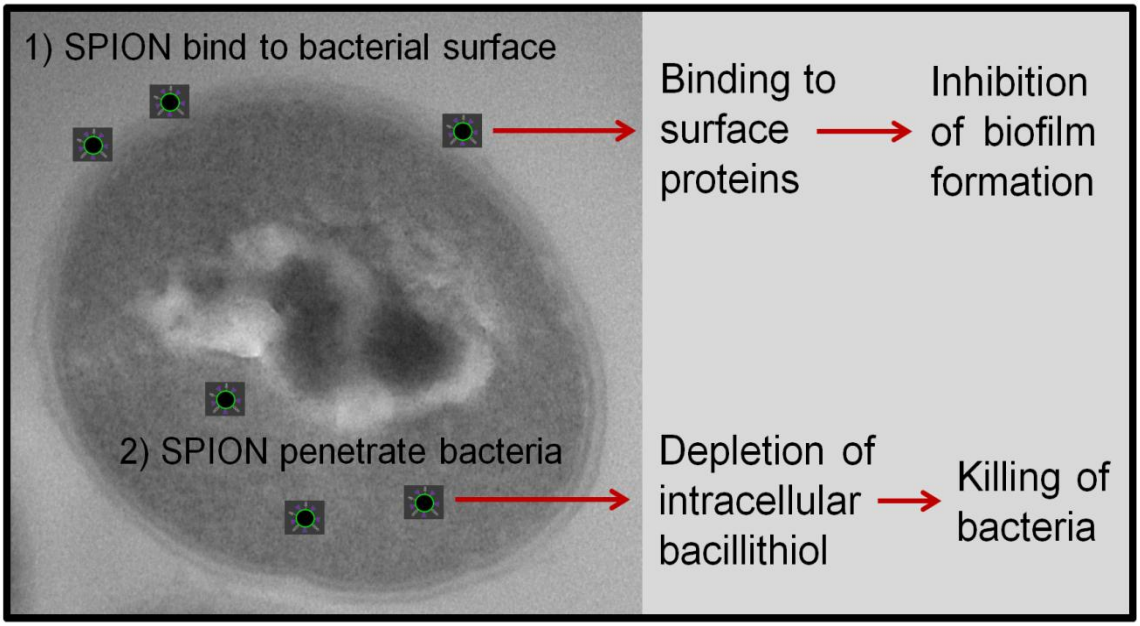

Figure 4.2 Hypothesized mechanisms of SPION action were probed. It was determined that 1) SPION bind to the bacterial surface, blocking biofilm formation through a zinc dependent receptor, and/or 2) that SPION penetrate bacteria, resulting in depletion of intracellular bacillithiol, and subsequently, bacteria death.

4.3.5 Conclusion

In conclusion, we report here for the first time that SPION reduced biofilm formation after the addition of iron, silver, or zinc, and reduce planktonic growth. It was found here that SPION attached to the bacterial surface, leading to a reduction in biofilms, where zinc conjugated SPION were the most effective at inhibiting biofilm formation at very low concentrations, unlike ionic (not nanoparticulate) compounds. These results were compared to traditional antibiotics used clinically including penicillin, oxacillin, gentamycin, streptomycin, and vancomycin. Although antibiotics did inhibit planktonic bacterial growth, all antibiotics caused an increase in biofilm, except vancomycin which had no effect on biofilm formation.

4.4 Magnetic manipulation of SPION and bacteria

4.4.1 Magnetic control of bacteria

Moving forward from the first evidence that SPION are useful for treating various infections related to medical devices, or other biofilm mediated or antibiotic resistant infections, we began to investigate magnetic manipulation of SPION and bacteria *in vitro*. This research is promising, demonstrating the coating of SPION with various antibacterial metals such as iron, zinc, and silver leading to improved antibacterial properties. The study also demonstrated methods for the magnetic control of SPION, mediating biofilm penetration or separation of flocculated bacteria. SPION alone have interesting antibacterial and anti-biofilm properties which should be further explored for treatment of device related infections, especially when coupled with magnetic field.

4.4.2 Broad goals and conclusions

Biofilm infection is a significant medical problem that is difficult to treat because of antibiotic resistant strains (such as MRSA) and due to biofilm formation. Prosthetic infection (or other orthopedic device related infections) and osteomyelitis are two examples of infection that are difficult to treat by conventional therapy and that require invasive and harmful procedures for the patient. Specifically, *Staphylococcus aureus* is a relevant biofilm forming organisms that need to be addressed in these infections.

SPION demonstrated critical anti-bacterial and anti-biofilm activity, which could be

modulated in a magnetic field, and thus SPION should be further explored as a new method for treating infections beyond (or possibly in combination with) antibiotics.

Finally, SPION were demonstrated here to exhibit crucial multifunctional activity. Importantly, the magnetic properties of SPION were utilized to target biofilms and bacteria, bind to bacteria, and kill bacteria, a combination this is impossible to achieve currently with traditional antibiotics alone **(Figure 4.3).**

Through the use of antibacterial nanoparticles (such as SPION) and development of more chemically active SPION, specific treatment of infection is becoming a possibility. SPION are also showing promise as therapeutic agents to regenerate native tissues especially for orthopaedic applications. Finally, methods for SPION targeting using magnetic drug delivery with MRI and ultrasound imaging as therapy feedback are being developed and could potentially be adapted to orthopedic or infection related applications. New applications of SPION provide strategies for therapeutic use of nanoparticles. Such insight could be expanded for other types of infection (other biofilm related, skin infection, etc.) or provide treatment of diseases never thought possible. Additionally, research into nanomaterials activity with bacteria improves environmental and health knowledge about nanoparticle toxicity which is a great concern when considering their various medical and other industrial uses.

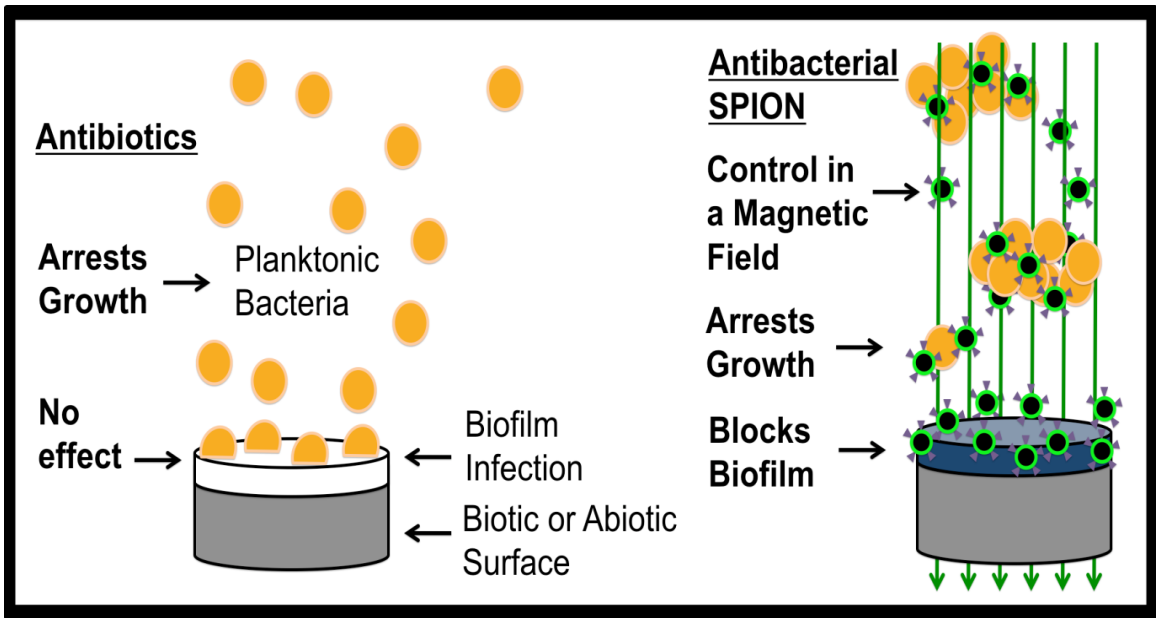

Figure 4.3 Studies were conducted to determine the antibacterial activity of antibiotics versus antimicrobial conjugated SPION. It was determined that antibiotics consistently decreased planktonic bacterial growth, and yet biofilm formation was either not affected, or, more frequently, increased in every case except vancomycin. SPION formulations also inhibited planktonic growth, especially through conjugation of antibacterial metal ions, and also blocked biofilm formation. SPION could also be controlled in a magnetic field, for possible concentration at the site of infection, or separation of free-floating bacteria. Therefore, SPION seem to exhibit crucial multifunctional behavior that may allow them to outperform antibiotics in the clinical treatment of device related infections.

4.5 Environmental and health considerations

4.5.1 Health Considerations

Consideration of safety for SPION use in humans is potential iron toxicity, immune response, and magnetic resonance imaging (MRI) safety. In particular, free iron is used in medicine as a therapeutic for treatment of anemia, and as SPION for MRI as an United States Food and Drug Administration (FDA) approved contrast agent.[262] Also, nanomaterials could cause macrophage activation; it will be considered below if this is a deleterious response, or could be advantageous in the presence of SPION.

Free iron is used in treatment of iron deficiency in anemia with a therapeutic dose from 3-6 mg/kg/day.[263] These treatments can also have toxic effects, with noticeable symptoms beginning at 10-20 mg/kg/day for elemental iron.[263] Such symptoms usually occur within 6 hours after an excessive amount of iron is swallowed, and severe toxicity occurs at ingestions of more than 50 mg/kg of elemental iron; at a toxic dose, iron corrodes your intestinal lining and is a direct irritant to the stomach, can cause severe vomiting, diarrhea, abdominal pain, dehydration and lethargy if not treated, and a bloody stool; shock and death can occur if poisoning is profound and inadequately treated.

With considerations of potential iron toxicity, we must consider if SPION are also toxic in the body. With SPION synthesized here, it was found that all SPION were effective at a concentration of 1000 μg/ml (~370 μg/ml Fe) which is equivalent to 24.667 to 28.461 mg/kg Fe for a 65 kg (143.300 pounds) or 75 kg adult (165.347 pounds) adult, respectively. If this was delivered as elemental iron, there could be concerns over iron

toxicity (or 49% to 57% of the toxic dose resulting in severe iron toxicity for free iron). Yet, some formulations were effective at inhibiting planktonic growth at lower concentrations of either 100 μg/ml (silver conjugated SPION) or inhibiting biofilm at a concentration of 10 μg/ml (zinc 1 mmol conjugated or iron 4 mmol conjugated SPION), equivalent to ~37 and ~3.7 μg/ml; these concentrations would be equivalent, or less, than those used clinically as an magnetic resonance imaging (MRI) contrast agent, where concentrations are usually utilized in the range of 2.5-4.2 mg/kg Fe.[262] Moreover, SPION dosages up to 500 mg/kg Fe have been safely tested in animals.[262] Some of these differences between SPION and elemental iron toxicity might be because SPION, other nanoparticles, and drug delivery vesicles in general help to encapsulate free metal ions, decrease bioavailability, and lower cytotoxicity compared to elemental preparations,[119,167,262] and in particular, the formulations here are coated with DMSA, which is a clinically used chelator of iron (the coating of nanomaterials can also limit release of metal ions).[167] Moreover, the research presented here demonstrates that in only one hour, SPION could be concentrated into biofilms in the presence of a magnet; the ability to concentrate SPION therapeutics might enable the translation of this research into the clinic if magnetic fields could be designed to enable SPION concentration at the infection site *in vivo*; yet safety concerns about biodistribution, pharmacokinetics, and biodegradation must be considered, especially in the presence of strong magnetic fields, such as produced by an MRI.

One other consideration is if SPION would cause immune activation. In particular, SPION are known to be taken up by macrophages, and size dependent uptake has been observed; smaller SPION have a longer circulation time than larger particles,[262] whereas

large nanoparticles (≥300 nm) are limited by a short blood-circulation time, due to rapid clearing from the blood stream, either by mechanical trapping, or uptake into macrophages of the reticuloendothelial system, particularly in the liver and spleen.[118,225] Some researchers have considered using this property of SPION as an advantage, for imaging of inflammatory activity, where macrophages are present,[262] and could be an advantage for treatment of infections if macrophages were activated in the presence of SPION, increasing immune activity at the infection site. Such properties of SPION, causing immune system activation, or uptake up by macrophages, should be the focus of future *in vivo* device related infection studies, and could easily by monitored by MRI.[262]

4.5.2 Industrial applications of nanomaterials and environmental considerations

Lastly, although there has been much promise for the use of nanomaterials (whether nanoparticles or nanostructured surface features) to fight infection, it would be remiss not to mention the possible, yet largely unknown, environmental consequences of nanomaterials. In particular, recent research has exposed the possible environmental and toxicological concerns of nanomaterials. This is especially true when considering that nanotechnology was estimated in 2008 to be a US$10.5 billion industry in the USA (eg, through the use of nanotechnology in sunscreens, paints, and antimicrobial agents) that is expected to grow to 1 trillion by 2015.[264,265] Therefore, concerns about the accidental release of nanomaterials (during manufacturing or use) into the environment are growing. Concerns have also been raised about damage to naturally occurring bacteria in the environment. For example, a study by Kang et al examined the potential release of

carbon-based nanomaterials (CBNs), determining that patterns of cytotoxicity occurred with SWNT inactivating *Pseudomonas aeruginosa*, *E. coli*, and *S. epidermidis*, but not *Bacillus subtilis*.[130] High rates of inactivation were also found in wastewater effluent and river water, especially with SWNTs, implying that certain CBNs might reduce microbial activity and potentially decrease microbial diversity.[130] In a similar type of study by Bradford et al, it was shown that silver nanoparticles in a model of river estuarine sediments did not reduce microbial diversity (as determined by genetic diversity).[266] Yet, separate concerns about the environmental release of silver nanoparticles have been raised, such as the potential spread of silver resistance in bacteria.[267,268] Studies like these also help raise our awareness about the use of nanomaterials in humans for medical purposes, where microbial diversity (of natural microbial flora, which prevents the spread of virulent organisms) and resistance to nanomaterials (similar to current problems of antibiotic resistance) are of paramount concern.

4.5.3 Conclusions

In the area of prevention and treatment of infection, it has been proposed that materials not only be used by professionals (such as during infection treatment by clinicians in hospitals) but also by every person (such as nanoparticles in paints for use at home or over the counter nanodrugs). For this reason, future work must rely on collaboration among engineers, clinicians, and environmental scientists (and those from other fields as well) to fully characterize such nanomaterials in terms of chemistry, impurities, and toxicity. With the establishment of safe usage guidelines, nanomaterials can be safely

used for the important and growing area of antibacterial material design. We should be excited (not frightened) about what the future holds for nanotechnology in these collaborative anti-infection efforts.

5. References

1. Hall-Stoodley L, Costerton JW, Stoodley P. Bacterial biofilms: from the Natural environment to infectious diseases. Nat Rev Micro 2004;2(2):95-108.
2. Donlan RM, Costerton JW. Biofilms: Survival mechanisms of clinically relevant microorganisms. Clinical Microbiology Reviews 2002;15(2):167-+.
3. Donlan RM. Biofilms and device-associated infections. Emerging Infectious Diseases 2001;7(2):277-281.
4. Taylor EN, Webster TJ. The use of superparamagnetic nanoparticles for prosthetic biofilm prevention. International Journal of Nanomedicine 2009;4:145-152.
5. Puckett SD, Taylor E, Raimondo T, Webster TJ. The relationship between the nanostructure of titanium surfaces and bacterial attachment. Biomaterials 2010;31(4):706-713.
6. Taylor E, Webster TJ. Reducing infections through nanotechnology and nanoparticles. International Journal of Nanomedicine 2011;6:1463-1473.
7. Colon G, Ward BC, Webster TJ. Increased osteoblast and decreased Staphylococcus epidermidis functions on nanophase ZnO and TiO2. Journal of Biomedical Materials Research Part A 2006;78A(3):595-604.
8. Siegel RW, Fougere GE. Mechanical properties of nanophase metals. Nanostructured Materials 1995;6(1–4):205-216.
9. Cardo D, Horan T, Andrus M, Dembinski M, Edwards J, Peavy G, Tolson J, Wagner D, Syst N. National Nosocomial Infections Surveillance (NNIS) System Report, data summary from January 1992 through June 2004, issued October 2004. American Journal of Infection Control 2004;32(8):470-485.
10. O'Grady NP, Alexander M, Dellinger EP, Gerberding JL, Heard SO, Maki DG, Masur H, McCormick RD, Mermel LA, Pearson ML and others. Guidelines for the prevention of intravascular catheter-related infections. Centers for Disease Control and Prevention. MMWR. Recommendations and reports : Morbidity and mortality weekly report. Recommendations and reports / Centers for Disease Control 2002;51(RR-10):1-29.
11. Rello J, Ochagavia A, Sabanes E, Roque M, Mariscal D, Reynaga E, Valles J. Evaluation of outcome of intravenous catheter-related infections in critically ill patients. American Journal of Respiratory and Critical Care Medicine 2000;162(3):1027-1030.
12. Dimick JB, Pelz RK, Consunji R, Swoboda SM, Hendrix CW, Lipsett PA. Increased resource use associated with catheter-related bloodstream infection in the surgical intensive care unit. Archives of Surgery 2001;136(2):229-234.
13. Mermel LA. Prevention of intravascular catheter-related infections (vol 132, pg 391, 2000). Annals of Internal Medicine 2000;133(5):395-395.
14. Gristina AG. BIOMATERIAL-CENTERED INFECTION - MICROBIAL ADHESION VERSUS TISSUE INTEGRATION. Science 1987;237(4822):1588-1595.
15. Darouiche RO. Current concepts - Treatment of infections associated with surgical implants. New England Journal of Medicine 2004;350(14):1422-1429.
16. Moroni A, Vannini F, Mosca M, Giannini S. Techniques to avoid pin loosening and infection in external fixation. Journal of Orthopaedic Trauma 2002;16(3):189-195.
17. Mahan J, Seligson D, Henry SL, Hynes P, Dobbins J. FACTORS IN PIN TRACT

INFECTIONS. Orthopedics 1991;14(3):305-308.
18. Zlowodzki M, Prakash JS, Aggarwal NK. External fixation of complex femoral shaft fractures. International Orthopaedics 2007;31(3):409-413.
19. Green SA, Ripley MJ. CHRONIC OSTEOMYELITIS IN PIN TRACKS. Journal of Bone and Joint Surgery-American Volume 1984;66A(7):1092-1098.
20. Vonrecum AF, Park JB. PERMANENT PERCUTANEOUS DEVICES. Crc Critical Reviews in Bioengineering 1981;5(1):37-77.
21. Puckett SD, Lee PP, Ciombor DM, Aaron RK, Webster TJ. Nanotextured titanium surfaces for enhancing skin growth on transcutaneous osseointegrated devices. Acta Biomaterialia 2010;6(6):2352-2362.
22. Stanton T HJ, Phillips M, Immerman I. Study points to savings with infection-screening program before TJR. AAOS Now 2010; 2011.
23. Bozic KJ, Kurtz SM, Lau E, Ong K, Vail TP, Berry DJ. The Epidemiology of Revision Total Hip Arthroplasty in the United States. J Bone Joint Surg Am 2009;91(1):128-133.
24. Bozic KJ, Kurtz SM, Lau E, Ong K, Chiu V, Vail TP, Rubash HE, Berry DJ. The Epidemiology of Revision Total Knee Arthroplasty in the United States. Clinical Orthopaedics and Related Research 2010;468(1):45-51.
25. Davis N, Curry A, Gambhir AK, Panigrahi H, Walker CRC, Wilkins EGL, Worsley MA, Kay PR. Intraoperative bacterial contamination in operations for joint replacement. Journal of Bone and Joint Surgery-British Volume 1999;81B(5):886-889.
26. Lina G, Boutite F, Tristan A, Bes M, Etienne J, Vandenesch F. Bacterial competition for human nasal cavity colonization: Role of staphylococcal agr alleles. Applied and Environmental Microbiology 2003;69(1):18-23.
27. Otto M, Echner H, Voelter W, Gotz F. Pheromone cross-inhibition between Staphylococcus aureus and Staphylococcus epidermidis. Infection and Immunity 2001;69(3):1957-1960.
28. Schlapp M, Friess W. Collagen/PLGA microparticle composites for local controlled delivery of gentamicin. Journal of Pharmaceutical Sciences 2003;92(11):2145-2151.
29. Palma M, Haggar A, Flock JI. Adherence of Staphylococcus aureus is enhanced by an endogenous secreted protein with broad binding activity. Journal of Bacteriology 1999;181(9):2840-2845.
30. Atiyeh BS, Costagliola M, Hayek SN, Dibo SA. Effect of silver on burn wound infection control and healing: Review of the literature. Burns 2007;33(2):139-148.
31. Burd A, Kwok CH, Hung SC, Chan HS, Gu H, Lam WK, Huang L. A comparative study of the cytotoxicity of silver-based dressings in monolayer cell, tissue explant, and animal models. Wound Repair and Regeneration 2007;15(1):94-104.
32. Hopkins CG, McHugh PE, McGarry JP. Computational Investigation of the Delamination of Polymer Coatings During Stent Deployment. Annals of Biomedical Engineering 2010;38(7):2263-2273.
33. Kollef MH, Afessa B, Anzueto A, Veremakis C, Kerr KM, Margolis BD, Craven DE, Roberts PR, Arroliga AC, Hubmayr RD and others. Silver-Coated Endotracheal Tubes and Incidence of Ventilator-Associated Pneumonia. JAMA: The Journal of the American Medical Association 2008;300(7):805-813.
34. Betsch BY, Eggli S, Siebenrock KA, Tauber MG, Muhlemann K. Treatment of joint prosthesis infection in accordance with current recommendations improves outcome. Clinical Infectious Diseases 2008;46(8):1221-1226.
35. Bernard L, Hoffmeyer P, Assal M, Vaudaux P, Schrenzel J, Lew D. Trends in the treatment of orthopaedic prosthetic infections. Journal of Antimicrobial Chemotherapy 2004;53(2):127-129.

36. Marculescu CE, Berbari EF, Hanssen AD, Steckelberg JM, Harmsen SW, Mandrekar JN, Osmon DR. Outcome of prosthetic joint infections treated with debridement and retention of components. Clinical Infectious Diseases 2006;42(4):471-478.
37. Hendriks JGE, van Horn JR, van der Mei HC, Busscher HJ. Backgrounds of antibiotic-loaded bone cement and prosthesis-related infection. Biomaterials 2004;25(3):545-556.
38. Klein E, Smith DL, Laxminarayan R. Hospitalizations and deaths caused by methicillin-resistant Staphylococcus aureus, United States, 1999-2005. Emerging Infectious Diseases 2007;13(12):1840-1846.
39. Hidron AI, Edwards JR, Patel J, Horan TC, Sievert DM, Pollock DA, Fridkin SK, Natl Healthcare Safety Network T, Participating Natl Healthcare S. Antimicrobial-Resistant Pathogens Associated With Healthcare-Associated Infections: Annual Summary of Data Reported to the National Healthcare Safety Network at the Centers for Disease Control and Prevention, 2006-2007. Infection Control and Hospital Epidemiology 2008;29(11):996-1011.
40. Rosenthal VD, Maki DG, Jamulitrat S, Medeiros EA, Todi SK, Gomez DY, Leblebicioglu H, Abu Khader I, Novales MGM, Berba R and others. International Nosocomial Infection Control Consortium (INICC) report, data summary for 2003-2008, issued June 2009. American Journal of Infection Control 2010;38(2):95-U31.
41. Neu HC. The Crisis in Antibiotic Resistance. Science 1992;257(5073):1064-1073.
42. Mingeot-Leclercq MP, Glupczynski Y, Tulkens PM. Aminoglycosides: Activity and resistance. Antimicrobial Agents and Chemotherapy 1999;43(4):727-737.
43. Sanglard D, Odds FC. Resistance of Candida species to antifungal agents: molecular mechanisms and clinical consequences. Lancet Infectious Diseases 2002;2(2):73-85.
44. Jabra-Rizk MA, Falkler WA, Meiller TF. Fungal biofilms and drug resistance. Emerging Infectious Diseases 2004;10(1):14-19.
45. Pfaller MA, Diekema DJ, Gibbs DL, Newell VA, Nagy E, Dobiasova S, Rinaldi M, Barton R, Veselov A, the Global Antifungal Surveillance Group. Candida krusei, a Multidrug-Resistant Opportunistic Fungal Pathogen: Geographic and Temporal Trends from the ARTEMIS DISK Antifungal Surveillance Program, 2001 to 2005. J. Clin. Microbiol. 2008;46(2):515-521.
46. Bugg TDH, Dutka-Malen S, Arthur M, Courvalin P, Walsh CT. Identification of vancomycin resistance protein VanA as a D-alanine:D-alanine ligase of altered substrate specificity. Biochemistry 1991;30(8):2017-2021.
47. Chambers HF. Penicillin-binding protein-mediated resistance in pneumococci and staphylococci. Journal of Infectious Diseases 1999;179:S353-S359.
48. Wikipedia.org. Antibiotic Resistance. Drug Resistance. Volume 2012: www.wikipedia.org; 20 January, 2012.
49. Izano EA, Amarante MA, Kher WB, Kaplan JB. Differential Roles of Poly-N-Acetylglucosamine Surface Polysaccharide and Extracellular DNA in Staphylococcus aureus and Staphylococcus epidermidis Biofilms. Appl. Environ. Microbiol. 2008;74(2):470-476.
50. Rohde H, Burandt EC, Siemssen N, Frommelt L, Burdelski C, Wurster S, Scherpe S, Davies AP, Harris LG, Horstkotte MA and others. Polysaccharide intercellular adhesin or protein factors in biofilm accumulation of Staphylococcus epidermidis and Staphylococcus aureus isolated from prosthetic hip and knee joint infections. Biomaterials 2007;28(9):1711-1720.
51. Costerton JW, Stewart PS, Greenberg EP. Bacterial biofilms: A common cause of persistent infections. Science 1999;284(5418):1318-1322.
52. Fux CA, Costerton JW, Stewart PS, Stoodley P. Survival strategies of infectious

biofilms. Trends in Microbiology 2005;13(1):34-40.
53. Otto M. Staphylococcus epidermidis - the 'accidental' pathogen. Nature Reviews Microbiology 2009;7(8):555-567.
54. LaPlante KL, Woodmansee S. Activities of Daptomycin and Vancomycin Alone and in Combination with Rifampin and Gentamicin against Biofilm-Forming Methicillin-Resistant Staphylococcus aureus Isolates in an Experimental Model of Endocarditis. Antimicrobial Agents and Chemotherapy 2009;53(9):3880-3886.
55. Ceri H, Olson M, Stremick C, Read R, Morck D, Buret A. The Calgary Biofilm Device: New technology for rapid determination of antibiotic susceptibilities in bacterial biofilms. Journal of Clinical Microbiology 1999;37:1771 - 1776.
56. Kaplan JB, Jabbouri S, Sadovskaya I. Extracellular DNA-dependent biofilm formation by Staphylococcus epidermidis RP62A in response to subminimal inhibitory concentrations of antibiotics. Research in Microbiology 2011;162(5):535-541.
57. Frank KL, Reichert EJ, Piper KE, Patel R. In vitro effects of antimicrobial agents on planktonic and biofilm forms of Staphylococcus lugdunensis clinical isolates. Antimicrobial Agents and Chemotherapy 2007;51(3):888-895.
58. Rachid S, Ohlsen K, Witte W, Hacker J, Ziebuhr W. Effect of subinhibitory antibiotic concentrations on polysaccharide intercellular adhesin expression in biofilm-forming Staphylococcus epidermidis. Antimicrobial Agents and Chemotherapy 2000;44(12):3357-3363.
59. O'Toole GA, Stewart PS. Biofilms strike back. Nat Biotech 2005;23(11):1378-1379.
60. Hess DJ, Henry-Stanley MJ, Wells CL. Gentamicin Promotes Staphylococcus aureus Biofilms on Silk Suture. Journal of Surgical Research 2011;170(2):302-308.
61. Vuong C, Kidder JB, Jacobson ER, Otto M, Proctor RA, Somerville GA. Staphylococcus epidermidis polysaccharide intercellular adhesin production significantly increases during tricarboxylic acid cycle stress. Journal of Bacteriology 2005;187(9):2967-2973.
62. Lim Y, Jana M, Luong TT, Lee CY. Control of glucose- and NaCI-induced biofilm formation by rbf in Staphylococcus aureus. Journal of Bacteriology 2004;186(3):722-729.
63. Deighton M, Borland R. REGULATION OF SLIME PRODUCTION IN STAPHYLOCOCCUS-EPIDERMIDIS BY IRON LIMITATION. Infection and Immunity 1993;61(10):4473-4479.
64. Rachid S, Ohlsen K, Wallner U, Hacker J, Hecker M, Ziebuhr W. Alternative transcription factor sigma(B) is involved in regulation of biofilm expression in a Staphylococcus aureus mucosal isolate. Journal of Bacteriology 2000;182(23):6824-6826.
65. Cramton SE, Ulrich M, Gotz F, Doring G. Anaerobic conditions induce expression of polysaccharide intercellular adhesin in Staphylococcus aureus and Staphylococcus epidermidis. Infection and Immunity 2001;69(6):4079-4085.
66. Knobloch JKM, Bartscht K, Sabottke A, Rohde H, Feucht HH, Mack D. Biofilm formation by Staphylococcus epidermidis depends on functional RsbU, an activator of the sigB operon: Differential activation mechanisms due to ethanol and salt stress. Journal of Bacteriology 2001;183(8):2624-2633.
67. Massonet C, Pintens V, Merckx R, Anne J, Lammertyn E, Van Eldere J. Effect of iron on the expression of sirR and sitABC in biofilm-associated Staphylococcus epidermidis. Bmc Microbiology 2006;6.
68. McWhirter MJ, Bremer PJ, Lamont IL, McQuillan AJ. Siderophore-mediated covalent bonding to metal (oxide) surfaces during biofilm initiation by Pseudomonas aeruginosa bacteria. Langmuir 2003;19(9):3575-3577.

69. Johnson M, Cockayne A, Morrissey JA. Iron-regulated biofilm formation in Staphylococcus aureus Newman requires ica and the secreted protein Emp. Infection and Immunity 2008;76(4):1756-1765.
70. Musk DJ, Banko DA, Hergenrother PJ. Iron salts perturb biofilm formation and disrupt existing biofilms of Pseudomonas aeruginosa. Chemistry & Biology 2005;12(7):789-796.
71. Allison KR, Brynildsen MP, Collins JJ. Metabolite-enabled eradication of bacterial persisters by aminoglycosides. Nature 2011;473(7346):216-+.
72. Gottlieb T, Atkins BL, Shaw DR. Infectious diseases - 7: Soft tissue, bone and joint infections. Medical Journal of Australia 2002;176(12):609-615.
73. Stoodley P, Cargo R, Rupp CJ, Wilson S, Klapper I. Biofilm material properties as related to shear-induced deformation and detachment phenomena. Journal of Industrial Microbiology & Biotechnology 2002;29(6):361-367.
74. Nair SP, Meghji S, Wilson M, Reddi K, White P, Henderson B. Bacterially induced bone destruction: Mechanisms and misconceptions. Infection and Immunity 1996;64(7):2371-2380.
75. Smeltzer MSaN, C.L. , editor. Osteomyelitis and septic arthritis. 2001 ed. New York , NY: Kluwer Academic/Plenum Publishing Corp.; 2001. 213-246 p.
76. Subbiahdoss G, Kuijer R, Grijpma DW, van der Mei HC, Busscher HJ. Microbial biofilm growth vs. tissue integration: "The race for the surface" experimentally studied. Acta Biomaterialia 2009;5(5):1399-1404.
77. Schaible ME, Kaufmann SHE. Iron and microbial infection. Nature Reviews Microbiology 2004;2(12):946-953.
78. school Hm. Update on osteoporosis drugs. Harvard Women's Health Watch: http://www.health.harvard.edu/newsweek/Update_on_osteoporosis_drugs.htm; 2004.
79. Hughes DE, Wright KR, Uy HL, Sasaki A, Yoneda T, Roodman DG, Mundy GR, Boyce BF. Bisphosphonates promote apoptosis in murine osteoclasts in vitro and in vivo. Journal of Bone and Mineral Research 1995;10(10):1478-1487.
80. Hughes DE, Macdonald BR, Russell RGG, Gowen M. INHIBITION OF OSTEOCLAST-LIKE CELL-FORMATION BY BISPHOSPHONATES IN LONG-TERM CULTURES OF HUMAN-BONE MARROW. Journal of Clinical Investigation 1989;83(6):1930-1935.
81. Reinholz GG, Getz B, Pederson L, Sanders ES, Subramaniam M, Ingle JN, Spelsberg TC. Bisphosphonates directly regulate cell proliferation, differentiation, and gene expression in human osteoblasts. Cancer Research 2000;60(21):6001-6007.
82. Adami S, Zamberlan N. Adverse effects of bisphosphonates. A comparative review. Drug safety : an international journal of medical toxicology and drug experience 1996;14(3):158-70.
83. Allan SM, Rothwell NJ. Inflammation in central nervous system injury. Philosophical Transactions of the Royal Society of London Series B-Biological Sciences 2003;358(1438):1669-1677.
84. Tan R, Feng Q, She Z, Wang M, Jin H, Li J, Yu X. In vitro and in vivo degradation of an injectable bone repair composite. Polymer Degradation and Stability 2010;95(9):1736-1742.
85. Martin P, Leibovich SJ. Inflammatory cells during wound repair: the good, the bad and the ugly. Trends in Cell Biology 2005;15(11):599-607.
86. James M A. Chapter 4 Mechanisms of inflammation and infection with implanted devices. Cardiovascular Pathology;2(3, Supplement):33-41.
87. Sivakumar M, Kumar Dhanadurai KS, Rajeswari S, Thulasiraman V. Failures in stainless steel orthopaedic implant devices: A survey. Journal of Materials Science

Letters 1995;14(5):351-354.
88. Mark S. Smeltzer CLN, and Richard P. Evans, editor. Biofilms and Aseptic Loosening. Volume 1. Berling: Springer; 2008.
89. Vuong C, Voyich JM, Fischer ER, Braughton KR, Whitney AR, DeLeo FR, Otto M. Polysaccharide intercellular adhesin (PIA) protects *Staphylococcus epidermidis* against major components of the human innate immune system. Cellular Microbiology 2004;6(3):269-275.
90. Lai YP, Villaruz AE, Li M, Cha DJ, Sturdevant DE, Otto M. The human anionic antimicrobial peptide dermcidin induces proteolytic defence mechanisms in staphylococci. Molecular Microbiology 2007;63(2):497-506.
91. Woo KM, Chen VJ, Ma PX. Nano-fibrous scaffolding architecture selectively enhances protein adsorption contributing to cell attachment. Journal of Biomedical Materials Research Part A 2003;67A(2):531-537.
92. Khang D, Kim SY, Liu-Snyder P, Palmore GTR, Durbin SM, Webster TJ. Enhanced fibronectin adsorption on carbon nanotube/poly(carbonate) urethane: Independent role of surface nano-roughness and associated surface energy. Biomaterials 2007;28(32):4756-4768.
93. Webster TJ, Ergun C, Doremus RH, Siegel RW, Bizios R. Specific proteins mediate enhanced osteoblast adhesion on nanophase ceramics. Journal of Biomedical Materials Research 2000;51(3):475-483.
94. Puckett S, Pareta R, Webster TJ. Nano rough micron patterned titanium for directing osteoblast morphology and adhesion. International Journal of Nanomedicine 2008;3(2):229-241.
95. Ercan B, Taylor E, Alpaslan E, Webster TJ. Diameter of titanium nanotubes influences anti-bacterial efficacy. Nanotechnology 2011;22(29).
96. Bjursten LM, Rasmusson L, Oh S, Smith GC, Brammer KS, Jin S. Titanium dioxide nanotubes enhance bone bonding in vivo. Journal of Biomedical Materials Research Part A 2010;92A(3):1218-1224.
97. von Wilmowsky C, Bauer S, Lutz R, Meisel M, Neukam FW, Toyoshima T, Schmuki P, Nkenke E, Schlegel KA. In Vivo Evaluation of Anodic TiO(2) Nanotubes: An Experimental Study in the Pig. Journal of Biomedical Materials Research Part B-Applied Biomaterials 2009;89B(1):165-171.
98. Puckett S. Select Nanofabricated Titanium Materials for Enhancing Bone and Skin Growth of Intraosseous Transcutaneous Amputation Prostheses. Providence, RI: Brown University; 2010.
99. Anagnostou F, Debet A, Pavon-Djavid G, Goudaby Z, Helary G, Migonney V. Osteoblast functions on functionalized PMMA-based polymers exhibiting Staphylococcus aureus adhesion inhibition. Biomaterials 2006;27(21):3912-3919.
100. Kinnari TJ, Peltonen LI, Kuusela T, Kivilahti J, Kononen M, Jero J. Bacterial adherence to titanium surface coated with human serum albumin. Otology & Neurotology 2005;26(3):380-384.
101. Park J, Bauer S, von der Mark K, Schmuki P. Nanosize and vitality: TiO2 nanotube diameter directs cell fate. Nano Letters 2007;7(6):1686-1691.
102. Oh S, Brammer KS, Li YSJ, Teng D, Engler AJ, Chien S, Jin S. Stem cell fate dictated solely by altered nanotube dimension. Proceedings of the National Academy of Sciences of the United States of America 2009;106(7):2130-2135.
103. Webster TJ, Siegel RW, Bizios R. Osteoblast adhesion on nanophase ceramics. Biomaterials 1999;20(13):1221-1227.
104. Yao C, Slamovich EB, Webster TJ. Enhanced osteoblast functions on anodized titanium with nanotube-like structures. Journal of Biomedical Materials Research

Part A 2008;85A(1):157-166.
105. Alpaslan E, Ercan B, Webster TJ. Anodized 20 nm diameter nanotubular titanium for improved bladder stent applications. International Journal of Nanomedicine 2011;6:219-225.
106. Rajyalakshmi A, Ercan B, Balasubramanian K, Webster TJ. Reduced adhesion of macrophages on anodized titanium with select nanotube surface features. International Journal of Nanomedicine 2011;6:1765-1771.
107. Ercan B. Anodized Nanotubular Titanium as and Orthopedic Implant and the Effect of Electrical Stimulation. Providence, RI: Brown University; 2011.
108. Ercan B, Kummer KM, Tarquinio KM, Webster TJ. Decreased Staphylococcus aureus biofilm growth on anodized nanotubular titanium and the effect of electrical stimulation. Acta Biomaterialia 2011;7(7):3003-3012.
109. Wentworth JS, Austin FE, Garber N, Gilboa-Garber N, Paterson CA, Doyle RJ. Cytoplasmic lectins contribute to the adhesion of Pseudomonas aeruginosa. Biofouling 1991;4(1-3):99-104.
110. Yoshinari M, Oda Y, Kato T, Okuda K. Influence of surface modifications to titanium on antibacterial activity in vitro. Biomaterials 2001;22(14):2043-2048.
111. Yoshinari M, Oda Y, Kato T, Okuda K, Hirayama A. Influence of surface modifications to titanium on oral bacterial adhesion in vitro. Journal of Biomedical Materials Research 2000;52(2):388-394.
112. Wan YZ, Raman S, He F, Huang Y. Surface modification of medical metals by ion implantation of silver and copper. Vacuum 2007;81(9):1114-1118.
113. Li B, Logan BE. Bacterial adhesion to glass and metal-oxide surfaces. Colloids and Surfaces B: Biointerfaces 2004;36(2):81-90.
114. Eick S, Glockmann E, Brandl B, Pfister W. Adherence of Streptococcus mutans to various restorative materials in a continuous flow system. Journal of Oral Rehabilitation 2004;31(3):278-285.
115. Katsikogianni M, Spiliopoulou I, Dowling D, Missirlis Y. Adhesion of slime producing <i>Staphylococcus epidermidis</i> strains to PVC and diamond-like carbon/silver/fluorinated coatings. Journal of Materials Science: Materials in Medicine 2006;17(8):679-689.
116. Correa CB, Pires JR, Fernandes-Filho RB, Sartori R, Vaz LG. Fatigue and Fluoride Corrosion on Streptococcus mutans Adherence to Titanium-Based Implant/Component Surfaces. Journal of Prosthodontics 2009;18(5):382-387.
117. Karlsson HL, Cronholm P, Gustafsson J, Möller L. Copper Oxide Nanoparticles Are Highly Toxic: A Comparison between Metal Oxide Nanoparticles and Carbon Nanotubes. Chemical Research in Toxicology 2008;21(9):1726-1732.
118. Kreuter J. Nanoparticles and microparticles for drug and vaccine delivery. Journal of Anatomy 1996;189:503-505.
119. Lee J-E, Park J-C, Lee KH, Oh SH, Kim J-G, Suh H. An Infection-Preventing Bilayered Collagen Membrane Containing Antibiotic-Loaded Hyaluronan Microparticles: Physical and Biological Properties. Artificial Organs 2002;26(7):636-646.
120. Lee J-E, Park J-C, Lee Kwang H, Oh Sang H, Suh H. Laminin Modified Infection-Preventing Collagen Membrane Containing Silver Sulfadiazine–Hyaluronan Microparticles. Artificial Organs 2002;26(6):521-528.
121. Yenice I, Calis S, Atilla B, Kas HS, Ozalp M, Ekizoglu M, Bilgili H, Hincal AA. In vitro/in vivo evaluation of the efficiency of teicoplanin-loaded biodegradable microparticles formulated for implantation to infected bone defects. Journal of Microencapsulation 2003;20(6):705-717.
122. Raghupathi KR, Koodali RT, Manna AC. Size-Dependent Bacterial Growth Inhibition

and Mechanism of Antibacterial Activity of Zinc Oxide Nanoparticles. Langmuir 2011;27(7):4020-4028.
123. Jiang W, Mashayekhi H, Xing BS. Bacterial toxicity comparison between nano- and micro-scaled oxide particles. Environmental Pollution 2009;157(5):1619-1625.
124. Jones N, Ray B, Ranjit KT, Manna AC. Antibacterial activity of ZnO nanoparticle suspensions on a broad spectrum of microorganisms. Fems Microbiology Letters 2008;279(1):71-76.
125. Lipovsky A, Tzitrinovich Z, Friedmann H, Applerot G, Gedanken A, Lubart R. EPR Study of Visible Light-Induced ROS Generation by Nanoparticles of ZnO. The Journal of Physical Chemistry C 2009;113(36):15997-16001.
126. Sawai J, Kawada E, Kanou F, Igarashi H, Hashimoto A, Kokugan T, Shimizu M. Detection of active oxygen generated from ceramic powders having antibacterial activity. Journal of Chemical Engineering of Japan 1996;29(4):627-633.
127. Sawai J, Kojima H, Igarashi H, Hashimoto A, Shoji S, Takehara A, Sawaki T, Kokugan T, Shimizu M. Escherichia coli damage by ceramic powder slurries. Journal of Chemical Engineering of Japan 1997;30(6):1034-1039.
128. Sawai J, Shoji S, Igarashi H, Hashimoto A, Kokugan T, Shimizu M, Kojima H. Hydrogen peroxide as an antibacterial factor in zinc oxide powder slurry. Journal of Fermentation and Bioengineering 1998;86(5):521-522.
129. Zhang L, Jiang Y, Ding Y, Povey M, York D. Investigation into the antibacterial behaviour of suspensions of ZnO nanoparticles (ZnO nanofluids). Journal of Nanoparticle Research 2007;9(3):479-489.
130. Kang S, Mauter MS, Elimelech M. Microbial Cytotoxicity of Carbon-Based Nanomaterials: Implications for River Water and Wastewater Effluent. Environmental Science & Technology 2009;43(7):2648-2653.
131. Sirivisoot S, Pareta R, Webster TJ. Electrically controlled drug release from nanostructured polypyrrole coated on titanium. Nanotechnology 2011;22(8).
132. Sirivisoot S, Webster TJ. Multiwalled carbon nanotubes enhance electrochemical properties of titanium to determine in situ bone formation. Nanotechnology 2008;19(29):295101.
133. Sirivisoot S, Yao C, Xiao X, Sheldon BW, Webster TJ. Greater osteoblast functions on multiwalled carbon nanotubes grown from anodized nanotubular titanium for orthopedic applications. Nanotechnology 2007;18(36).
134. Aslan S, Loebick CZ, Kang S, Elimelech M, Pfefferle LD, Van Tassel PR. Antimicrobial biomaterials based on carbon nanotubes dispersed in poly(lactic-co-glycolic acid). Nanoscale 2010;2(9):1789-1794.
135. Kang S, Herzberg M, Rodrigues DF, Elimelech M. Antibacterial effects of carbon nanotubes: Size does matter. Langmuir 2008;24(13):6409-6413.
136. Kang S, Mauter MS, Elimelech M. Physicochemical determinants of multiwalled carbon nanotube bacterial cytotoxicity. Environmental Science & Technology 2008;42(19):7528-7534.
137. Kang S, Pinault M, Pfefferle LD, Elimelech M. Single-walled carbon nanotubes exhibit strong antimicrobial activity. Langmuir 2007;23(17):8670-8673.
138. Minnikanti S, Pereira MGAG, Jaraiedi S, Jackson K, Costa-Neto CM, Li Q, Peixoto N. In vivo electrochemical characterization and inflammatory response of multiwalled carbon nanotube-based electrodes in rat hippocampus. Journal of Neural Engineering 2010;7(1):016002.
139. Misra SK, Watts PCP, Valappil SP, Silva SRP, Roy I, Boccaccini AR. Poly(3-hydroxybutyrate)/Bioglass ® composite films containing carbon nanotubes. Nanotechnology 2007;18(7):075701.

140. Naguib NN, Mueller YM, Bojczuk PM, Rossi MP, Katsikis PD, Gogotsi Y. Effect of carbon nanofibre structure on the binding of antibodies. Nanotechnology 2005;16(4):567.
141. Sinha N, Yeow JTW. Carbon nanotubes for biomedical applications. NanoBioscience, IEEE Transactions on 2005;4(2):180-195.
142. Vecitis CD, Zodrow KR, Kang S, Elimelech M. Electronic-Structure-Dependent Bacterial Cytotoxicity of Single-Walled Carbon Nanotubes. ACS Nano 2010;4(9):5471-5479.
143. Webster TJ, Waid MC, McKenzie JL, Price RL, Ejiofor JU. Nano-biotechnology: carbon nanofibres as improved neural and orthopaedic implants. Nanotechnology 2004;15(1):48-54.
144. Aninwene GE, Yao C, Webster TJ. Enhanced osteoblast adhesion to drug-coated anodized nanotubular titanium surfaces. International Journal of Nanomedicine 2008;3(2):257-264.
145. Cohen A, Liu-Synder P, Storey D, Webster TJ. Decreased fibroblast and increased osteoblast functions on ionic plasma deposited nanostructured Ti coatings. Nanoscale Research Letters 2007;2(8):385-390.
146. Ercan B, Webster TJ. Greater osteoblast proliferation on anodized nanotubular titanium upon electrical stimulation. International Journal of Nanomedicine 2008;3(4):477-485.
147. Tang M, Zhang T, Xue YY, Wang S, Huang MM, Yang Y, Lu MY, Lei H, Kong L, Pu YP. Dose Dependent In Vivo Metabolic Characteristics of Titanium Dioxide Nanoparticles. Journal of Nanoscience and Nanotechnology 2010;10(12):8575-8583.
148. Yao C, Webster TJ. Anodization: A promising nano-modification technique of titanium implants for orthopedic applications. Journal of Nanoscience and Nanotechnology 2006;6(9-10):2682-2692.
149. Popat KC, Eltgroth M, La Tempa TJ, Grimes CA, Desai TA. Titania nanotubes: A novel platform for drug-eluting coatings for medical implants? Small 2007;3(11):1878-1881.
150. Popat KC, Eltgroth M, LaTempa TJ, Grimes CA, Desai TA. Decreased Staphylococcus epidermis adhesion and increased osteoblast functionality on antibiotic-loaded titania nanotubes. Biomaterials 2007;28(32):4880-4888.
151. Hsu SH, Tseng HJ, Lin YC. The biocompatibility and antibacterial properties of waterborne polyurethane-silver nanocomposites. Biomaterials 2010;31(26):6796-6808.
152. Hung HS, Hsu SH. Biological performances of poly(ether)urethane-silver nanocomposites. Nanotechnology 2007;18(47).
153. Kumar A, Vemula PK, Ajayan PM, John G. Silver-nanoparticle-embedded antimicrobial paints based on vegetable oil. Nature Materials 2008;7(3):236-241.
154. Zheng Z, Yin W, Zara JN, Li W, Kwak J, Mamidi R, Lee M, Siu RK, Ngo R, Wang J and others. The use of BMP-2 coupled – Nanosilver-PLGA composite grafts to induce bone repair in grossly infected segmental defects. Biomaterials 2010;31(35):9293-9300.
155. Harrison JJ, Ceri H, Stremick CA, Turner RJ. Biofilm susceptibility to metal toxicity. Environmental Microbiology 2004;6(12):1220-1227.
156. Baker C, Pradhan A, Pakstis L, Pochan DJ, Shah SI. Synthesis and antibacterial properties of silver nanoparticles. Journal of Nanoscience and Nanotechnology 2005;5(2):244-249.
157. Makhluf S, Dror R, Nitzan Y, Abramovich Y, Jelinek R, Gedanken A. Microwave-

assisted synthesis of nanocrystalline MgO and its use as a bacteriocide. Advanced Functional Materials 2005;15(10):1708-1715.
158. Maki DG. Coming to Grips with Foodborne Infection - Peanut Butter, Peppers, and Nationwide Salmonella Outbreaks. New England Journal of Medicine 2009;360(10):949-953.
159. Xia T, Kovochich M, Liong M, Mädler L, Gilbert B, Shi H, Yeh JI, Zink JI, Nel AE. Comparison of the Mechanism of Toxicity of Zinc Oxide and Cerium Oxide Nanoparticles Based on Dissolution and Oxidative Stress Properties. ACS Nano 2008;2(10):2121-2134.
160. Wang B, Feng W, Wang M, Wang T, Gu Y, Zhu M, Ouyang H, Shi J, Zhang F, Zhao Y and others. Acute toxicological impact of nano- and submicro-scaled zinc oxide powder on healthy adult mice. Journal of Nanoparticle Research 2008;10(2):263-276.
161. Caballero L, Whitehead KA, Allen NS, Verran J. Photoinactivation of Escherichia coli on acrylic paint formulations using fluorescent light. Dyes and Pigments 2010;86(1):56-62.
162. Sunada K, Kikuchi Y, Hashimoto K, Fujishima A. Bactericidal and detoxification effects of TiO(2) thin film photocatalysts. Environmental Science & Technology 1998;32(5):726-728.
163. Heller A. Chemistry and Applications of Photocatalytic Oxidation of Thin Organic Films. Accounts of Chemical Research 1995;28(12):503-508.
164. Shiraishi K, Koseki H, Tsurumoto T, Baba K, Naito M, Nakayama K, Shindo H. Antibacterial metal implant with a TiO(2)-conferred photocatalytic bactericidal effect against Staphylococcus aureus. Surface and Interface Analysis 2009;41(1):17-22.
165. Choi MG, Koh HS, Kluess D, O'Connor D, Mathur A, Truskey GA, Rubin J, Zhou DXF, Sung KLP. Effects of titanium particle size on osteoblast functions in vitro and in vivo. Proceedings of the National Academy of Sciences of the United States of America 2005;102(12):4578-4583.
166. Ellis JR. The Many Roles of Silver in Infection Prevention. American Journal of Infection Control 2007;35(5):E26-E26.
167. Liu J, Sonshine DA, Shervani S, Hurt RH. Controlled Release of Biologically Active Silver from Nanosilver Surfaces. ACS Nano 2010;4(11):6903-6913.
168. McDonnell G, Russell AD. Antiseptics and disinfectants: Activity, action, and resistance (vol 12,pg 147, 1999). Clinical Microbiology Reviews 2001;14(1):227-228.
169. Liau SY, Read DC, Pugh WJ, Furr JR, Russell AD. Interaction of silver nitrate with readily identifiable groups: relationship to the antibacterial action of silver ions. Letters in Applied Microbiology 1997;25(4):279-283.
170. Park H-J, Kim JY, Kim J, Lee J-H, Hahn J-S, Gu MB, Yoon J. Silver-ion-mediated reactive oxygen species generation affecting bactericidal activity. Water Research 2009;43(4):1027-1032.
171. Hwang ET, Lee JH, Chae YJ, Kim YS, Kim BC, Sang B-I, Gu MB. Analysis of the Toxic Mode of Action of Silver Nanoparticles Using Stress-Specific Bioluminescent Bacteria. Small 2008;4(6):746-750.
172. Rivardo F, Martinotti MG, Turner RJoseph, Ceri H. The activity of silver against Escherichia coli biofilm is increased by a lipopeptide biosurfactant. Canadian Journal of Microbiology 2010;56(3):272-278.
173. Lewis K. Riddle of Biofilm Resistance. Antimicrobial Agents and Chemotherapy 2001;45(4):999-1007.
174. Silver S. Bacterial silver resistance: molecular biology and uses and misuses of silver

compounds. FEMS Microbiology Reviews 2003;27(2-3):341-353.
175. Touati D. Iron and oxidative stress in bacteria. Archives of Biochemistry and Biophysics 2000;373(1):1-6.
176. Weinberg ED. Iron loading and disease surveillance. Emerging Infectious Diseases 1999;5(3):346-352.
177. Lee C, Kim JY, Lee WI, Nelson KL, Yoon J, Sedlak DL. Bactericidal Effect of Zero-Valent Iron Nanoparticles on Escherichia coli. Environmental Science & Technology 2008;42(13):4927-4933.
178. Phenrat T, Long TC, Lowry GV, Veronesi B. Partial Oxidation ("Aging") and Surface Modification Decrease the Toxicity of Nanosized Zerovalent Iron. Environmental Science & Technology 2008;43(1):195-200.
179. Auffan Ml, Achouak W, Rose Jr, Roncato M-A, Chanéac C, Waite DT, Masion A, Woicik JC, Wiesner MR, Bottero J-Y. Relation between the Redox State of Iron-Based Nanoparticles and Their Cytotoxicity toward Escherichia coli. Environmental Science & Technology 2008;42(17):6730-6735.
180. Zhang J, Spallholz JE. Toxicity of Selenium Compounds and Nano-Selenium Particles. General, Applied and Systems Toxicology: John Wiley & Sons, Ltd; 2009.
181. Tran PA, Sarin L, Hurt RH, Webster TJ. Opportunities for nanotechnology-enabled bioactive bone implants. Journal of Materials Chemistry 2009;19(18):2653-2659.
182. Tran PA, Webster TJ. Selenium nanoparticles inhibit Staphylococcus aureus growth. International Journal of Nanomedicine 2011;6.
183. Tran PA. Nanostructured Selenium for Biomedical Applications: from Theory to Practice. Providence, RI: Brown University; 2010.
184. Kamencic H, Lyon A, Paterson PG, Juurlink BHJ. Monochlorobimane fluorometric method to measure tissue glutathione. Analytical Biochemistry 2000;286(1):35-37.
185. delCardayre SB, Stock KP, Newton GL, Fahey RC, Davies JE. Coenzyme A disulfide reductase, the primary low molecular weight disulfide reductase from Staphylococcus aureus - Purification and characterization of the native enzyme. Journal of Biological Chemistry 1998;273(10):5744-5751.
186. Newton GL, Rawat M, La Clair JJ, Jothivasan VK, Budiarto T, Hamilton CJ, Claiborne A, Helmann JD, Fahey RC. Bacillithiol is an antioxidant thiol produced in Bacilli. Nature Chemical Biology 2009;5(9):625-627.
187. Newton GLF, R. C.; Rawat, M. Detoxification of toxins by bacillithiol in Staphylococcus aureus. Microbiology 2012;10(1099):5715.
188. Gaballa A, Newton GL, Antelmann H, Parsonage D, Upton H, Rawat M, Claiborne A, Fahey RC, Helmann JD. Biosynthesis and functions of bacillithiol, a major low-molecular-weight thiol in Bacilli. Proceedings of the National Academy of Sciences of the United States of America 2010;107(14):6482-6486.
189. Gomes SAO, Vieira CS, Almeida DB, Santos-Mallet JR, Menna-Barreto RFS, Cesar CL, Feder D. CdTe and CdSe Quantum Dots Cytotoxicity: A Comparative Study on Microorganisms. Sensors 2011;11(12):11664-11678.
190. Kolosnjaj J, Szwarc H, Moussa F. Toxicity Studies of Carbon Nanotubes
Bio-Applications of Nanoparticles. In: Chan WCW, editor: Springer New York; 2007. p 181-204.
191. Lam C-w, James JT, McCluskey R, Arepalli S, Hunter RL. A Review of Carbon Nanotube Toxicity and Assessment of Potential Occupational and Environmental Health Risks. Critical Reviews in Toxicology 2006;36(3):189-217.
192. Poland CA, Duffin R, Kinloch I, Maynard A, Wallace WAH, Seaton A, Stone V, Brown S, MacNee W, Donaldson K. Carbon nanotubes introduced into the abdominal cavity of mice show asbestos-like pathogenicity in a pilot study. Nat Nano 2008;3(7):423-

428.
193. Suci PA, Berglund DL, Liepold L, Brumfield S, Pitts B, Davison W, Oltrogge L, Hoyt KO, Codd S, Stewart PS and others. High-density targeting of a viral multifunctional nanoplatform to a pathogenic, biofilm-forming bacterium. Chemistry & Biology 2007;14(4):387-398.
194. Gu HW, Ho PL, Tong E, Wang L, Xu B. Presenting vancomycin on nanoparticles to enhance antimicrobial activities. Nano Letters 2003;3(9):1261-1263.
195. Mohammed Fayaz A, Girilal M, Mahdy SA, Somsundar SS, Venkatesan R, Kalaichelvan PT. Vancomycin bound biogenic gold nanoparticles: A different perspective for development of anti VRSA agents. Process Biochemistry 2011;46(3):636-641.
196. Xing BG, Ho PL, Yu CW, Chow KH, Gu HW, Xu B. Self-assembled multivalent vancomycin on cell surfaces against vancomycin-resistant enterococci (VRE). Chemical Communications 2003(17):2224-2225.
197. Greenhalgh K, Turos E. In vivo studies of polyacrylate nanoparticle emulsions for topical and systemic applications. Nanomedicine-Nanotechnology Biology and Medicine 2009;5(1):46-54.
198. Wang GQ, Hindler JF, Ward KW, Bruckner DA. Increased vancomycin MICs for Staphylococcus aureus clinical isolates from a university hospital during a 5-year period. Journal of Clinical Microbiology 2006;44(11):3883-3886.
199. Liu LH, Xu KJ, Wang HY, Tan PKJ, Fan WM, Venkatraman SS, Li LJ, Yang YY. Self-assembled cationic peptide nanoparticles as an efficient antimicrobial agent. Nature Nanotechnology 2009;4(7):457-463.
200. Zheng Z, Yin W, Zara JN, Li WM, Kwak J, Mamidi R, Lee M, Siu RK, Ngo R, Wang J and others. The use of BMP-2 coupled - Nanosilver-PLGA composite grafts to induce bone repair in grossly infected segmental defects. Biomaterials 2010;31(35):9293-9300.
201. Fujie T, Saito A, Kinoshita M, Miyazaki H, Ohtsubo S, Saitoh D, Takeoka S. Dual therapeutic action of antibiotic-loaded nanosheets for the treatment of gastrointestinal tissue defects. Biomaterials 2010;31(24):6269-6278.
202. Fujie T, Matsutani N, Kinoshita M, Okamura Y, Saito A, Takeoka S. Adhesive, Flexible, and Robust Polysaccharide Nanosheets Integrated for Tissue-Defect Repair. Advanced Functional Materials 2009;19(16):2560-2568.
203. Fujie T, Kinoshita M, Shono S, Saito A, Okamura Y, Saitoh D, Takeoka S. Sealing effect of a polysaccharide nanosheet for murine cecal puncture. - Mosby; 2010. p 48.
204. Fujie T, Kinoshita M, Shono S, Saito A, Okamura Y, Saitoh D, Takeoka S. Sealing effect of a polysaccharide nanosheet for murine cecal puncture. Surgery 2010;148(1):48-58.
205. Weissleder R, Bogdanov A, Neuwelt EA, Papisov M. LONG-CIRCULATING IRON-OXIDES FOR MR-IMAGING. Advanced Drug Delivery Reviews 1995;16(2-3):321-334.
206. Berry CC, Curtis ASG. Functionalisation of magnetic nanoparticles for applications in biomedicine. Journal of Physics D-Applied Physics 2003;36(13):R198-R206.
207. Gilchrist RK, Medal R, Shorey WD, Hanselman RC, Parrott JC, Taylor CB. SELECTIVE INDUCTIVE HEATING OF LYMPH NODES. Annals of Surgery 1957;146(4):596-606.
208. Oliveira DM, Lacava ZGM, Lima ECD, Morais PC, Tedesco AC. Zinc phthalocyanine/magnetic fluid complex: A promising dual nanostructured system for cancer treatment. Journal of Nanoscience and Nanotechnology 2006;6(8):2432-2437.
209. Thunemann AF, Schutt D, Kaufner L, Pison U, Mohwald H. Maghemite nanoparticles protectively coated with poly(ethylene imine) and poly(ethylene oxide)-block-

poly(glutamic acid). Langmuir 2006;22(5):2351-2357.
210. Schwertmann U, Cornell RM. Frontmatter. Iron Oxides in the Laboratory: Wiley-VCH Verlag GmbH; 2007. p i-xviii.
211. Xu CJ, Sun SH. Monodisperse magnetic nanoparticles for biomedical applications. Polymer International 2007;56(7):821-826.
212. Reimer P, Weissleder R. Development and experimental application of receptor-specific MR contrast media. Radiologe 1996;36(2):153-163.
213. Chouly C, Pouliquen D, Lucet I, Jeune JJ, Jallet P. Development of superparamagnetic nanoparticles for MRI: Effect of particle size, charge and surface nature on biodistribution. Journal of Microencapsulation 1996;13(3):245-255.
214. Gupta PK, Hung CT. MAGNETICALLY CONTROLLED TARGETED MICRO-CARRIER SYSTEMS. Life Sciences 1989;44(3):175-186.
215. Lee H, Purdon AM, Chu V, Westervelt RM. Controlled Assembly of Magnetic Nanoparticles from Magnetotactic Bacteria Using Microelectromagnets Arrays. Nano Letters 2004;4(5):995-998.
216. Sun C, Lee JSH, Zhang M. Magnetic nanoparticles in MR imaging and drug delivery. Advanced Drug Delivery Reviews 2008;60(11):1252-1265.
217. Harris MM, Houtkooper LB, Stanford VA, Parkhill C, Weber JL, Flint-Wagner H, Weiss L, Going SB, Lohman TG. Dietary iron is associated with bone mineral density in healthy postmenopausal women. Journal of Nutrition 2003;133(11):3598-3602.
218. Parelman M, Stoecker B, Baker A, Medeiros D. Iron restriction negatively affects bone in female rats and mineralization of hFOB osteoblast cells. Experimental Biology and Medicine 2006;231(4):378-386.
219. Abraham R, Walton J, Russell L, Wolman R, Wardley-Smith B, Green JR, Mitchell A, Reeve J. Dietary determinants of post-menopausal bone loss at the lumbar spine: a possible beneficial effect of iron. Osteoporosis International 2006;17(8):1165-1173.
220. Le NTV, Richardson DR. Iron chelators with high antiproliferative activity up-regulate the expression of a growth inhibitory and metastasis suppressor gene: a link between iron metabolism and proliferation. Blood 2004;104(9):2967-2975.
221. Tran N, Webster TJ. Increased osteoblast functions in the presence of hydroxyapatite-coated iron oxide nanoparticles. Acta Biomaterialia 2011;7(3):1298-1306.
222. Shimizu K, Ito A, Yoshida T, Yamada Y, Ueda M, Honda H. Bone tissue engineering with human mesenchymal stem cell sheets constructed using magnetite nanoparticles and magnetic force. Journal of Biomedical Materials Research Part B-Applied Biomaterials 2007;82B(2):471-480.
223. Dobson J. Remote control of cellular behaviour with magnetic nanoparticles. Nature Nanotechnology 2008;3(3):139-143.
224. Walker LM, Holm A, Cooling L, Maxwell L, Oberg A, Sundqvist T, El Haj AJ. Mechanical manipulation of bone and cartilage cells with 'optical tweezers'. Febs Letters 1999;459(1):39-42.
225. Ferrari M, Lee AP. BioMEMS and biomedical nanotechnology: Springer; 2006.
226. Dobretsov KG, Afon'kin VY, Kirichenko AK, Ladygina VP, Stolyar SV, Bayukov OA, Sipkin AV. A Method for Introduction of Magnetic Nanoparticles into Tissues by Means of Magnetic Field Gradient: An Experimental Study. Bulletin of Experimental Biology and Medicine 2009;147(6):750-752.
227. Shapiro BW, DC, US), Emmert-buck, Michael R. (Easton, MD, US) Methods And Systems For Using Therapeutic, Diagnostic or Prophylactic Magnetic Agents. 2009.
228. Chertok B, Moffat BA, David AE, Yu FQ, Bergemann C, Ross BD, Yang VC. Iron oxide

nanoparticles as a drug delivery vehicle for MRI monitored magnetic targeting of brain tumors. Biomaterials 2008;29(4):487-496.
229. Oh J, Feldman MD, Kim J, Condit C, Emelianov S, Milner TE. Detection of magnetic nanoparticles in tissue using magneto-motive ultrasound. Nanotechnology 2006;17(16):4183-4190.
230. Polyak B, Fishbein I, Chorny M, Alferiev I, Williams D, Yellen B, Friedman G, Levy RJ. High field gradient targeting of magnetic nanoparticle-loaded endothelial cells to the surfaces of steed stents. Proceedings of the National Academy of Sciences of the United States of America 2008;105(2):698-703.
231. Kadurugamuwa JL, Sin L, Albert E, Yu J, Francis K, DeBoer M, Rubin M, Bellinger-Kawahara C, Parr TR, Contag PR. Direct continuous method for monitoring biofilm infection in a mouse model. Infection and Immunity 2003;71(2):882-890.
232. Felfoul O, Mohammadi M, Martel S. Magnetic resonance imaging of Fe3O4 nanoparticles embedded in living magnetotactic bacteria for potential use as carriers for in vivo applications. Conference proceedings : ... Annual International Conference of the IEEE Engineering in Medicine and Biology Society. IEEE Engineering in Medicine and Biology Society. Conference 2007;2007:1463-6.
233. Kang YS, Risbud S, Rabolt JF, Stroeve P. Synthesis and Characterization of Nanometer-Size Fe3O4 and γ-Fe2O3 Particles. Chemistry of Materials 1996;8(9):2209-2211.
234. Gupta AK, Gupta M. Cytotoxicity suppression and cellular uptake enhancement of surface modified magnetic nanoparticles. Biomaterials 2005;26(13):1565-1573.
235. Suchanek W, Yashima M, Kakihana M, Yoshimura M. Hydroxyapatite/hydroxyapatite-whisker composites without sintering additives: Mechanical properties and microstructural evolution. Journal of the American Ceramic Society 1997;80(11):2805-2813.
236. Wan J, Cai W, Meng X, Liu E. Monodisperse water-soluble magnetite nanoparticles prepared by polyol process for high-performance magnetic resonance imaging. Chemical Communications 2007(47):5004-5006.
237. Maity D, Kale SN, Kaul-Ghanekar R, Xue J-M, Ding J. Studies of magnetite nanoparticles synthesized by thermal decomposition of iron (III) acetylacetonate in tri(ethylene glycol). Journal of Magnetism and Magnetic Materials 2009;321(19):3093-3098.
238. Cai W, Wan J. Facile synthesis of superparamagnetic magnetite nanoparticles in liquid polyols. Journal of Colloid and Interface Science 2007;305(2):366-370.
239. Yantasee W, Warner CL, Sangvanich T, Addleman RS, Carter TG, Wiacek RJ, Fryxell GE, Timchalk C, Warner MG. Removal of Heavy Metals from Aqueous Systems with Thiol Functionalized Superparamagnetic Nanoparticles. Environmental Science & Technology 2007;41(14):5114-5119.
240. Yavuz CT, Mayo JT, Yu WW, Prakash A, Falkner JC, Yean S, Cong LL, Shipley HJ, Kan A, Tomson M and others. Low-field magnetic separation of monodisperse Fe3O4 nanocrystals. Science 2006;314(5801):964-967.
241. Conrady DG, Brescia CC, Horii K, Weiss AA, Hassett DJ, Herr AB. A zinc-dependent adhesion module is responsible for intercellular adhesion in staphylococcal biofilms. Proceedings of the National Academy of Sciences of the United States of America 2008;105(49):19456-19461.
242. Roger J, Pons JN, Massart R, Halbreich A, Bacri JC. Some biomedical applications of ferrofluids. European Physical Journal-Applied Physics 1999;5(3):321-325.
243. Fauconnier N, Pons JN, Roger J, Bee A. Thiolation of maghemite nanoparticles by dimercaptosuccinic acid. Journal of Colloid and Interface Science 1997;194(2):427-

433.
244. Di Marco M, Sadun C, Port M, Guilbert I, Couvreur P, Dubernet C. Physicochemical characterization of ultrasmall superparamagnetic iron oxide particles (USPIO) for biomedical application as MRI contrast agents. International Journal of Nanomedicine 2007;2(4):609-622.
245. George GN, Prince RC, Gailer J, Buttigieg GA, Denton MB, Harris HH, Pickering IJ. Mercury Binding to the Chelation Therapy Agents DMSA and DMPS and the Rational Design of Custom Chelators for Mercury. Chemical Research in Toxicology 2004;17(8):999-1006.
246. Oprea C, Ciupina V, Prodan G. Investigation of nanocrystals using TEM micrographs and electron diffraction technique. Romanian Journal of Physics 2008;53(1-2):223-230.
247. Webster TJ, Schadler LS, Siegel RW, Bizios R. Mechanisms of enhanced osteoblast adhesion on nanophase alumina involve vitronectin. Tissue Engineering 2001;7(3):291-301.
248. Wu W, Xiao X, Zhang S, Li H, Zhou X, Jiang C. One-Pot Reaction and Subsequent Annealing to Synthesis Hollow Spherical Magnetite and Maghemite Nanocages. Nanoscale Research Letters 2009;4(8):926-931.
249. Hu Q, Chen F, Li B, Shen J. Preparation of three-dimensional nano-magnetite/chitosan rod. Materials Letters 2006;60(3):368-370.
250. Xu C, Xie J, Ho D, Wang C, Kohler N, Walsh EG, Morgan JR, Chin YE, Sun S. Au–Fe3O4 Dumbbell Nanoparticles as Dual-Functional Probes. Angewandte Chemie International Edition 2008;47(1):173-176.
251. Webster TJ, Ergun C, Doremus RH, Siegel RW, Bizios R. Enhanced osteoclast-like cell functions on nanophase ceramics. Biomaterials 2001;22(11):1327-1333.
252. Stoimenov PK, Klinger RL, Marchin GL, Klabunde KJ. Metal oxide nanoparticles as bactericidal agents. Langmuir 2002;18(17):6679-6686.
253. Egorova LG, Okonishn.Ie, Nirenbur.Vl, Postovsk.Iy. COMPARATIVE STUDY OF INTERACTION OF SPACIAL ISOMERS OF DIMERCAPTOSUCCINIC ACID WITH SOME METALS. Khimiko-Farmatsevticheskii Zhurnal 1971;5(1):26-&.
254. Malvern. Hydrodynamic radius - what is it? : http://www.malvern.com/labeng/industry/protein/hydrodynamic_radius.htm; 2011.
255. Qiang Y, Antony J, Sharma A, Nutting J, Sikes D, Meyer D. Iron/iron oxide core-shell nanoclusters for biomedical applications. Journal of Nanoparticle Research 2006;8(3):489-496.
256. Fluit AC, Wielders CLC, Verhoef J, Schmitz FJ. Epidemiology and susceptibility of 3,051 Staphylococcus aureus isolates from 25 university hospitals participating in the European SENTRY study. Journal of Clinical Microbiology 2001;39(10):3727-3732.
257. Pearson L. Joint Replacement: Does this Look Infected to You? : AAOS Now 2010; 2010.
258. Aarestrup FM, Cavaco L, Hasman H. Decreased susceptibility to zinc chloride is associated with methicillin resistant Staphylococcus aureus CC398 in Danish swine. Veterinary Microbiology 2010;142(3-4):455-457.
259. Ansari MA KH, Khan AA, Malik A, Sultan A, Shahid M, Shujatullah F, Azam A. Evaluation of antibacterial activity of silver nanoparticles against MSSA MRSA on isolates from skin infections. Biology and Medicine 2011;3(2):141-146.
260. Corrigan RM, Rigby D, Handley P, Foster TJ. The role of Staphylococcus aureus surface protein SasG in adherence and biofilm formation. Microbiology-Sgm

2007;153:2435-2446.
261. Helmann JD. Bacillithiol, a New Player in Bacterial Redox Homeostasis. Antioxidants & Redox Signaling 2011;15(1):123-133.
262. Corot C, Robert P, Idée J-M, Port M. Recent advances in iron oxide nanocrystal technology for medical imaging. Advanced Drug Delivery Reviews 2006;58(14):1471-1504.
263. WebMD. Iron Poisoning. In: Edmundson A, editor. WebMD Medical Reference from eMedicineHealth: http://www.webmd.com/a-to-z-guides/iron-poisoning?page=3; 2006.
264. Aitken RJ, Chaudhry MQ, Boxall ABA, Hull M. Manufacture and use of nanomaterials: current status in the UK and global trends. Occupational Medicine-Oxford 2006;56(5):300-306.
265. Handy RD, von der Kammer F, Lead JR, Hassellov M, Owen R, Crane M. The ecotoxicology and chemistry of manufactured nanoparticles. Ecotoxicology 2008;17(4):287-314.
266. Bradford A, Handy RD, Readman JW, Atfield A, Muhling M. Impact of Silver Nanoparticle Contamination on the Genetic Diversity of Natural Bacterial Assemblages in Estuarine Sediments. Environmental Science & Technology 2009;43(12):4530-4536.
267. Gupta A, Silver S. Molecular genetics - Silver as a biocide: Will resistance become a problem? Nature Biotechnology 1998;16(10):888-888.
268. Chopra I. The increasing use of silver-based products as antimicrobial agents: a useful development or a cause for concern? - Author's response. Journal of Antimicrobial Chemotherapy 2007;60(2):447-448.